2023-08-01

Design And Development Of Transition Metal-Based Electrocatalysts For Environmentally Friendly And Efficient Hydrogen Evolution Reactions (her)

Navid Attarzadeh
University of Texas at El Paso

DESIGN AND DEVELOPMENT OF TRANSITION METAL-BASED ELECTROCATALYSTS FOR ENVIRONMENTALLY FRIENDLY AND EFFICIENT HYDROGEN EVOLUTION REACTIONS (HER)

NAVID ATTARZADEH

Doctoral Program in Environmental Science and Engineering

APPROVED:

Chintalapalle V Ramana, Ph.D., Chair

Ahmed El-Gendy, Ph.D.

Skye Fortier, Ph.D.

Debabrata Das, Ph.D.

Stephen L. Crites, Jr., Ph.D.
Dean of the Graduate School

Dedication

I dedicate this dissertation to my parents, who loved me truly.

DESIGN AND DEVELOPMENT OF TRANSITION METAL-BASED ELECTROCATALYSTS FOR ENVIRONMENTALLY FRIENDLY AND EFFICIENT HYDROGEN EVOLUTION REACTIONS (HER)

by

NAVID ATTARZADEH, M.Sc.

DISSERTATION

Presented to the Faculty of the Graduate School of

The University of Texas at El Paso

in Partial Fulfillment

of the Requirements

for the Degree of

DOCTOR OF PHILOSOPHY

Environmental Science and Engineering

THE UNIVERSITY OF TEXAS AT EL PASO

August 2023

Acknowledgments

I would like to thank Prof. CV Ramana and extend my gracious, most sincere gratitude to my mentor for making this journey possible. I cannot thank him enough. He has been a constant companion during my PhD and kept me pushing to achieve the best version of me. It is because of his "bigger picture" approach, I could excel and experiment as a researcher. My PhD degree is possible because of a great mentorship, and I have been fortunate to have landed with a guide like Professor Ramana

I would like to thank Dr. Debobrate Das, for his assistance and help during my research at CMR.
I would like to thank Dr. Skye Fortier, Dr. Ahmed El-Gendi, for guidance on my dissertation, and the member of the Center for Advanced Materials Research (CMR).
I would like to thank Prof. Creg Tweedie, for his continuous support during my Ph.D. education. He encouraged me while there were many obstacles along my path.

I would like to thank Ms. Fabiola Alvarez, Ms. Lina Hamadan.

I also acknowledge, with pleasure, support from the National Science Foundation (NSF) with NSF-PREM grant #DMR-1827745.

Abstract

Hydrogen fuel is a clean energy source primarily because it emits no carbon dioxide (CO_2). Sustainable energy alternatives have attracted the scientific community and policymakers as concerns over global warming and depletion of fossil fuels have increased significantly. Substituting H_2 gas as a primary source for our daily energy consumption under the guideline of the hydrogen economy concept has not progressed as anticipated because of inadequate efficiency associated with the generation (electrolyzer) and utilization (fuel cell) devices. However, there are challenges associated with hydrogen that must be overcome for it to become a truly sustainable and widespread energy source. The full potential of electrocatalysts fabricated from earth-abundant metals has yet to be exploited to replace Pt-group metals due to inadequate efficiency and insufficient design strategies to meet the ever-increasing demands for renewable energies. To improve the electrocatalytic performance, the primary challenge is to optimize the structure and electronic properties by enhancing the intrinsic catalytic activity and expanding the active catalytic surface area. A significant overpotential limits the HER, while efficient electrocatalysts based on platinum group metals (PGMs) have demonstrated relatively low overpotentials across a wide pH range of electrolytes. However, the large-scale utilization of PGM-based electrocatalysts is hindered by two main factors: scarcity and high cost. This dissertation focused on developing alternative catalysts that could replace or reduce the reliance on PGMs. The presented work employed abundant and low-cost transition metals such as Ni and Mo to discover and optimize new materials with maintaining high catalytic activity and stability for the HER. First, we report synthesizing a 3D nanoarchitecture of aligned Ni_5P_4-Ni_2P/NiS (plate/nanosheets) using a phospho-sulfidation process. The durability and unique design of prickly pear cactus in desert environments by adsorbing moisture through its extensive surface and ability to bear fruits at the edges of leaves

inspire this study to adopt a similar 3D architecture and utilize it to design an efficient heterostructure catalyst for HER activity. The catalyst comprises two compartments of the vertically aligned Ni_5P_4-Ni_2P plates and the NiS nanosheets, resembling the role of leaves and fruits in the prickly pear cactus. The Ni_5P_4-Ni_2P plates deliver charges to the interface areas, and the NiS nanosheets significantly influence H_{ad} and transfer electrons for the HER activity. Indeed, the synergistic presence of heterointerfaces and the epitaxial NiS nanosheets can substantially improve the catalytic activity compared to nickel phosphide catalysts. Secondly, we report synthesizing a 3D structure of Mo_2N-MoP@Mo heterostructured catalysts. To attain the current densities of 10 and 100 mA cm^{-2}, the Ni-catalyst showed overpotentials of 75 and 115 mV, and Mo-catalyst exhibited 65 and 110 mV, respectively. The Tafel slopes were found to be 50 and 65 mV dec^{-1} for the champions. The longevity of both catalysts was investigated, and the electrochemical impedance spectroscopy (EIS) revealed inducing S and N non-metals was the underlying reason for the modification and durability of structures.

Table of Contents

List of Tables

List of Figures

List of Illustrations

Chapter 1: Application of Transition Metal Phosphides to Electrocatalysis

1.1. INTRODUCTION

Preserving the environment by establishing global-scale sustainable energy systems has emerged as one of the most vital and critical challenges for the future generation. The projection of energy demands required for the growing world population and industrialization expansion illustrates 24-26 TW under scenarios of "new policies" or "current policies", while carbon dioxide emission will reach 37-44 Gt per year in 2040 (She et al. 2017). The energy supply demands immediate impetus to diversify energy sources, emphasizing environmental challenges aroused by fossil fuel consumption. The current momentum is to broaden the traditional power supply and narrow fossil fuel usage. The daily aggravation of demands for clean and economical energy resources endows excellent opportunities for designing and exploring new electrocatalysts which can address current global challenges regarding environment and sustainability. For instance, a rational strategy is to employ electrocatalysts for converting water as an environmentally abundant source to higher-value energy sources, including hydrogen and oxygen. Nanostructured transitional metal phosphides have improved electrocatalytic activity compared to many bulk materials (Browne, Sofer, and Pumera 2019). The efficacy of electrocatalysis is controlled by the electrode materials, which in turn determines the kinetics of hydrogen release and adsorption/desorption at the electrode-electrolyte interface. Figure 1.1 represents the schematic of applications of transition metal phosphides in various energy segments.

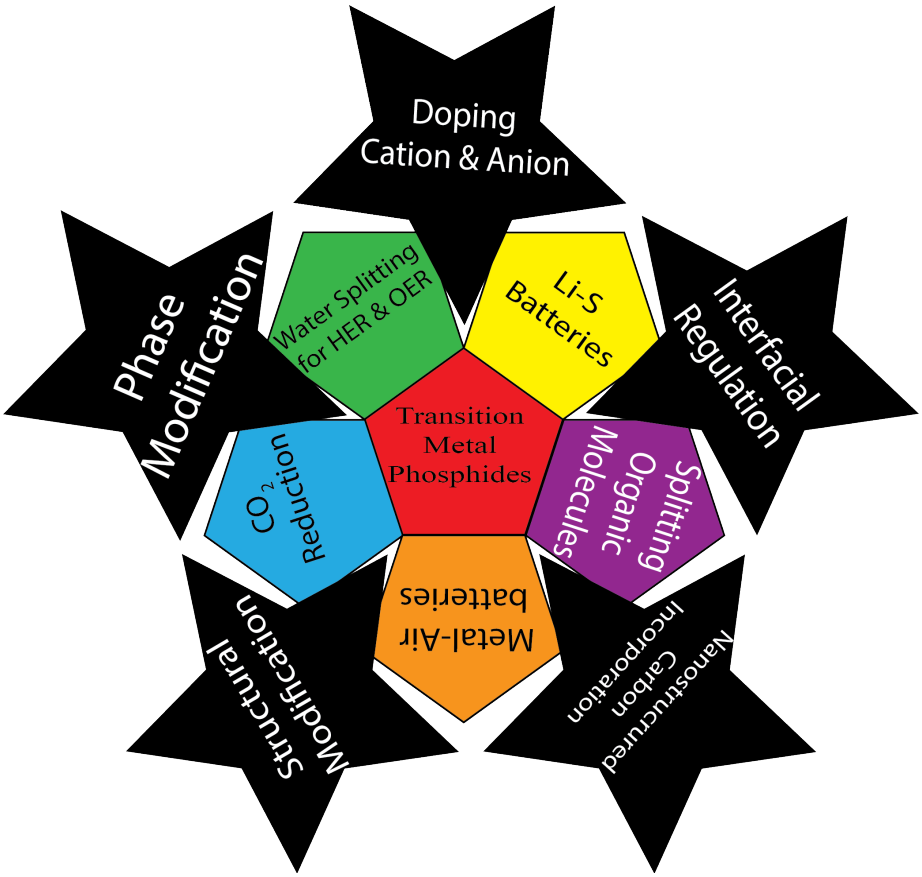

Figure 1-1: Schematic representation of modulated strategies for modification of transition metal phosphides for energy-related applications as electrocatalysts.

Employing electrocatalysts for either splitting water for hydrogen evolution reaction (HER) and oxygen evolution reaction (OER) or operating the cathodic process of oxygen reduction reaction (ORR) indicates a remarkable potential to maximize energy density economically and efficiently in fuel cells. In this respect, the essential goal is to develop precious metal-free catalysts demonstrating well-controlled nanostructures that augment the number of active sites and high durability and sufficient intrinsic activity at each site. The application of nanostructured electrodes made from transition metals (Ni, Co, Mo, etc.) has been studied extensively as electrocatalysts because of their abundant earth reserves and active properties. In recent decades, electrocatalysts composed of earth-rich transition metals that are utilized for energy transformation could be

categorized as follows: transition metal oxides (TMO) (Cheng et al. 2009), metal nitrides (TMN) (M. Liu et al. 2013; Dong et al. 2013), metal dichalcogenides (TMDs) (Mahmood et al. 2013; Y. Sun et al. 2017; Kong et al. 2013), metal carbides (TMC) (H. bin Wu et al. 2015), and insulated single atoms of transition metals (TMs) (K. Jiang et al. 2018). For example, the well-known electrocatalysts developed for specific reactions are MoS_2 for HER (Lukowski et al. 2013; Yanguang Li et al. 2011) and Co_3O_4 for OER/ORR (L. Xu et al. 2016; J. Xu, Gao, and Zhao 2012). Despite the current progress of noble metal-free paradigms, a few challenges, such as inadequate active sites and weak electron conductivity, have yet to be addressed to achieve the primary milestones in the development of electrocatalysts. TMPs have demonstrated significant physicochemical characteristics, such as desirable electronic features, because metal-rich metal phosphides are metallic, even acting as superconductors (Callejas et al. 2016a). Crystalline surfaces in TMPs provide more active sites, in contrast to 2D TMDs, where catalytic activity relies on the edges of stacking layers (Y. Wang et al. 2017). Broader stability in various pH conditions endows greater applicability to TMP structures. Due to excellent physicochemical features and several fabrication methods, TMP electrocatalysts surpass constraints seen in TMO, TMN, and TMDs and represent greater feasibility to replace noble metal catalysts. All elements known as transition metals in the periodic table enable to react with phosphorous to form TMPs. Phosphides demonstrate complex chemistry because different crystalline structures emerge from different stoichiometric ratios, and minor variations in the ratio of metal to phosphorous result in a significant alteration in physicochemical characteristics (Yang Lv and Wang 2017). Thus, it seems rational to record better electron conductivity and chemical stability when metal-rich or monophosphide TMP structures are provided because of adequate metal-metal bonds and metal-phosphorous bonds compared to phosphorus-rich TMPs with good phosphorous-phosphorous

bands (Callejas et al. 2016a). Therefore, the favorable physicochemical features of TMPs can be tuned successfully by altering their corresponding compositions and structures (Yang Li, Dong, and Jiao 2020a). For instance, a key frontier in the synthesis of new structures is to tailor the composition and structure of electrocatalysts to operate at various conditions while researchers pursue improving the longevity and selectivity of catalysts to realize the prospects of replacing renewable energy with fossil fuels.

The reversible reaction of hydrogen evolution, reaction 1, occurs on the electrode surface and requires to be catalyzed by an electronic conductor (Kibler 2006):

$$H^+_{(aq)} + e^- \rightarrow {}^1\!/_2\, H_{2(g)} \qquad (1)$$

Indeed, the chemical composition and surface structure of the electrode strongly influences the rate of hydrogen evolution, known as electrocatalytic activity. Generally, the hydrogen evolution (HER) can be categorized in three steps in the acidic environment (Kibler 2006):

1. Volmer or discharge reaction:

$$H^+_{(aq)} + e^- \rightarrow H_{ad} \qquad (2)$$

2. Tafel or combination reaction:

$$2H_{ad} \rightarrow H_{2,ad} \qquad (3)$$

3. Heyrowsky or ion + atom reaction

$$H^+_{(aq)} + H_{ad} \rightarrow H_{2,ad} \qquad (4)$$

Subsequent to the reaction between electrons from electrode and protons from solution, the surface of the catalyst requires adsorption of H_{ad} and formation of molecular hydrogen gas. The electrocatalytic activity can be defined using the Butler–Volmer equation (Kibler 2006), relating the reaction current density j to overpotential η, and the exchange current density, j_0, and is proportional to the reaction rate, as shown by equation (5):

$$j = j_0[\exp\left(\frac{\alpha F\eta}{RT}\right) - \exp\left(\frac{-(1-\alpha)F\eta}{RT}\right)] \quad (5)$$

Electrocatalytic activity relates to the composition, morphology, microstructure, and surface/interface features of the materials involved. This study summarizes the effective strategies to fabricate transition metal phosphides to form a significant number of exposable active sites with modified composition and structure. It focuses on regulations and effective approaches in synthesizing TMPs such as elemental doping, phase modification, structural and interfacial engineering, and incorporation of other effective supports like nanocarbon. The future outlook and prospects are presented to offer impetus for fabricating TMP electrocatalysts with robust efficacy.

1.2. Fabrication Strategies of Transition Metal Phosphides

The methods of preparation for transition metal phosphides are presented nowadays with new strategies, which endow scale-up fabrication lines for hydrogen electrocatalyst production. Several strategies are developed to control the size, composition, and morphology of prepared nanostructured TMPs. The fundamentals of fabrication methods are categorized into processes that are tightly associated with phosphorous sources. For instance, the preparation of active HER catalysts such as Ni_2P nanoparticles, FeP nanosheets, and CoP nanoparticles have suffered from incorporating several tedious steps involving organic solvents (Popczun et al. 2014; Y. Xu et al. 2013; Feng et al. 2014; Popczun et al. 2013a). Subsequently, studies shifted towards developing organic solvent-free strategies such as phosphorizing Co_3O_4 at 300 °C for two hours to prepare highly active HER catalysts of hybrid CoP nanocrystals supported by carbon nanotubes (CoP/CNT) (Q. Liu et al. 2014). Sun's group has conducted pioneering studies on a series of nanostructured metal hydroxides (including Co, Ni, Fe, and Cu) and synthesized nanostructured assays of TMPs without the involvement of organic phosphorous sources (Q. Liu et al. 2014; Tian, Liu, Asiri, et al. 2014; Q. Li et al. 2014a; P. Jiang, Liu, and Sun 2014; Y. Liang et al. 2014; P.

Jiang et al. 2014; Tian, Liu, Cheng, et al. 2014). In this study, we focus on fabrication strategies that rely on inorganic phosphorous sources. The flammable and noxious natures of organic phosphorous sources have hampered the development of methods using them. However, implementing inorganic and elemental phosphorous sources has resulted in the progress of multiple eco-friendly fabrication strategies. Sun et al. fabricated CoP on carbon cloth (CC) using phosphorization in a porcelain boat at 300 °C for 60 min in a static Ar atmosphere (Tian, Liu, Asiri, et al. 2014). They also electrodeposited nanosheet arrays of α-$Co(OH)_2$ on a Ti plate at room temperature followed by phosphorization in a porcelain boat with $Na_2H_2PO_2$ at 300 °C for one hour (Pu et al. 2014). The merit of growing nanostructure arrays on the current collectors such as carbon cloth (CC) is to prevent using a polymer binder, while TMP arrays remain well-retained and coupled tightly with the electrode (Tian, Liu, Asiri, et al. 2014).

1.2.1. Solution-Phase Reaction Methods

This fabrication method usually proceeds in highly boiling point solvents, including 1-octadecene and oleylamine at an elevated reaction temperature of approximately 300°C to cleave strong C-P bonds in organophosphorous such as trioctylphosphine (TOP), or triphenylphosphine (TPP) and their analogs as phosphorous sources (M. Sun et al. 2016a). For instance, metal acetylacetonates as the metal precursor participate in a reaction with TOP (P. Xiao, Chen, and Wang 2015), given by the following chemical formula:

$$(C_8H_{17})_3P + M(AcetylAcetonate)_2 \rightarrow MP_x \qquad (6)$$

After cleaving C-P bonds at high temperatures, the phosphorous atoms can coordinate with metal atoms to create metal phosphides. This reaction route can end up producing well-defined crystalline and nanostructured 3d, 4d, and 5d transition metal phosphides (Callejas et al. 2016b).

One of the early studies to prepare TMPs through the solution-phase method reported the formation of single crystalline Ni_2P nanowires, in which the ratio of TOP to oleic acid controlled the formation of one-dimensional nanowires (Y. Chen et al. 2009). For instance, the preparation of Ni_2P nanoparticles supported on SiO_2 through a reaction between $Ni(AcetylAcetonate)_2$ and trioctylphosphine resulted in the formation of a uniform particle size distribution and the efficient evolution of H species relating to a facile transfer of H species from nickel sites to the support (K. Yan et al. 2015). Henkes et al. also reported a solution-mediated reaction involving TOP and preformed transition metal nanoparticles as precursors (Amanda E. Henkes, Yolanda Vasquez, and Schaak 2007). They produced a broad range of transition metal phosphides, including Ni_2P, Rh_2P, Au_2P_3, PtP_2, and PdP_2, and could tune size, size disparity, and hollow sphere formation by controlling the parameters of the metal nanoparticle precursors. Stern et al. prepared highly uniformly distributed Ni_2P nanowires by heating $Ni(AcetylAcetonate)_2$ in a solution containing Oleic acid, trioctylamine, and tri-n-octylphosphine (Stern et al. 2015). They compared the catalytic activity of Ni_2P in the two structures of nanowires and nanoparticles, which was synthesized through a simple thermal reaction of NaH_2PO_2 and $NiCl_2.6H_2O$. They found that the nanoparticles exhibited lower overpotentials at the same loading quantity on the carbon substrate. Therefore, the characteristics of TMPs can be controlled by tailoring organic solvents, the molar ratio of metal to phosphorous, and the reaction temperature. This method requires rigorous control of the reaction condition and continuous purge of inert gas to prevent leakage of flammable gases (Y. Chen et al. 2009).

On the other hand, electrodeposition is an eco-friendly method that will not release highly toxic substances into the environment. In this approach, a thin film of Ni is fabricated using the electrodeposition method from ethylene glycol/choline chloride (EG/ChCl), and then is

phosphorized into Ni-P using organic phosphorous solution (Lu et al. 2013). A crystalline/amorphous Co/CoP film is also prepared on Ni foam using one-step electrodeposition at ambient conditions (Bai et al. 2016). The obtained Co-P film shows catalytic activity and strong bonding with the substrate resembling low interface resistance and intensified H evolution. The constraints of this method are its limited applications to specific Ni-P and Co-P compositions and the lack of uniformity of the deposited metal phosphides, while their structures are also amorphous [38]. Recently, the electrodeposition process has been utilized to fabricate nanocomposite of NiP_x/TNAs. The NiP_x/TNAs composites show superior electrocatalysts activity toward HER due to enhanced electrocatalytic active sites from amorphous NiP_x. Figure 1.2 illustrates the performance and preparation steps for NiP_x/TNAs nanocomposite electrocatalysts. TEM and HRTEM images of the sample are shown in Figure 1.2. The lattice spacing of 0.35 nm relates to the anatase titanium oxide phase with (101) plane, while a low quantity of NiP_x crystal phase is detected. The detailed elemental distribution of NiP_x/TNAs nanocomposites is shown by EDS analyses of participating elements (Gao et al. 2021a).

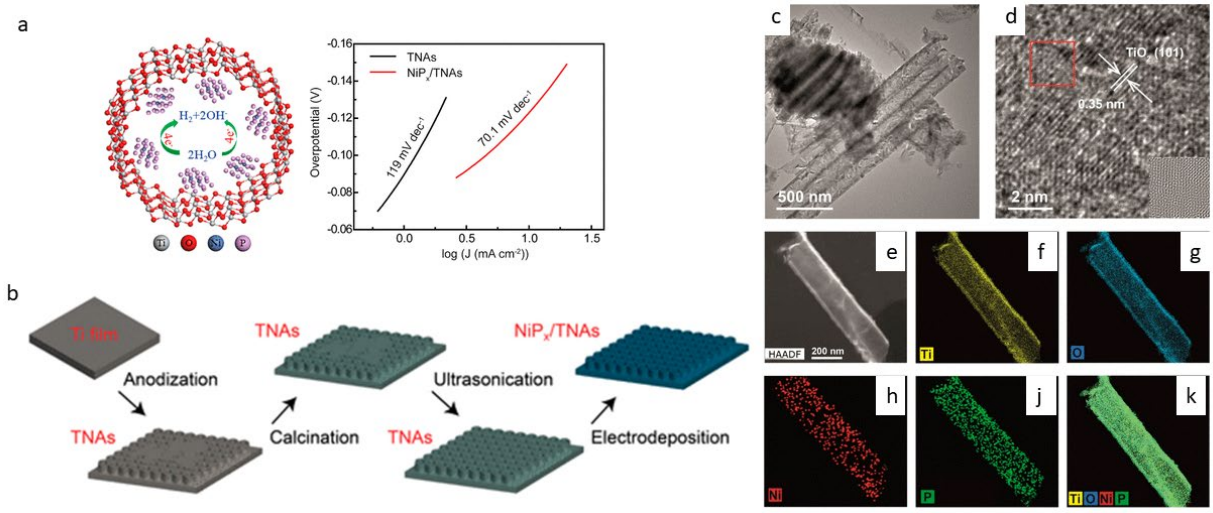

Figure 1-2: (a) Illustration of the participating element in the prepared catalysts and the performance of the catalysts. (b) Schematic process of the NiP_x/TNAs preparation steps. (c,d) TEM and HRTEM images of NiP_x/TNAs nanocomposites. (e-k) EDS mapping profiles of participating elements in the NiP_x/TNAs nanocomposits (Gao et al. 2021a). Reproduced with permission.

1.2.2. Gas-Phase Reaction Methods

Transition metal phosphides can be obtained after reaction between highly active phosphorous steam source and either metal vapor or nanostructured metal precursors at temperatures ranging from 300 to 900 °C, and the chemical formula can be expressed as MP_x. The adverse outcome can be the possibility of producing P-rich metal phosphides (i.e., CoP_3) and even some unstable metal phosphides (Callejas et al. 2016b). Besides, a much cautious approach needs to be taken at elevated temperatures to prevent the escape of noxious phosphorous source gases like phosphine, and the seal of the reaction furnace needs rigorous control. Metal hydroxides as the precursor and hypophosphite (NaH_2PO_2, $NH_4H_2PO_2$) as the phosphorous source can also be used in the reaction furnace at the upstream and at the downstream, respectively. At temperatures over 250 °C, PH_3 is released and reacts with the metal oxides to produce metal phosphides. Employing this strategy is

beneficial because the nanostructure morphology of metal oxides is most likely retained after reaction at a temperature of 300 °C for approximately two hours.

Plasma assisted synthesis of TMPs also shows promising results for catalytically producing oxygen and hydrogen. This finding has inspired researchers to perform many interesting studies benefiting from PH_3 plasma conditions to obtain NiFe-P, NiCo-P (H. Liang and Alshareef 2017). Low-temperature phosphorization of bimetallic metal-organic frameworks such as MOF-74 is an interesting method for controlling the synthesis of NiCo-P nanotubes as highly efficient electrocatalysts (L. Yan et al. 2017). Optimizing the molar ratio of Co/Ni atoms in the MOF structure could result in a variety of synthesized Co_xNi_yP catalysts. The produced nanotubes show good HER and OER catalytic performance in an alkaline electrolyte, offering a low overpotential of 129 mV for H_2 and 245 mV for O_2 productions at a current density of 10 mA/cm^2. In a recent study, a multicomponent reactive low-temperature plasma assisted simultaneous MOF decomposition and phosphorization, offering high chemical reactivity combined with low-temperature conditions, has been demonstrated (Guo et al. 2020). Ultrafine $Ni_{12}P_5$ nanoparticles encapsulated in a thin layer of N-doped carbon (NC) show a superior HER performance under a broad pH range. The crystal structure of Ni MOF-74, as shown in Figure 1.3, is grown on Ni foam (NF) through the solvothermal reaction. Plasma conversion is performed in a horizontal quartz tube furnace, as shown in Figure 1.3b. The temperature is maintained at 300 °C for evaporation of red phosphorous, and NH_3 and H_2 are introduced into the chamber. The plasma glow covers the entire hot zone where phosphorization of precursors takes place, and samples are treated with NH_3-plasma and H_2-plasma, respectively. The SEM images reveal a comparative illustration of two different structures of nickel phosphide that are well dispersed in their encapsulated situations. XRD patterns reveal two different phases of $Ni_{12}P_5$ and Ni_2P formed by NH_3-plasma and H_2-

plasma, respectively, indicating that the phase structure is affected strongly by the plasma. The measurement of *in situ* optical emission spectroscopy (OES) reveals the presence of PH radicals in both the plasma assisted situations, in which the PH radicals are the main precursors for phosphorization at low temperatures. The ultrafine $Ni_{12}P_5$ particles, encapsulated in N-doped carbon shells, successfully show a promising performance of the hydrogen evolution reaction in a broad pH range. The plasma assisted phosphorization method offers exciting opportunities to prepare various bimetallic phosphides.

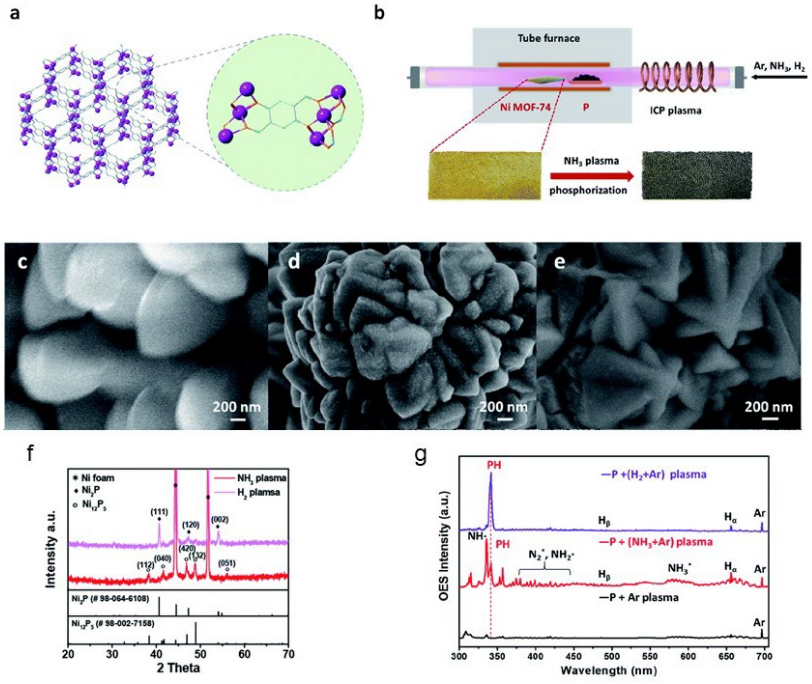

Figure 1-3: Multicomponent plasma conversion of MOF-74 to ultrafine nickel phosphide encapsulated in carbon layers. (a) Structural representation of Ni MOF-74 unit. (b) Schematic of the plasma-assisted phosphorization system with precursors. (c-e) SEM images of pristine Ni MOF-74, NH_3-plasma sample, and H_2-plasma sample, respectively. (f) XRD patterns for structural characterization of NH_3-plasma and H_2-plasma samples. (g) Optical emission spectra (OES) of P + (H_2+ Ar), P + (NH_3+ Ar) and P + Ar plasma (Guo et al. 2020). Reproduced with permission.

1.2.3. Other Novel Methods

In addition to the methods discussed in the previous section, novel strategies to synthesize transition metal phosphides, which are consistent with the environment, have been developed. For instance, using the nontoxic biomass phosphorous source has attracted significant interest. As an appealing phosphating reagent, phytic acid can quickly generate the phytic acid-metal cross-linked structure because of the intense affinity between its six phosphate groups and metal cations. The benefit of this method is the possibility of implementing large-scale production of transition metal phosphides. A nontoxic and facile method for synthesizing TMPs has been introduced by using phytic acid (PA) containing six phosphonic acid groups and obtained from plant sources (Pu et al. 2017). Pu et al. have used PA for pyrolysis of metal salts in combination with melamine as precursors to fabricate a series of TMPs encapsulated in N,P-codoped carbon (NPC) such as Ni_2P NPs@NPC, FeP NPs@NPC. They report that the encapsulation method enhances the catalytic activity in a broad range of pH. The environmentally friendly, cost-effective fabrication strategy of using PA opens up an avenue to prepare TMPs in large-scale production.

Recently, carbon derived from pinecones, in combination with ultrasound (US) and microwave (MW) techniques, have been used to anchor CoP and enhance the associated electrocatalytic activity (Zuliani et al. 2021). US/MW assisted techniques have been developed significantly for the synthesis of electrocatalysts (Hülsey, Lim, and Yan 2020). The benefits of preparation of TMPs from these techniques are due to the following: (i) direct transfer of energy to the proceeding reaction instead of applying heat, (ii) rate of conversion reactions are independent of applied heat, (iii) feasibility to apply heat in greater rates compared to the routine process, (iv) feasibility of using material-selective heating, and obtaining volumetric, and local heats (Cova et al. 2018; Zuliani, Muñoz-Batista, and Luque 2018). Zuliani et al. demonstrated the

feasibility of preparing active CoP catalysts through conversion of biomass using MW and US techniques (Figure 1.4).

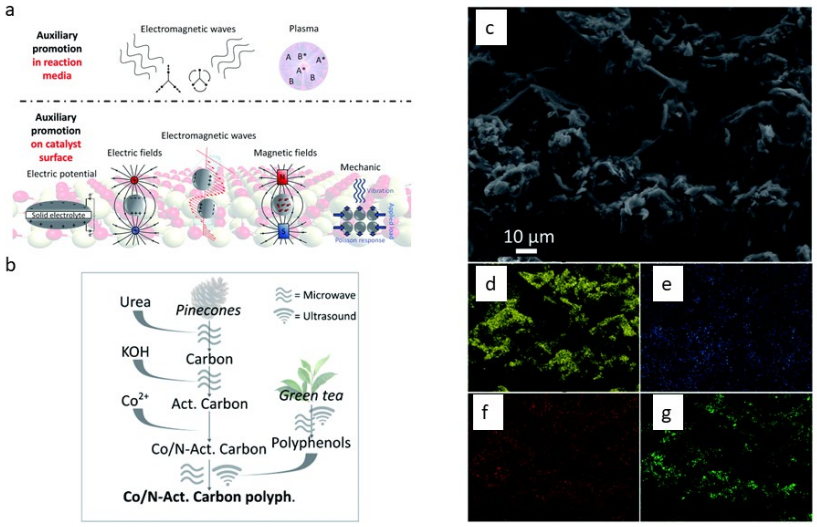

Figure 1-4: (a) An overview of techniques used for promoting reaction in the media or on the catalyst surface (Hülsey, Lim, and Yan 2020), (b) Schematic representation of the preparation of low quantity cobalt catalysts, (c) SEM-EDS images with mapping analysis of (a) Cobalt catalysts in N-doped forms, (d-g) demonstration of the presence of carbon, cobalt, nitrogen, and oxygen, respectively (Zuliani et al. 2021). Reproduced with permission.

1.3. Earth Abundant Transition Metal Phosphides

Figure 1-5 illustrates the most frequently used transition metal phosphides. We focus on their synthesis strategy, crystal morphology, features, and electrocatalytic performance in order to highlight the importance of TMPs. The successful application of nickel phosphide (Ni_2P) nanoparticles and their excellent stability in acidic solutions confirms the use of TMPs for electrocatalytic HER to produce H_2(g) with nearly faradaic yield (Yang Li, Dong, and Jiao 2020a). Recent investigations also confirm that TMPs can be employed as highly efficient catalysts in OER (Ryu et al. 2015; Doan-Nguyen et al. 2015), thereby broadening their applications to water

electrolyzers (Ledendecker et al. 2015), metal-air batteries (Qin et al. 2019), and fuel cells (Yuan Lv et al. 2018).

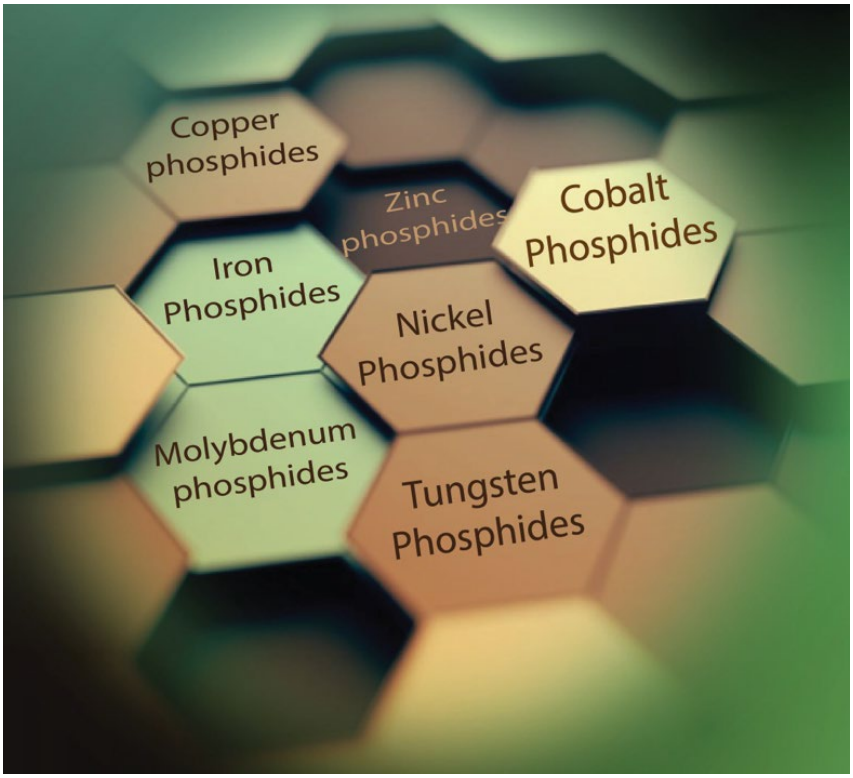

Figure 1-5: Frequently used transition metal phosphides as electrocatalysts

Covering a complete spectrum of TMPs is beyond the scope of this study. Therefore, two representative case studies, namely Ni and Co phosphides, are discussed in the following sections. It is worth mentioning that TMPs show several crystal structures, similar to different phases and structures already reported for transition metal oxides (TMOs) by our group (C. V. Ramana et al. 2006; Ramana, Mauger, and Julien 2021). The polyhedral lattice-based crystals of these phosphides are shown in Figure 1.6.

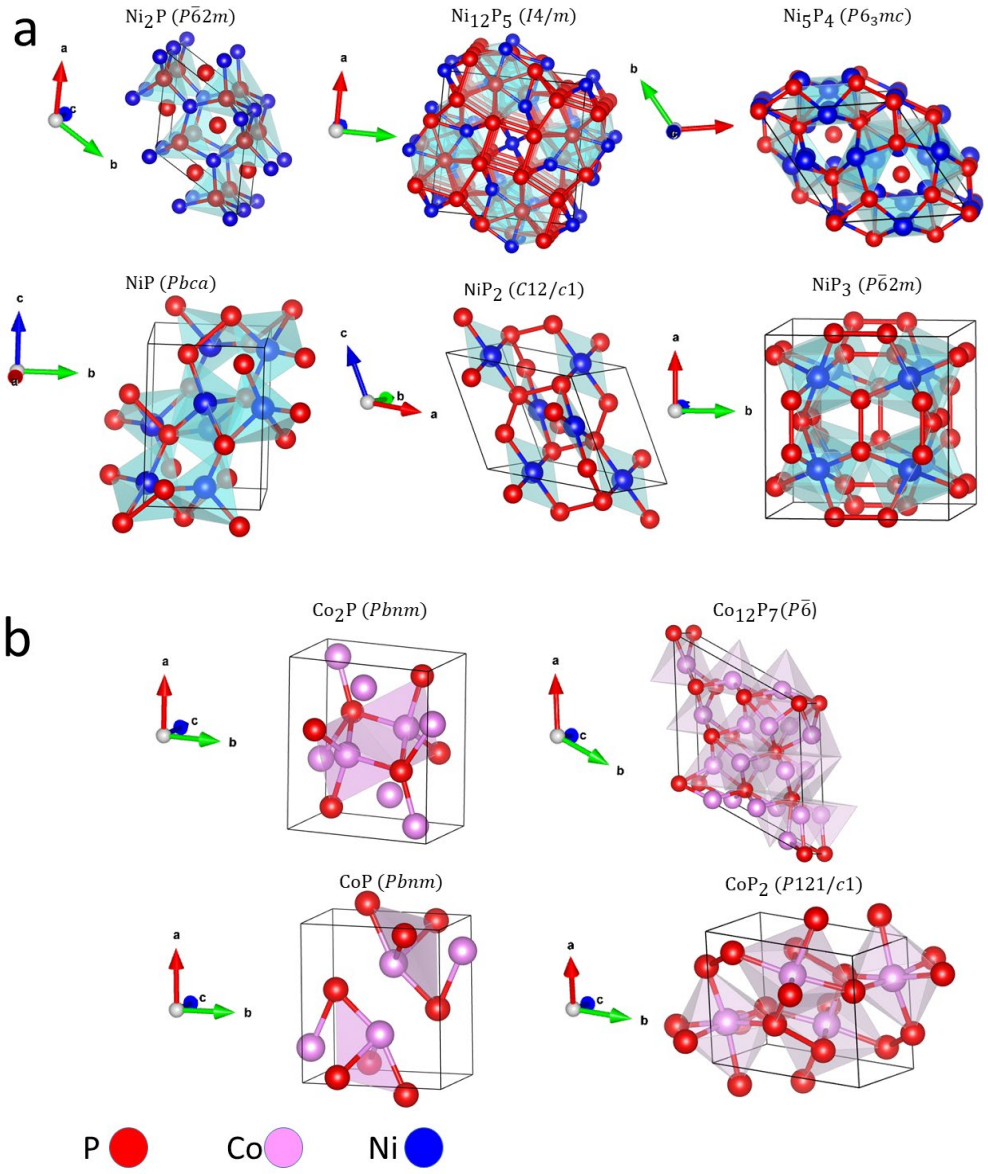

Figure 1-6: Selection of the most frequently used nickel phosphides and cobalt phosphides in their polyhedral lattice-based representation (Yang Li, Dong, and Jiao 2020b).

A minor change in metal/phosphorous stoichiometric ratio results in a noticeable variation in structures, and therefore, different physicochemical characteristics are presented. Higher electron conductivity, chemical stability, and thermal resistivity are observed in these structures. The favorable physicochemical properties of TMPs can be tested by changing composition and structure.

1.3.1. Cobalt phosphides

Electrocatalysts derived from CoP-based electrodes demonstrate a bifunctional catalyst. High HER activity of CoP has been observed over a broad range of morphologies, grain sizes, and preparation methods. Examples include the following: single crystals of hollow CoP nanoparticles with multiple facets on Ti foils (Popczun et al. 2014), films of CoP synthesized by cathodic deposition (Saadi et al. 2014), CoP particles on carbon cloth (Q. Li et al. 2014b) prepared using either reaction between pre-grown Co nanoparticles and octylphosphine, or phosphidation of cobalt oxide. The aforementioned HER-active CoP studies have been conducted on polycrystalline or multifaceted nanostructures. In contrast, no information on the proportion of different crystal facets with exposable and accessible sites has been provided. It can be added that cobalt phosphides do not show magnetic properties, unlike magnetic features in cobalt ferrite compounds (Puli, Adireddy, and Ramana 2015).

To better understand the reason for the high HER activity of CoP, Popczun et al. synthesized nanostructured CoP with multiple branches that were formed by nanorod protrusions of CoP single-crystals exposing significant density of accessible (111) facets (Popczun et al. 2015). They compared the HER performance of multifaceted CoP nanoparticles with branched CoP nanorods to evaluate the role of the morphology of transition metal phosphides. Due to lack of adequate stability, the branched CoP nanostructures showed lower HER activity compared to multifaceted CoP nanoparticles. The branched CoP nanostructures showed an overpotential of 117 mV for a current density of 20 mA/cm^2, while the multifaceted nanoparticles demonstrated a lower overpotential of 100 mV for the same current density. Therefore, despite both surface areas being mutually comparable, the multi-branched CoP nanostructures showed a lower HER activity than

the multifaceted CoP nanoparticles. The weak stability of the branched CoP nanostructures could be attributed to the poor adhesion of nanostructures to a Ti electrode surface.

Therefore, the importance of morphology or preparation method was opted out from bottlenecks about the high intrinsic activity of CoP-based catalysts. The general interest is to design nanoscale arrays to achieve better electrocatalytic performance and compete with the commercial Pt- and Ru/Ir-based catalysts. Two successful examples of engineered structures are ultrathin and holey nanosheets of CoP, as they facilitate significant HER activity due to the high surface area and super hydrophilicity at the surface (Chang et al. 2016; Z. Fang et al. 2018). Dang et al. integrated modified ultrathin and three-dimensional (3D) holey nanostructures to produce CoP phase on the carbon cloth (CC) as a bifunctional electrocatalyst for HER at 0-14 pH values and OER in an alkaline environment (Dang et al. 2019). Figure 1.7a shows the XRD characterization of the orthorhombic CoP phase and the scanning electron microscopy (SEM) images of uniformly deposited ultrathin cobalt hydroxide nanosheets (Figure 1.7b-d), while it is apparent that the earlier morphology is most likely retained after phosphidation at 300 °C for vertically grown nanosheets of CoP phases (Figure 1.7e-g). Promising electrocatalytic activity of CoP reflects the importance of the synergistic effects of 3D electrochemically grown structure facilitating the exit of gas bubbles and greatly improved effective electrolyte diffusion. Their work leads to an avenue for preparing binder-free HER electrodes in the prospect of renewable energy.

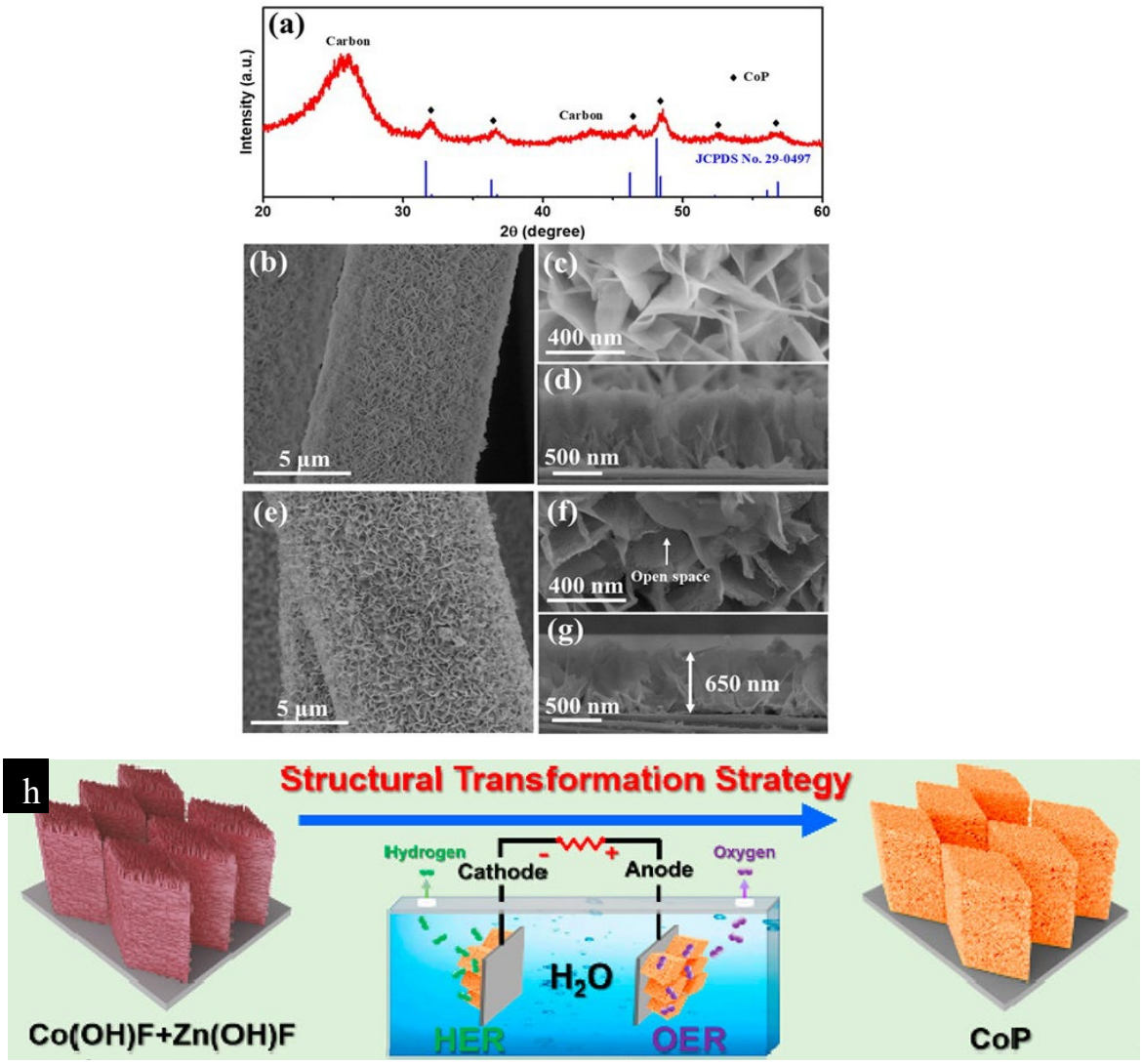

Figure 1-7: (a) XRD analysis of CoP supported on CC. (b-d) SEM images of cobalt hydroxide supported on CC. (e-g) SEM images of CoP supported on CC (Dang et al. 2019). (h) Schematic representation of the structural transformation of cobalt hydroxides to cobalt phosphides (Cao et al. 2020). Reproduced with permission from the American Chemical Society (ACS).

To produce 3D CoP porous structure, Cao et al. conducted a controllable structural transformation strategy on the phosphatized Ni foam (Cao et al. 2020). Removing the Zn-based compounds by alkali etching left porous Co-based compound arrays with nanoflake hierarchical structures. CoP arrays formed through the phosphorization process using $NaH_2PO_2.H_2O$ as the P

source. Figure 1.7h shows a schematic of the structural transformation steps. The prepared CoP@NF electrode showed excellent bifunctional electrocatalytic activity for both HER and OER in alkaline electrolytes. The enhanced performance could be ascribed to the presence of large, exposed surface areas with abundant active sites. The unique morphology of CoP promoted fast gas release and electrolyte diffusion for modified kinetics of the catalyst. A recent study also reported an innovative synthesis of Fe-doped CoP nanosheets (NS) using an etching-coordination method, inspired by the merit of the two-dimensional NS, heteroatom doping, and defective structure (T. Chen et al. 2021a). The catalysts demonstrated a large number of exposable active sites due to the unique topography of the two-dimensional NS structure. The doping of Fe element influenced the regulation of electron structure between Co and P.

The combination of doping with foreign elements and improving the morphology through engineered nanostructures will increase the intrinsic activity of each site and the number of active sites on a given electrocatalyst synergistically. Besides, one of the main challenges during the fabrication of cobalt phosphides is to prohibit preparation at elevated temperatures where agglomeration of phosphides hinders the mass and charge diffusion channels and diminishes the number of active sites (Vesborg, Seger, and Chorkendorff 2015). For this purpose, Han et al. fabricated Mo-doped porous CoP nanosheets supported by nickel foam, in which synthesizing porous nanostructures was originated from removing Al from CoMo(Al)-P (Han et al. 2019). The prepared nanocrystalline material was composed of $Co_{0.76}Mo_{0.24}P$ with an average particle size of 4.11 nm. The modification occurred on the electrocatalyst because the impingement of Mo^{6+} and Al^{3+} led to greater dispersion of Co^{2+} in its hydroxide precursors and inhibited the formation of agglomerated CoP nanocrystals during phosphorization at elevated temperatures. Besides, the incorporation of Mo into CoP modified the electronic structure and augmented the catalytic

activity by increasing the electrochemically active surface area and decreasing the resistance of the interface between catalysts and solution (Han et al. 2019). Jiang et al. also fabricated electrocatalysts consisting of CoMoP heterogeneous nanosheet arrays that were decorated with plenty of tiny CoP_3 nanoparticles (D. Jiang et al. 2019). A tremendous effort was taken to form bimetal phosphides, with the aim to weaken the H bonds on P active sites. However, the modification on anion sites may cause a stronger effect on HER activity than interring the metal for cation sites because the active sites of TMPs for HER is P. For instance, N doping at the P sites of CoP_2 supported on porous carbon cloth (PCC) showed a modified HER activity (L. Wang et al. 2019). It was realized that the N doping in the anion sites could ease not only the electron transit but also decrease the Gibbs free energy of hydrogen adsorption (ΔG_{H*}) on both Co and P sites, which ended up improving HER activity. Successful incorporation of a trace amount (<1%) of sulfur into Co_2P as a doping anion also caused modification of HER/OER catalyst activity (Anjum et al. 2018). Fabrication of N-doped Co_2P nanorod arrays, supported by carbon cloth, using a hydrothermal method confirmed enhanced electrical conductivity, increased exposure of active site number after N doping for all pH values (Men et al. 2019). Chen et al. also reported the fabrication of Fe-doped CoP that was inspired by the defective structure of 2D nanosheets and used an innovative approach of an etching-coordination strategy to prepare support for the catalysts (T. Chen et al. 2021b).

1.3.2. Nickel phosphides

A significant amount of research has been performed on nickel phosphide electrocatalysts, in which composition, morphology, and microstructures were controlled to obtain superior HER catalytic activity and stability in acidic and alkaline conditions. The performance of nickel

phosphides is primarily influenced by the P/Ni ratio (Popczun et al. 2013b; Pan et al. 2014; A. B. Laursen et al. 2015). Pan et al. reported a higher catalytic activity for the nanocrystals of Ni_5P_4 than the nanocrystals of $Ni_{12}P_5$ and Ni_2P (Pan et al. 2014). They ascribed the superior catalytic activity of Ni_5P_4 to the higher positive charge of Ni and a more substantial ensemble effect of P in nanocrystals of Ni_5P_4 (Rodriguez 2005). The ensemble effect is recognized in which the negatively charged P reduces the affinity between M-H bonds and facilitates the quicker release of H_2 gas during desorption (Du et al. 2017). Nickel phosphides could form in several phases, including Ni_3P, Ni_5P_2, $Ni_{12}P_5$, Ni_2P, and Ni_5P_4 (Anders B. Laursen et al. 2018; Chung et al. 2016; A. B. Laursen et al. 2015; Pan et al. 2014). Laursen et al. worked on the HER activity and electrochemical stability of Ni_3P, whose phosphorous content is the lowest among the thermodynamically stable nickel phosphide phases (Anders B. Laursen et al. 2018). Their work confirmed that the pure crystalline phase of Ni_3P microparticles could show excellent HER activity (slightly lower than that of Ni_5P_4) with high corrosion resistance in both acidic and alkali solutions despite its low phosphorous content. Figure 1.8a shows the chronopotentiometry (CP) analysis of Ni_3P, Ni_5P_4 microparticle catalysts comparatively in acidic and alkali solutions during 16 h. The cyclic voltammetry (CV) analysis of Ni_3P, Ni_5P_4, and Pt in acidic and alkali conditions is shown in Figure 1.8b. It is apparent that the Ni_3P phase could show a catalyst activity close to Ni_5P_4. Figure 1.8c depicts the plot of current density vs. overpotential for Ni_3P phase in acidic and alkali conditions. Figure 1.8d illustrates a comparison between electrocatalyst performance metrics for Ni_3P and other state-of-the-art HER electrocatalysts in acidic conditions. These results confirm the high intrinsic activity of Ni_3P microparticles and the excellent corrosion tolerance under reduction conditions for both acidic and alkali. Due to the added effect of ionic Ni-P bonding, this extra bonding for the case of Ni_3P causes a larger heat of formation and greater corrosion resistance.

The boosted stability of Ni_3P compared to Ni(s) can be quantified by the heat of formation of Ni_3P ($\Delta H_f = -220\ kJ/mol$) vs Ni(s) ($\Delta H_f = 0\ kJ/mol$). As P content rises for Ni_3P, Ni_5P_2, and Ni_2P, the per-atom stability stays relatively constant. The authors deduced that the change in the bonding configurations of the Ni_3-hollow could be attributed to the structural difference between the Ni-rich structure of Ni_3P and the P-rich structure of Ni_2P and Ni_5P_4, which influences ΔG_H of phases and the HER activity of catalysts (Anders B. Laursen et al. 2018).

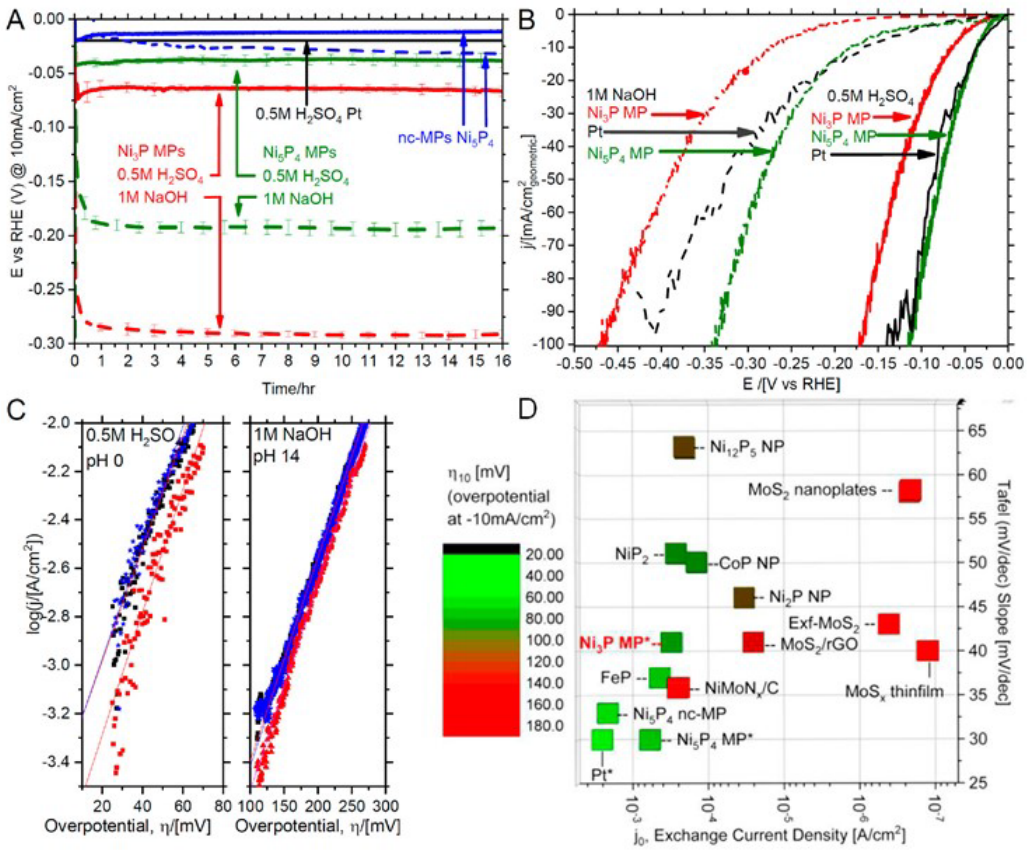

Figure 1-8: Chronopotentiometry of different electrodes in acidic and alkali condition, (b) Cyclic voltammetry of different electrode compositions in acidic and alkali condition at a scan rate of 1 mV/s, (c) Tafel plots of Ni_3P at acidic and alkali conditions, (d) Comparison of three electrocatalyst performance for different electrode materials (Anders B. Laursen et al. 2018). Reproduced with permission from American Chemical Society (ACS).

The general understanding is that the HER activity of nickel phosphides increases with the P/Ni ratio, while the work by Laursen et al. showed an exception. The relation between HER activity and the P extent has been described by the ensemble effect (Rodriguez 2005) or ligand effect (Ping Liu et al. 2005) between Ni and P. Similar to HER activity, tolerance against degradation can also be related to the P/Ni ratio, where the increasing ratio implies the formation of insoluble nickel phosphides in acidic condition (Pan et al. 2014). An innovative study of one-step TMP fabrication presents electrodeposition of highly stable nickel phosphide phases followed by a selective leaching process (Kim et al. 2019). In this study, the additional deposited metallic Ni is dissolved at positive potentials; the nickel phosphides are stable. The porous structures remaining after leaching metallic nickel result in more extensive surface contact for the intensified HER activity.

The application of bimetallic phosphides on the self-supported porous NiCuC foil represents an efficient HER performance (Yu et al. 2019). The porous Ni-Cu alloy template is prepared in association with graphite carbon using the powder metallurgy method, where the direct phosphorization at 300 °C produces a hierarchical porous structure of Ni_2P-Cu_3P@NICuC catalyst. The prepared catalyst consists of laterally grown Ni_2P aggregates with plenty of vertically attached small particles of Cu_3P, providing significant surface contacts and remarkable interaction in the system synergistically. The bimetallic phosphides are obtained with substantial control over the phase composition because of the porous structure of the Ni-Cu template and controlling Ni/Cu ratio using various quantities of both precursors (Yu et al. 2019). Recently, a super hydrophilic hierarchical bimetallic phosphide of Ni_2P-CuP_2 has been prepared on Ni-foam and graphene carbon nanotubes (CNTs) heterostructure using metallic electrodeposition followed by phosphorization (Riyajuddin et al. 2021). The porous chrysanthemum-flower-like heterostructure

provides significant superhydrophilic surface area for HER activity. Figure 1.9a shows the schematic representation of fabrication steps of bimetallic phosphide Ni_2P-CuP_2 on top of Ni-Gr-CNTs. It illustrates the deposition steps of Ni and Cu during the preparation of electrocatalysts. XRD patterns also confirm the formation of both phosphide phases on the CNT matrix. The detailed analyses of phases and structural configuration of the prepared catalysts are conducted by X-ray diffraction (XRD) shown in Figure 1.10 b.

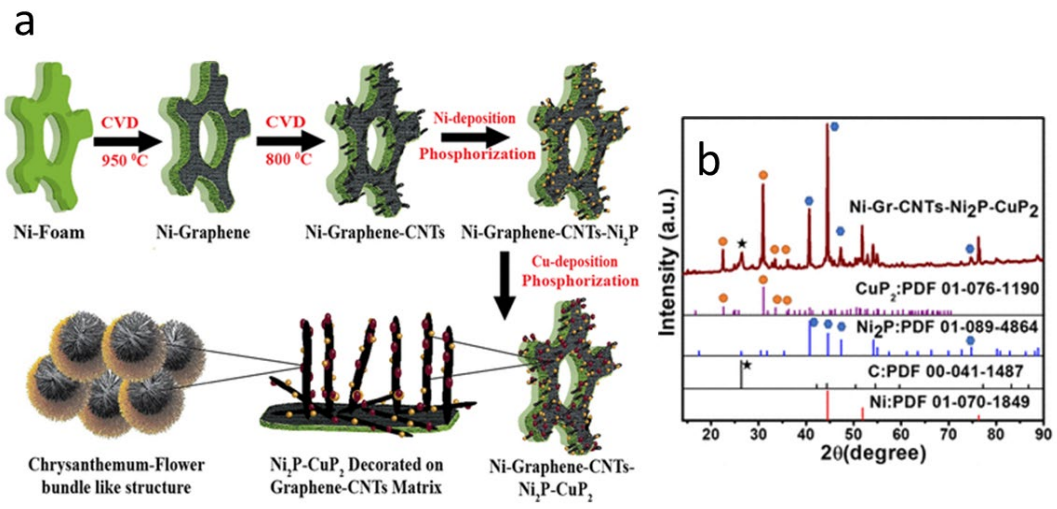

Figure 1-9: (a) Schematic illustration of the preparation path of the chrysanthemum-flower-like bundles of hierarchical bimetallic phosphide catalysts. (b) XRD pattern of Ni-Gr-CNTs-Ni2P-CuP2 (Riyajuddin et al. 2021). Reproduced with permission from the American Chemical Society (ACS).

Heterogeneous 3D-graphene on top of the 3D configuration of Ni foam boosts the feasibility of increased surface area for catalytic activity as illustrated in Figures 10 a, and b. Using CNTs with the random distribution provides a highly porous network, in which intertwined and interconnected branches facilitate passivation of the electrolyte ion diffusion, generating tunnels with high conductivity for electron transfer and facilitating modified electrode support. After electrodeposition of Ni uniformly on the CNT matrix, the anchored Ni_2P phases on the CNT bundles are generated using phosphorization, thereby forming a 3D porous Ni-Gr-CNTs-Ni_2P heterostructure (as shown in Figure 1.10 d). To further enhance the HER activity, CuP_2 is also

added to the system through electroplating Cu followed by phosphorization, as shown in Figure 1.10 e. The zoomed-in view shown in Figure 1.10 f illustrates the morphology of the bimetallic phosphide of Ni-Gr-CNTs-Ni_2P-CuP_2 resembling a chrysanthemum-flower-bundle-like structure where bundle size varies from 1 to 3 µm. The stability of the catalysts is confirmed by a chronoamperometry test at a cell voltage of 1.45 V, where Figure 1.10m illustrates that the catalysts can be maintained for at least for 40 hours with a negligible deviation of 3% from the current density. This result confirms the excellent and robust electrocatalytic performance for overall water splitting.

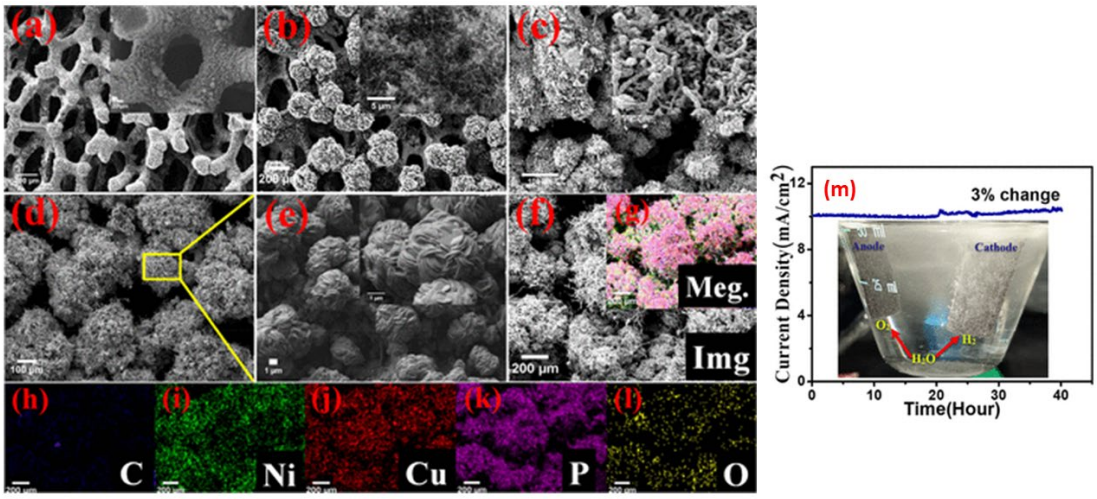

Figure 1-10: (a) SEM images of graphene deposited on nickel foam uniformly in which all areas are covered homogeneously, (b) A dense CNTs bundle on the graphene, where the inset confirms the random orientation and intertwining to each other, (c) Ni-Gr-CNTs-Ni2P heterostructure (NGCN), where Ni2P rods are anchored over CNT bundles. (d) Presence of Ni2P and CuP2 heterostructure on the Ni-Gr-CNTs matrix, (e) High-resolution image of Ni-Gr-CNTs- Ni2P-CuP2 heterostructure, with the chrysanthemum-flower-like structure. (h-i) EDS elemental mapping for the shown structure. (m) The choroamperometric study of stability at an applied voltage of 1.45 V in alkaline solution (Riyajuddin et al. 2021). Reproduced with permission.

The traditional fabrication techniques are strenuous and render a random distribution of nickel phosphides all over the electrode, thereby weakening the connection between the catalysts

and the current collector. Therefore, switching to novel, facile, and eco-friendly strategies for HER fabrication is desirable because they provide a high-surface-area current collector and immobilized earth-rich HER catalysts. The crucial concern is to optimize the interfacial contacts between nickel phosphides and electrode substrate to augment catalytic activity. For that purpose, the direct growth of nickel phosphides on the substrate, known as binder-free methods, has gained significant attention among researchers (Pu, Liu, Tang, et al. 2014; You et al. 2015). Recently, one-step synthesis of NiP_x electrocatalysts without subsequent phosphorization at elevated temperature has been reported by Gao et al. on TiO_2 nanotube arrays (Gao et al. 2021). First, the vertically aligned TiO_2 nanotube arrays are prepared by anodic dissolution. Then, the well-ordered nanotubes are used for co-deposition of nickel and phosphorous to provide a high-contact surface area and boost catalytic activity. This geometry provides an efficient charge transfer and significant capability for mass transport of hydrogen gas during electrocatalysis(Gao et al. 2021).

Chapter 2: Nature-Inspired Design of Nano-Architecture-Aligned Ni_5P_4-Ni_2P/NiS Arrays for Enhanced Electrocatalytic Activity of Hydrogen Evolution Reaction (HER)

2.1. INTRODUCTION

The skyrocketing demand for renewable energy and the aggravation of global warming with its ominous impact on climate change emphasizes the importance of research and development activities for clean and sustainable energy conversion systems.(de Luna et al. 2019) The nascent hydrogen (H_2) utilization economy is gaining popularity because of promising advances in employing state-of-the-art electrocatalysts for water splitting, reliable storage technologies, and efficient hydrogen consumption in fuel cells. The hydrogen evolution reaction (HER) is exceedingly constrained by a large dynamic overpotential beyond its thermodynamic potential during the cathodic half-reaction of water splitting.(Anantharaj et al. 2021) So far, efficient electrocatalysts derived from platinum (Pt) group metals (PGM) have shown slight overpotentials in a broad pH range of electrolytes, while their utilization on a large scale is limited due to the scarcity and their high cost.(H. Yin et al. 2015) Therefore, the paramount challenge is to explore novel methods for synthesizing low-cost and highly active electrocatalysts with high durability and relatively low overpotentials that can be substituted with PGM catalysts.(M. Sun et al. 2016b) Transition metal phosphides (TMPs) with metalloid compounds demonstrate widespread utilization for promoting the HER due to outstanding characteristics such as high durability, intrinsic catalytic activity, and good electrical connectivity.(M. Sun et al. 2016; Tang et al. 2017; Tingting Liu et al. 2017) Several strategies have been offered to develop high-performance electrocatalysts. These strategies can be categorized as enhancing the intrinsic activity of individual catalytic sites,(Cabán-Acevedo et al. 2015; W. Liu et al. 2016) increasing the population of active catalytic sites,(Z. Wu et al. 2017) fabricating seamless and 3D nanoarchitecture with highly conductive electrocatalysts,(Bae et al. 2017) and developing intermediate phases with suitable specific adsorption/desorption energy.(Zhang et al. 2020; Ye et al. 2016) While numerous modifications were implemented to the structure, composition, and synthesizing methods of TMPs

to develop versatile catalysts,(Attarzadeh, Nuggehalli, and Ramana 2022) finding alternatives for PGM catalysts demands substantial progress to fulfill the requirements for sustainable hydrogen production. Furthermore, in the context of advancements to be made, a detailed fundamental understanding of the materials is the key, and strategies, especially those that we see routinely and last long enough in nature, must be adopted to design and unlock the potential of electrocatalysts.

For transition metal phosphides, the consensus is that P centers in P-terminated surfaces of metal phosphide structures are negatively charged due to the induced polarization. Therefore, it creates a greater affinity for the adsorption of H* species by trapping positive-charged protons and synergistically enhances hydrogen desorption during the electrolysis process.(Shi and Zhang 2016) Combining multiple anions is currently an emerging strategy resulting in the development of chemical complexity and structural alternation to augment overall water splitting.(Y. Liu et al. 2022) The primary motivation for utilizing two anions with the difference in electronegativity, ionization potential, and atomic radius is to increase the population of active sites by expanding the electrochemical active surface area (ECSA) and enhancing the intrinsic catalytic activity by reducing the adsorption-free energy of intermediate reactions owing to tuning the electronic structure, thereby strengthening the electrocatalytic activity.(Song et al. 2017; Luo et al. 2017; Dai et al. 2017) Further, the synergistic presence of P and S atoms retards the surface oxidation of sulfide/phosphide, increasing the catalysts' durability. For instance, introducing sulfur to the surface of the prepared MoP showed significant improvements in catalytic activity and stability.(Kibsgaard et al. 2014)

Introducing both P and S anions for developing ternary transition metal catalysts has drawn significant attention among researchers.(Chang et al. 2018; J. Wang et al. 2020; Q. Liang et al. 2019; L. Fang et al. 2021; Z. Wu et al. 2017) Attention is primarily given to employing different synthesis methods, typically resulting in catalysts with various ratios of phosphide to sulfide and some degree of control over surface morphology. Luo et al. reported the preparation of three-dimensional $NiP_{0.62}S_{0.38}$ using sequential sulfidation and phosphidation processes on a nickel foam at 300 and 500 ◦C for 1 and 2 h, respectively.(Luo et al. 2017) Recent studies target improving

catalytic activity by optimizing the surface electronic and energy of intermediates via growing epitaxial interfaces with two different components.(Q. Liang et al. 2019; Zhu et al. 2018; An et al. 2019) The $NiPS_3/Ni_2P$ heterojunction was constructed by *in situ* epitaxial growth of Ni_2P on 2D $NiPS_3$ sheets using a desulfurization process under a partial H_2 atmosphere, and the electrocatalyst electrodes were prepared using the drop cast method.(Q. Liang et al. 2019) Liang et al. indicated modification of the electronic features of the fabricated catalysts. This study revealed that the energy barrier for the HER at the $NiPS_3/Ni_2P$ heterojunction showed a significant drop. The authors realized that the H* affinity significantly reduced on the Ni centers. However, the current literature lacks a seamless electrocatalyst synthesized using a 3D nanoarchitecture with modified epitaxial growth and heterointerfaces structures. This approach may result in an accelerated electron transfer due to a robust electronic interaction at the interface of epitaxial sheets.

Fascinated by the aforementioned scientific challenges, herein, we report highly efficient seamless electrocatalysts synthesized by a two-step chemical vapor process on ultrathin nickel meshes manufactured by electroplating into an etchable mask. The phosphidation of the nickel mesh creates vertically aligned Ni_5P_4-Ni_2P plates, which are used as template sites to synthesize the Ni_5P_4-Ni_2P/NiS (plates/nanosheets) 3D structures due to *in-situ* growth of epitaxial nanosheets and emerging abundant hetero-interfaces. We hypothesize that this modification optimizes the catalytic activity for hydrogen production. The epitaxial NiS nanosheets resemble prickly pear fruits thanks to their similarity in growing at the edges of their leaves. The electrochemical studies confirm that the growth of the epitaxial NiS nanosheets on the edges and steps of Ni_5P_4-Ni_2P plates reduces the overpotentials and the Tafel slopes, indicating a more significant number of active catalytic sites can be exposed to H^* species, and also the intrinsic catalytic activity is strengthened. The electrochemical impedance spectroscopy (EIS) results also confirm that the growth of NiS can modify the interaction with H^* species, and greater electron exchangeability prevails at interfaces. Furthermore, the prepared seamless architecture of the Ni_5P_4-Ni_2P/NiS 3D structure not only offers a broad surface area with abundant active sites for the hydrogen evolution reaction (HER) but also

facilitates hydrogen gas removal from the surface due to more significant spatial freedom compared to foam sheets.

2.2. EXPERIMENTAL METHODS

2.2.1. Synthesis

Preparation of porous nickel phosphide on nickel meshes: A piece of Ni mesh (1 cm × 2 cm, ~0.002 g, GOODFELLOW CAMBRIDGE Ltd.) was washed under ultrasonication in propanol and ethanol for 10 min to degrease and then rinsed with DI water and allowed to dry in an oven at 60℃. The Ni mesh features a thickness of 0.004 mm, a wireline width of 0.011 mm, and an open area of 60% (200 wire.cm^{-2}). Then, a quartz boat containing 0.2 g of red phosphorous powder (Sigma Aldrich, %99.99 pure) was covered partially by Ni mesh with keeping at 1 cm distance above the powders. After that, the boat and mesh together were placed gently inside the quartz tube of the MTI Corporation chemical vapor deposition (CVD) furnace. The tube furnace was kept under vacuum pumping, and Ar was also purged for 10 min at a flow rate of 200 SCCM to evacuate the air and replace it with Ar. The furnace was heated to 450 ℃ at 5 ℃ min^{-1}, kept at the final temperature for 1 h, and then cooled down to room temperature at the same rate while the Ar was purged continuously during the process at the flow rate of 10 SCCM.

The growth of the epitaxial NiS nanosheets at Ni_5P_4-Ni_2P plates: a quartz boat containing different sulfur powder shown in Table 2.1 with already prepared nickel phosphide structures was placed inside the furnace tube. The sulfidation process was followed according to the procedure shown in illustration 2.1.

2.2.2. Experimental design and motivations

The NiS crystals demonstrates that Ni^{2+} is bonded to six equivalent S^{2-} atoms to construct NiS_6 octahedra, where the tilt angle of the corner-sharing octahedrons is 50°and the Ni-S length bond is 2.37 Å, and S^{2-} is bonded in a 6-coordinate geometry to six equivalent Ni^{2+} atoms.

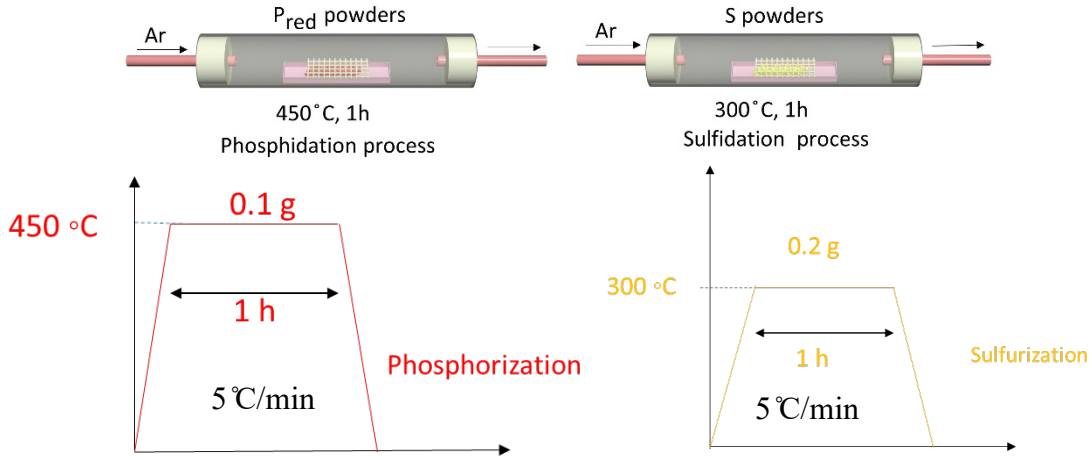

Illustration 2. 1. Schematic representation of preparation Nickel phosphor-sulfide and Schematic diagram of the phosphidation and sulfidation process

Table 2. 1. Ni-P-S electrocatalysts produced during phospho-sulfidation process of nickel.

Catalysts	P (g)	S (g)
NiP	0.2	0
NiS	0	0.1
NiPS1	0.2	0.1
NiPS2	0.2	0.15
NiPS3	0.2	0.2
NiPS4	0.1	0.1

2.2.3. Material Characterization

We utilized various analytical techniques to characterize the structure, phase, morphology and microstructure, and chemical composition of synthesized Ni-P-S materials. Scanning electron microscopy (SEM) images were collected using Hitachi S4800 by applying 10 kV and 15 µA. Transmission electron microscopy (TEM) images, energy-dispersive X-ray (EDX), and selected-area electron diffraction (SAED) patterns were collected using a Thermo Scientific (formerly FEI) Titan Themis 200 with an accelerator voltage of 200kV. X-ray diffraction (XRD) patterns were obtained using a Malvern Panalytical Empyrean Nano edition multipurpose X-ray diffractometer. To resolve peaks from the diffraction pattern, the step size and the integration time were 0.01 ̊and

0.85 s/step, respectively. A Cu Kα X-ray source with a wavelength of 0.154 nm was used to acquire the measurements. Rietveld refinement in Xpert highscore software was used to estimate the ratio of phases in the XRD pattern. X-ray photoelectron spectroscopic (XPS) scans of the best Ni-P-S electrocatalyst samples were obtained employing Kratos Axis Ultra DLD spectrometer using Al Kα monochromatic X-ray source (1486.6 eV) and a high-resolution hemispherical analyzer. The XPS survey and high-resolution scans were recorded, and the data obtained were analyzed with the help of CasaXPS software employing Gaussian/Lorentzian (GL(30)) line shape, line asymmetry, and Shirley background correction.

2.2.4. Electrochemical Characterization and Performance Evaluation

Hydrogen evolution reaction (HER) measurements were carried out on a Solartron analytical-ModuLab Xm workstation using a conventional three-electrode system with Ag/AgCl, a graphite rod (99.99%) as the reference electrode, and the counter electrode, respectively. The prepared electrocatalysts from ultrathin nickel mesh were working electrodes. The reference electrode was calibrated with respect to a reversible hydrogen electrode (RHE) before experiments. The electrolyte was 1.0 M H_2SO_4 aqueous solution made from DI water. The linear sweep voltammetry (LSV) was recorded at a scan rate of 5 mV s^{-1}. Before LSV measurement, the working electrode was kept at open circuit potential (OCP) for 15 min to reach a pseudo-Plato voltage. The electrochemical impedance spectroscopy (EIS) was collected using the same workstation at the applied overpotentials ranging from 100 to 450 mV. The amplitude was 5 mV, while the scan started from 100 kHz to 1 Hz. IR correction was performed to account for the cell resistance based on the EIS test at the open circuit potential (OCP). Cyclic voltammetry (CV) was performed at different scan rates ranging from 20 to 200 mV s^{-1} and at the non-Faradaic potential region. We prepared a Pt/C (20%) electrode using the conventional method. For that, 5 mg Pt/C (20%) was sonicated for 30 min in 1 ml solution of ethanol and Nafion (with the 9:1 ratio). We did drop-cast the prepared ink on the surface of a glassy carbon electrode. Then, the HER activity of the prepared

Pt/C electrode was evaluated in an identical condition that the synthesized ternary electrocatalysts were tested.

2.3. RESULTS AND DISCUSSION

2.3.1. Crystal Structure, Phase, Chemical Composition and Synthesis Process Optimization

The key to our successful synthesis of the Ni-P-S materials with desired morphology is the in-house designed chemical vapor deposition (CVD) chamber with a specific fabrication process schematically. The fabrication process results from direct reactions between Ni mesh and chemical vapors of phosphorous and sulfur at two temperatures of 450 and 300 ºC, respectively. The ultrathin Ni mesh is rationally selected to support a uniform transport of chemical vapors over the entire Ni mesh surface. The sufficient open-area of Ni mesh allows efficient chemical vapor infiltration through the mesh holes during the process, leading to a uniform phase alteration on both sides of the mesh. As a promising approach, nanodomain boundaries with two or three phases can be purposefully designed to enhance electronic interactions and increase active sites simultaneously. To emphasize the critical approach of the current study, the schematic illustration in Figure 2.2a displays the 3D nanoarchitecture of synthesized NiPS electrocatalysts. The schematics resemble the prickly pears cactus demonstrating the result of the phospho-sulfidation processes designed to improve the catalytic activity. The nickel phosphide phases, Ni_5P_4-Ni_2P, form as vertically aligned plates during the phosphidation process resembling leaves, and the NiS nanosheets resembling the prickly pear fruits form primarily at the edge of leaves during the sulfidation process. The key novelty in the designed strategy is to synthesize a ternary system with a 3D nanoarchitecture that provides abundant heterointerfaces and promising epitaxial NiS nanosheets. We hypothesize that the synthesized nanostructure can significantly improve the HER catalytic activity due to enhancing electronic interaction at the nanodomain scale and boundaries of different phases.

After completing the sulfidation process, we understand that a heteroepitaxial growth prevails between Ni_2P and NiS phases, where the involving planes in both crystal structures are shown in Figure 2.2b. Indeed, heteroepitaxy is a specific case of heterogeneous nucleation in which a peculiar crystallographic relationship prevails between substrate orientation and the growing crystals. Generally, a geometric match of the dimensions between the substrate and new crystals is considered the main criterion of epitaxial growth.(Marghussian 2015) In addition, the origin of the epitaxial growth can also be the structural features of the substrate crystal facets, where emerging kinks, steps, and dislocations may facilitate the epitaxial growth of a new crystalline phase.(Habelitz et al. 1999) The NiS crystallizes in the hexagonal $P6_3/mmc$ space group.(Halim et al. 2016) The involved phases of Ni_5P_4 and Ni_2P crystallize in the hexagonal $P6_3mc$ and $\bar{P}62m$ space groups, respectively. Beyond strengthening the electronic interaction, another aspect is the synergistic generation of heterointerfaces at the boundary of the Ni_2P and NiS phases, increasing exposure at the active catalytic sites, as illustrated schematically in Figure 2.2c. The 2D crystal structure of Ni_2P and NiS is shown in Figure 2.2d, where the generation of epitaxy with strong interfacial interaction led to an accelerated electron exchangeability.

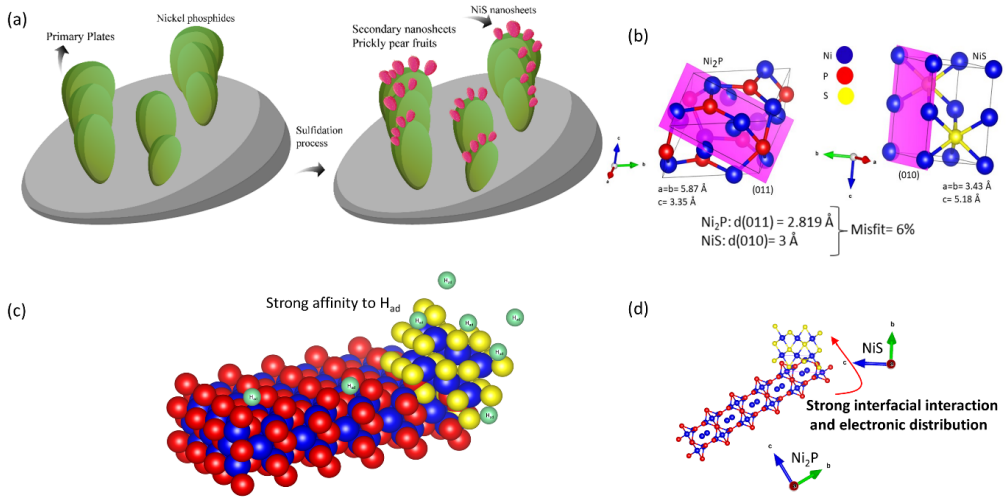

Figure 2-2: (a) Schematic illustration of prickly pear cactus for generation of the Ni5P4-Ni2P/NiS (plate/nanosheets) structures, (b) Ni2P and NiS crystal structures, (c) schematic illustration for enhanced hydrogen evolution at the newly grown NiS nanosheets, (d) schematic illustration for generation of the heterointerfaces, their synergistic interaction effects and the crystals connections between Ni2P and NiS. Blue, red, and yellow balls represent nickel, phosphor, and sulfur.

X-ray diffraction (XRD) examines the composition and crystal structure of phases formed during phospho-sulfidation. Figure 2.3 a-c shows the XRD patterns of pristine Ni mesh, nickel phosphide (NiP), and nickel sulfide (NiS) phases forming during the phosphidation and sulfidation processes. The XRD pattern for the ternary nickel phosphosulfide (NiPS3) is also shown in Figure 2.3d. After the phosphidation at 450 ◦C for 1 h, the XRD result in Figure 2.3b confirms the successful formation of two hexagonal nickel phosphide phases of Ni_5P_4 and Ni_2P, confirming previous reports by Wang et al.(X. Wang et al. 2015) Characteristic peaks and crystallographic planes corresponding to these nickel phosphides are illustrated. The development of characteristic diffraction peaks: crystalline planes at 15.1°: (010), 16.12°: (002), 22.12°: (012), 28.7°: (013), 30.3°: (020), 31.4°: (021), 34.5°: (022), 36.08°: (014), 41.36°: (121), 43.85°: (122), 45.16°: (024), 47°: (031), 47.8°: (123), 52.91°: (124), and 54°: (220) indicates the formation of Ni_5P_4 (ICDD 98-024-9340) phase. Further, the development of different characteristic diffraction peaks: crystalline planes at 30.3°: (110), 40.58°: (111), and 47°: (120) represents the formation of the Ni_2P (ICDD 98-064-6108) phase. These results are consistent with the nickel phosphide phases obtained from the phosphidation process of nickel foams.(X. Wang et al. 2015; S. Liu et al. 2019) The XRD pattern for the sulfurized mesh represents the formation of the hexagonal nickel sulfide phase of NiS, with some unreacted nickel remaining after the process (Figure 2.3c). The characteristic diffraction peaks: crystalline phases at 30.11°: (010), 34.48°: (011), 44.43°: (011), 53.57°: (110) are indicative of the NiS (ICDD 98-064-6340) phase. After performing the joint phosphidation and sulfidation processes consecutively, as shown in Figure 2.3. The XRD pattern in Figure 2.3d related to NiPS3 electrocatalyst reveals the formation of Ni_5P_4 and Ni_2P phases with strong diffraction peaks, while weak diffraction peaks can also be attributed to the NiS phase. Therefore, peaks corresponding to Ni_5P_4, Ni_2P, and NiS phases are assigned in the powder XRD pattern. Raising the heating temperature at the first step can change the formed nickel phosphides' crystal structure, surface morphology, and mechanical stability. We realize that the vertical Ni_5P_4-Ni_2P plates, used as templates for growing the NiS nanosheets, disappear after heating above 500 °C. The surface morphology alteration was also reported by Wang et al. in their study of various phases formed on

the nickel foam during the phosphidation process.(X. Wang et al. 2015) They found that the formation of different nickel phases via raising the heating temperature above 500 °C decreased HER electrocatalytic activities, while the surface morphology changed, and the brittleness of the foams increased. Likewise, we find out that the mechanical stability also drops significantly, where the durability of the catalysts formed at 450°C is significant during electrochemical experiments rather than those formed at 500 °C.

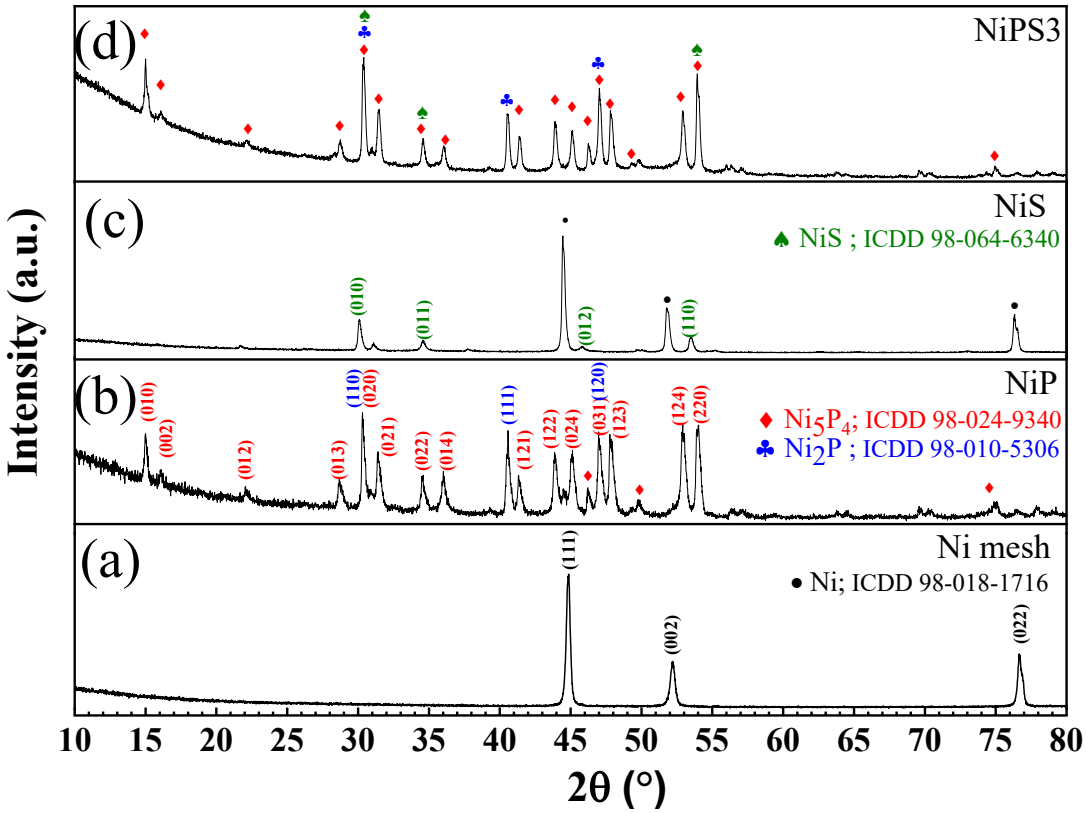

Figure 2-3: Powder XRD patterns for (a) Ni mesh, (b) Ni_5P_4-Ni_2P phases, (c) NiS, (d) heterostructure of Ni_5P_4-Ni_2P/NiS (plates/nanosheets)

To reveal detailed information about the formation of different phases, particularly NiS nanosheets, we perform X-ray photoelectron spectroscopy (XPS) on the NiPS3 electrocatalyst. Thus, the chemical state and molecular environment corresponding to the formed phases are characterized using the casaXPS software.(Ramana, Roy, et al. 2021; Ramana, Bandi, et al. 2021) The XPS survey spectrum in Figure 2.4a confirms the presence of Ni, P, and S. As shown in Figure 2.4b, the core level spectra of Ni $2p_{3/2}$ display a peak at 853.62 eV in the Ni 2p region,

corresponding well to the $Ni^{\delta+}$ species in Ni_5P_4. The high-resolution XPS spectrum of the Ni 2p signal for the NiPS3 catalyst containing Ni_5P_4, Ni_2P, and NiS phases indicates that nickel is primarily at the +3 valance state.(H. Sun et al. 2017). The appearance of the peaks at 857 and 875.42 eV are related to the Ni 2P satellite peaks. Further, the appearance of the peak at 862.76 eV in the Ni 2p spectrum of the heterostructure catalyst can be attributed to the formation of Ni-S species because of the epitaxial NiS nanosheets.(Z. Qin et al. 2016) The core level spectra of Ni $2p_{1/2}$ also display a peak at 870.9 eV. Regarding the core-level P 2p spectrum (Figure 2.4c), the first two peaks at 130 and 130.8 eV can be assigned to the P $2p_{3/2}$ and P $2p_{1/2}$, respectively. The peak at 134.2 eV can be ascribed to the P-O bond for forming $NiPO_4$ compounds, which is related to partial surface oxidation and agrees well with the previous study on transition metal phosphides.(H. Sun et al. 2017) Noticeably, we realize the peak emerging at 131.9 eV is related to the formation of P_4S_3 compounds due to the partial release of phosphorous during the sulfidation process at 300 ◦C and its combination with the present sulfur vapor at the surface. The narrow scan for the S 2p spectrum is deconvoluted to several peaks, shown in Figure 2.4d. Two peaks at 161.9 and 162.9 eV can be attributed to the S $2p_{3/2,}$ and S $2p_{1/2}$ orbitals of divalent sulfide ions (S^{2-}) in Ni-S, which agrees well with the NiS spectrum reported earlier.(Z. Qin et al. 2016) The peak at 164 eV can be ascribed to the formation of S_8 during the vapor deposition treatment.

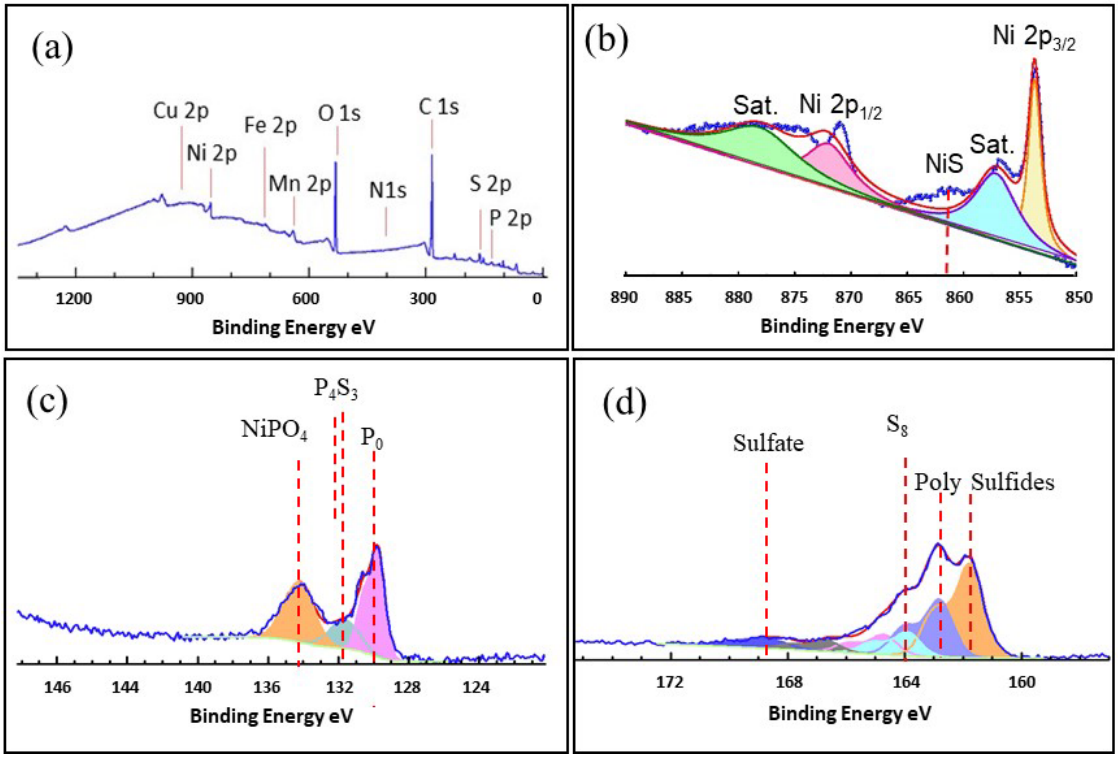

Figure 2-4: (a) the wide X-ray photoelectron survey for the prepared NiPS3 catalysts, (b) high-resolution Ni 2p, (c) P 2p, (d) S 2p XPS spectra of the heterostructure of Ni_5P_4-Ni_2P/NiS

2.3.2. Surface and Interface Morphology and Microstructure

The structure and surface morphology of the prepared catalysts are examined using scanning electron microscopy (SEM) and transition electron microscopy (TEM) to understand the effect of the sulfidation process. We realize that Ni_5P_4 and Ni_2P phases cover the entire mesh surface after the phosphidation process, while Ni_5P_4 is the dominant phase on the surface. As illustrated in Figure 2.5a, b, two surface features are noticeable, protrusions and vertically aligned plates, where protrusions encompass plates. Energy dispersive spectroscopy (EDS) analysis reveals that protrusions are Ni_5P_4 phases. A broad view of nickel mesh after the phosphidation process is shown in Figure 2.5a to illustrate the uniform distribution of plates and protrusions over the mesh surface. The magnified SEM image in Figure 2.5b reveals that the vertically aligned plates adopt several steps throughout the facet surface or at the edges, while the overall thickness stays approximately

below 100 nm. We postulate that these steps/shearlines form on the facets due to the extra strains derived from the synergistic presence of Ni_5P_4 and Ni_2P phases. Thus, these are called Ni_5P_4-Ni_2P plates to highlight the simultaneous presence of both phases. Furthermore, we envisage that these steps/shearlines work as preferential sites with a lower barrier energy for initiating the growth of the epitaxial NiS nanosheets.(Habelitz et al. 1999) As displayed in Figure 2.5c, d, the population of the NiS nanosheets is the highest for NiPS3 electrocatalysts. EDS analyses are performed for two regions of A and B, as depicted in Figure 2.5e, where A and B are rich and scarce in sulfur, respectively. The EDS analyses indicate the formation of nickel sulfide in region A, while nickel phosphide is the dominant phase in region B. The atomic ratio of P/Ni implies that Ni_5P_4 is the dominant phase in vertically aligned plates before and after the sulfidation process, verified by the XRD and Rietveld analyses earlier. The EDS analysis confirms the formation of Ni_5P_4 as a dominant phase in the protrusion feature areas. The NiS nanosheets appear at the edges of the plates resembling the prickly pear fruits (Figure 2.5e, f), and Ni_5P_4-Ni_2P plates represent the cactus leaves remarkably (Figure 2.5f). We discussed the formation of the prickly pear cactus in the schematic illustration shown in Figure 1a, where the primary nickel phosphide plates, Ni_5P_4-Ni_2P, form during the phosphidation process, and the NiS nanosheets form during the sulfidation process.

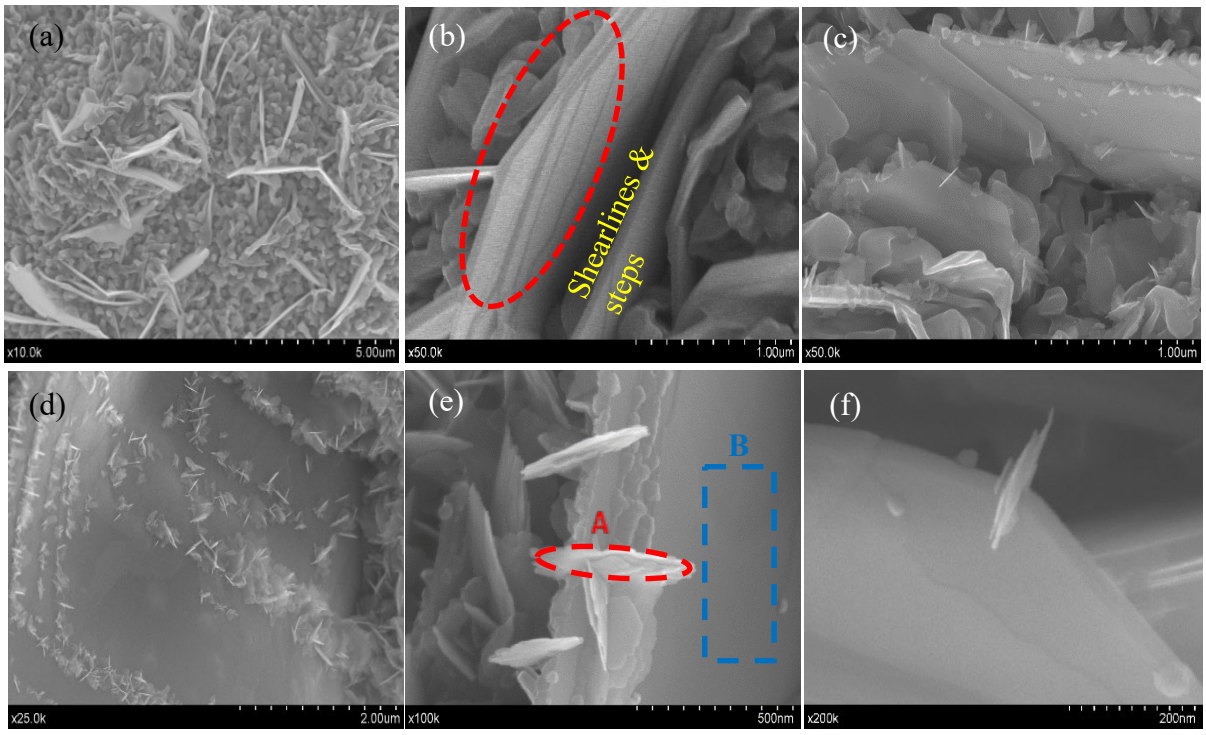

Figure 2-5: SEM images from (a, b) nickel phosphides, (c) NiPS1 catalyst, (d) NiPS3 catalyst, (e, f) high magnification images from NiS nanosheets growing at the edges

TEM images in Figure 2.6 remarkably demonstrate the nanostructure features appearing after the joint phospho-sulfidation process, where the NiS nanosheets start growing on the edge of Ni_5P_4-Ni_2P plates. The TEM image in Figure 2.6a shows a broad view of a nickel phosphide plate accompanied by nickel sulfide nanosheets. As shown in Figure 2.6b, e, the sulfidation process generates heterogeneous interfaces because of the synergistic presence of different phases, particularly in the vicinity of the NiS roots, where the epitaxial NiS nanosheets initiate growing. These heterointerfaces can act as suitable regions for enhanced electron transfer and intensified electron exchangeability between catalytic sites and H* species (H protons). As magnified in Figure 2.6e, the NiS nanosheets grow outward in random directions, and thereby, various crystallographic planes appear in the selected-area electron-diffraction (SAED) pattern shown in Figure 2.6c. The SAED pattern obtained from the nanosheet's apex (the prickly pear fruit) confirms the formation of the hexagonal NiS structure. By carefully investigating the SAED pattern (Figure 2.6d) collected from the Ni_5P_4-Ni_2P plate (the cactus leaf), we observe a localized

vibration at each shinning spot that can be attributed to the simultaneous diffraction from two hexagonal crystal structures corresponding to the Ni_5P_4 and Ni_2P phases (Danielsen et al. 2006). It can be noted that many spots overlap in the diffraction pattern since the pattern is obtained from the contribution of both crystal structures. Thus, corresponding planes are identified for both phases. The simultaneous presence of several phases, including Ni_5P_4, Ni_2P, and NiP_2 (semi-stable), was also reported by evaluating the SAED pattern corresponding to the synthesized nickel phosphide nanosheets (C. Hu et al. 2020). The magnified TEM image shown in Figure 5e is used as a reference for further characterization. High-resolution TEM (HRTEM) images taken from red-marked circles regions near NiS nanosheets and its root are displayed in Figure 5f-h. As demonstrated in Figure 5f, the lattice fringes with a spacing of 0.290 nm are indicative of the interplanar spacing of (110) planes from the hexagonal Ni_2P phase, while various lattice fringes with a spacing of 0.173, 0.175, and 0.285 can be related to the interplanar spacing of (033), (025), and (021) planes from the hexagonal Ni_5P_4 phase, respectively. Indeed, the synergistic presence of both Ni_5P_4 and Ni_2P phases can also be realized from the HRTEM image in Figure 2.6f, representing the internal structural discontinuity in the Ni_5P_4 phase due to a random distribution of the Ni_2P phase marked by yellow circles (Makeswaran et al. 2021). This interference leads to the generation of Ni_5P_4/Ni_2P heterointerfaces at the nanoscale. Remarkably, the HRTEM image in Figure 2.6g confirms the formation of the epitaxial NiS nanosheets, where NiS ($d_{(010)}$= 0.300 nm) and Ni_2P ($d_{(011)}$= 0.281 nm) approximately share similar lattice distances, yielding to a decent d-spacing (interplanar space) matching between the Ni_2P phase and the epitaxial NiS phase (An et al. 2019; Zhu et al. 2018; Q. Liang et al. 2019).

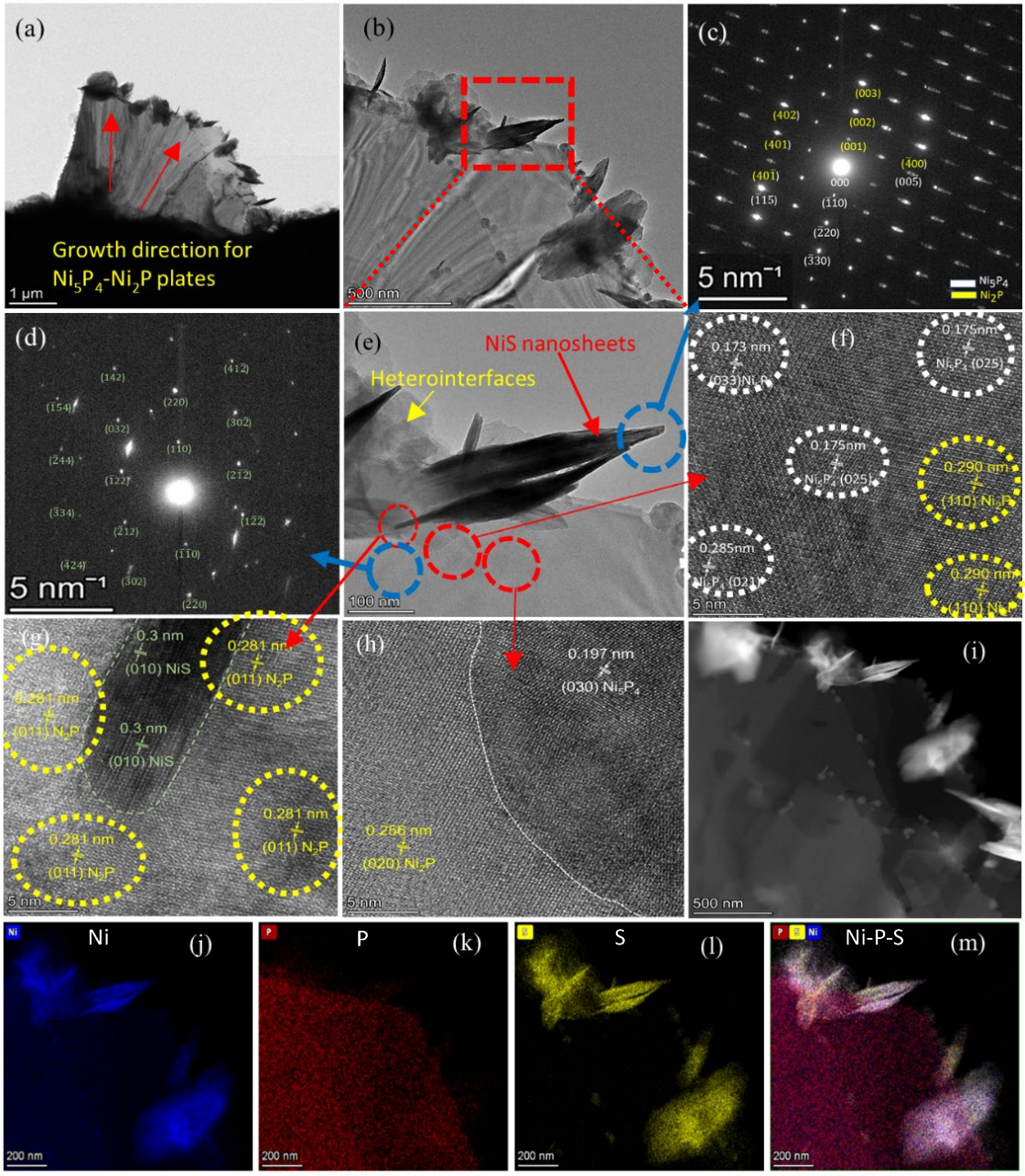

Figure 2-6: (a and b) The TEM images of the Ni_5P_4-Ni_2P/NiS heterostructure, (c, d) SAED images from the selected regions shown in e, (e) The magnified TEM images, (f, g, and h) HRTM images of the selected regions shown in e, (i) dark-field STEM image, (j-m) corresponding EDS elemental mapping of Ni, P, S for the Ni_5P_4-Ni_2P/NiS heterostructure.

Therefore, the epitaxial interfacing between Ni_2P and NiS crystals occurs along the (011) facets from Ni_2P thanks to the negligible interfacial strain (Figure 2.2b). The dark-field scanning transmission electron microscopy (STEM) image also reveals the growth of NiS nanosheets from

edges and the complex structure of the vertically grown Ni_5P_4-Ni_2P plate (Figure 2.6i). The EDS mapping obtained under STEM mode reveals the uniform distribution of Ni and P in the vertically grown plates,(Ramana et al. 2006) while Ni and S are only present in the epitaxial NiS nanosheets (Figure 2.6j, m). Considering these characterizations, we can verify emerging epitaxial interfaces between Ni_2P and NiS phases at the nanoscale, which can facilitate electron transport during the electrocatalytic activity and strengthen the structure of the nanosheets.

The implications of the structure-chemistry relationship in these Ni-P-S nanomaterials, as revealed by the XRD, SEM, TEM, and XPS analyses, can be described as follows. Note that the structural tuning of electrocatalysts has been recognized as one the most effective approaches to enhance interfacial interactions between electrocatalysts and electrolytes, leading to more significant HER performance. Specifically, one successful strategy is to judiciously grow epitaxial nanosheets out of the dominating phases, thereby expanding the active catalytic surface area and optimizing electronic features. It also tunes the energetics of intermediates via developing heterointerfaces (An et al. 2019; Zhu et al. 2018). This strategy eventually leads to more significant hydrogen production and emphasizes the importance of using the conventional electrocatalyst as an appreciable substrate for constructing epitaxial nanosheets. Employing a sulfidation process leads to growing the epitaxial NiS nanosheets on the vertically aligned Ni_5P_4-Ni_2P plates. Therefore, we expect our work to benefit from both simultaneous formation of Ni_5P_4 and Ni_2P with nanodomain interfaces and the generation of the epitaxial NiS out of Ni_2P phase. This unique 3D architecture resembles the prickly pear cactus. We provide detailed electrochemical studies to validate the effectiveness of these Ni-P-S nanostructures for enhanced HER performance.

2.3.3. Electrochemical Characterization and HER Performance Evaluation

The electrocatalytic activities of the Ni_5P_4-Ni_2P/NiS (plates/nanosheets) heterostructures are investigated specifically for the HER performance. We aim to determine the effect of the epitaxial NiS nanosheets and generated heterointerfaces in hydrogen production. The HER activities are

evaluated using electrochemical measurements in Ar saturated 0.5 M H_2SO_4 solution with a reference electrode of Ag/AgCl, calibrated to a reversible hydrogen electrode (RHE). We also use the normalized electrocatalytic current density by considering the catalysts' geometry and surface area. As shown in Figure 2.7a, the IR-corrected linear sweep voltammetry (LSV) at a scan rate of 5 $mV.s^{-1}$ demonstrates that the epitaxial growth of NiS nanosheets can boost the catalytic activities. In contrast, the NiP catalyst displays a lower HER activity. The NiPS3 electrocatalyst shows the lowest HER onset overpotential of 35 mV, which is a decent value compared to the commercial Pt/c electrode and lower than that of the NiP electrocatalyst (70 mV).(S. Liu et al. 2019) A noticeable feature related to the onset overpotential is that it is intrinsic to the catalyst's surface properties regardless of its loading.(Anantharaj et al. 2021) For the HER performance, overpotentials at the current density of 10 and 100 mA cm^{-2} are obtained from LSV curves and shown in Figure 2.7b. It reveals that the overpotential is significantly decreased for NiPS3 and other NiPS series. However, the NiP electrocatalyst contains the highest overpotentials. This noticeable catalytic activity confirms the importance of reinforcing intrinsic catalytic sites and expanding the active surface area by developing the epitaxial growth of NiS nanosheets upon the sulfidation process. Although the overpotential values for the NiPS3 electrode at the current densities of 10 and 100 mA cm^{-2} (70 and 115 mV, respectively) do not surpass the catalytic performance of the Pt group catalysts, this work demonstrates the importance of improving the electronic and structural features for boosting the electrocatalytic activity (Q. Liang et al. 2019; An et al. 2019). It is worth mentioning that the primary goal of the current study is not to introduce a champion electrocatalyst dominating the sophisticated Pt group catalysts. Further, it endows a new avenue for constructing seamless electrocatalysts. A linear fitting by the Tafel equation is performed on the polarization curves based on the method explained by Murthy et al. (Murthy, Theerthagiri, and Madhavan 2018). Figure 2.7c shows the corresponding Tafel plots. Tafel slopes are inversely related to the charge transfer coefficient of HER, which directly demonstrates how efficiently electrons are exchanged across the interface. Tafel slopes also serve as indicators for controlling the mechanism of HER established across the interface. Noticeably, the Tafel slope

profile for the Ni_5P_4-Ni_2P/NiS heterostructure reflects a decreasing trend with increasing sulfur content during the sulfidation process, where NiPS3 shows the lowest slope (50 mV dec^{-1}) compared to other catalysts, particularly NiP (141 mV.dec^{-1}). These findings indicate efficient kinetics of HER due to the emerging NiS nanosheets.

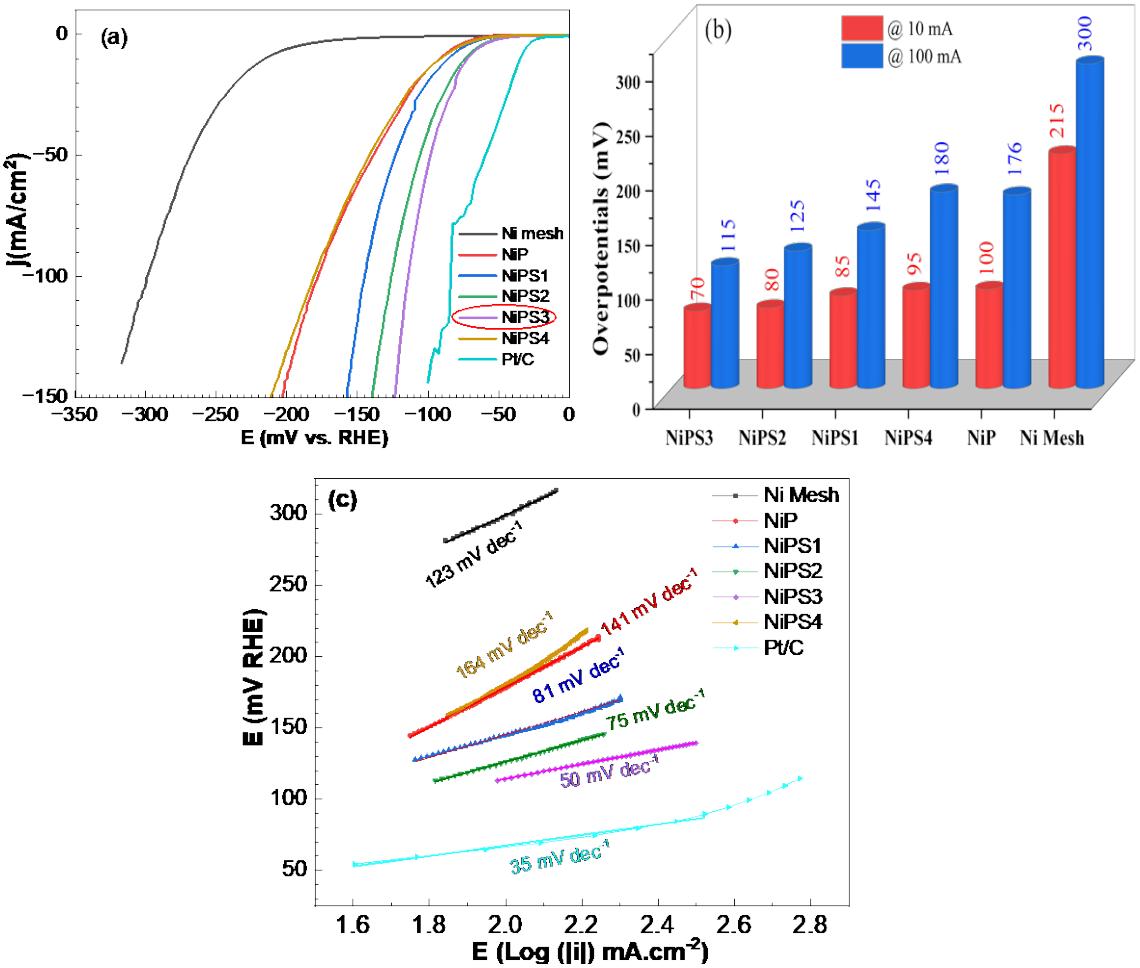

Figure 2-7: (a) IR-corrected linear sweep voltammetry (LSV) of HER (b) overpotential profiles of the prepared catalysts, (c) plot of Tafel slopes for the prepared catalysts

It is worth mentioning that estimating the turnover frequency (TOF), which is indicative of the number of transported electrons for each active site per second, is not feasible for the current study because determining the number of active sites for the complex heterostructures is cumbersome. Therefore, to construct a relation between the structural properties and active catalytic surface area of the electrocatalysts, we measure the double-layer capacitance (C_{dl}) from

the cyclic voltammetry (CV) curves in the limited cathodic range of 105 to 205 mV vs. RHE (Figure 2.8a-b). The electrochemically active surface area (ECSA) is directly proportional to the C_{dl}, ECSA = C_{dl}/C_s (Cs is the assumed specific capacitance), which is the linear slope of Δj as a function of a series of scan rates obtained from the CV curves. The measured C_{dl} values are 13.12 and 4.74 mF cm^{-2} for NiPS3 and NiP, respectively, indicating a nearly threefold higher ECSA for the electrocatalyst containing the epitaxial NiS nanosheets. The NiPS3 catalyst with the most significant C_{dl} indicates that the HER activity proceeds with a more enhanced adsorption of H^* on the active sites compared to other prepared electrocatalysts. Thus, electron exchangeability improves considerably between the active sites and adsorbed protons from the electrolyte, remarkably enhancing HER performance for the NiPS3 electrocatalyst. The characterization already performed, like LSV and CV, reveals the superior HER performance of the NiPS3 electrocatalyst. SEM images in Figure 2.5c, d illustrate that increasing the sulfur content during the sulfidation process causes the population of NiS to rise on the Ni_5P_4-Ni_2P plates. For the NiPS3 electrocatalyst, it is envisaged that the epitaxial NiS nanosheets can provide greater accommodation for adsorbed intermediates, and the interfacial interaction between the catalyst and intermediate species proceeds more efficiently. In addition, emerging abundant heterointerfaces may positively influence the catalytic activity. Therefore, the unique structure of Ni_5P_4-Ni_2P/NiS (plates/nanosheets) can boost the HER performance compared to the other prepared catalysts.

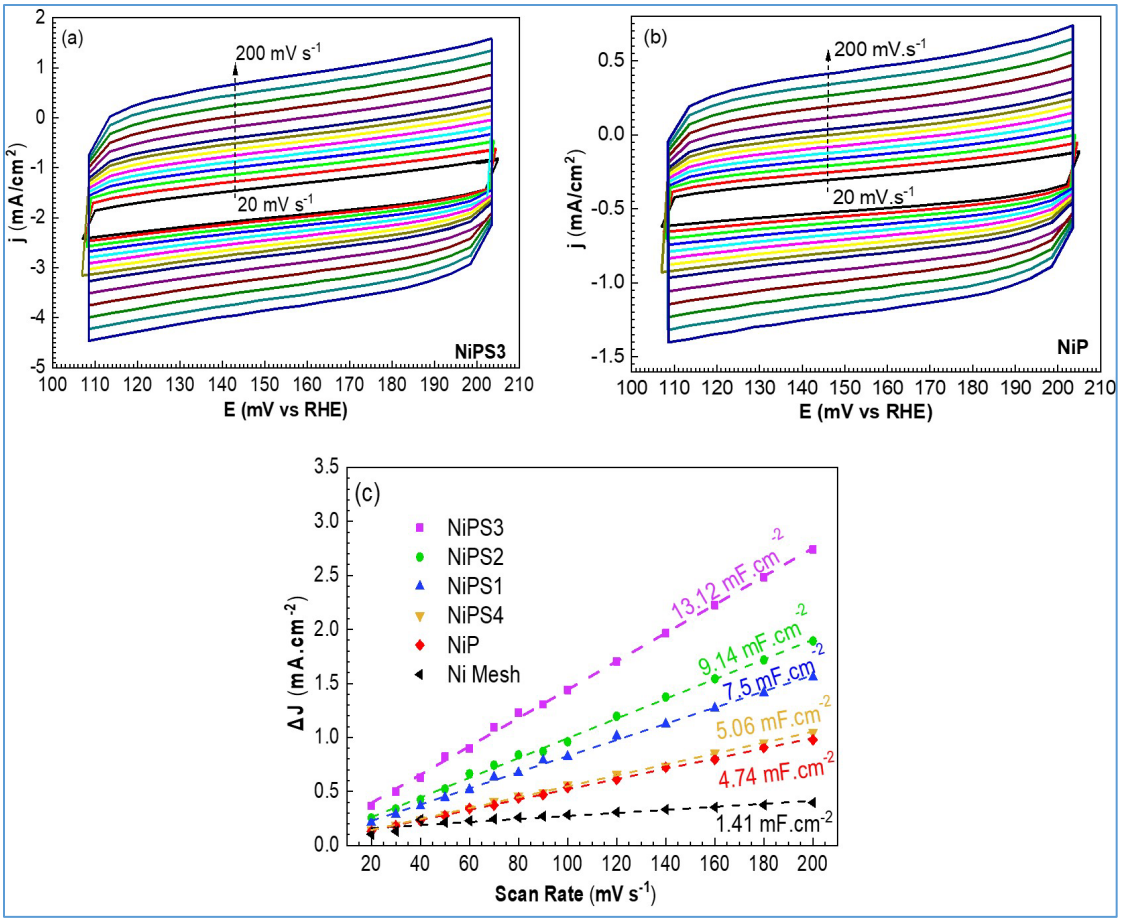

Figure 2-8: (a, b) cyclic voltammetry at scan rates from 20 to 200 mV s^{-1} for NiPS3 and NiP, respectively, (c) determination of C_{dl} for all prepared catalysts**.**

Furthermore, LSV results also confirm that the NiPS3 electrocatalyst offers the lowest overpotentials and Tafel slopes. These significant improvements imply the catalytic activity is enhanced, and the NiPS3 electrocatalyst demands the lowest electrical energy and shows the quickest hydrogen evolution kinetics. The CV studies and measuring the capacitances, as shown in Figure 2.8a-c, reflect that the NiPS3 electrocatalyst retains the largest capacitance, which can be attributed to the emerging epitaxial NiS nanosheets. The generation of the epitaxial NiS nanosheets increases the active surface area that synergistically accommodates a higher number of H_{ad} species and facilitates electron transition.(Y. Yin et al. 2017) Furthermore, the following EIS results also show that the interface between NiPS3 and electrolyte establishes the lowest charge transfer resistance, indicating an accelerated electron transfer occurs at interfaces. Thus, in the

conglomeration of the extensive studies with respect to the superiority of NiPS3, our evaluation suggests that the significant improvement in the catalytic performance of NiPS3 can be related to the growth of epitaxial NiS nanosheets compared to the other prepared catalysts.

To further understand the significance of the ternary nanostructured materials developed in this work and to elevate the technical approach used to synthesize such tailor-made prickly pears heterostructures, we compare our data with those reported in the literature. Table 2.2 represents electrocatalysts developed based on the ternary Ni-P-S system. The data presented in Table 2.3 demonstrates the significance of the current work compared to those already reported in the literature.

Table 2. 2: Comparison of various Ni-P-S electrocatalyst systems with their HER activity.

Source	Preparation process	Catalyst composition	solution	HER activity			Ref.
				η_{10} *	η_{100} *	Tafel Slope **	
NF	Sulfo-Phosphidation	NiS and Ni_8P_3	♣	68.4	130	46.6	(Duan, Chen, and Zhao 2018)
NF	One-step phospho-Sulfidation	NiS, $Ni_2P_2S_6$	♣	140	210	72.8	(X. Zhang et al. 2017)
NF	one-step electrodeposition	Ni-$NiSP_x$ (amorphous)	♠	46	145	86	(Chen et al. 2019)
NF	Hydrothermal + Sulfo-Plasma/Phosphidation	$S_{vacancy}$-$Ni_3S_{2-X}P_X$	♣	89	169	122.5	(Yang et al. 2021)
NF	Phospho-Sulfidation	$NiP_{0.62}S_{0.38}$	♣	52		52.3	(Luo et al. 2017)
NF	Phospho-sulfidation	$NiPS_3$	♣	74	175	86	(Fang et al. 2021)
Ni_5P_4 nanoplates	Phospho-sulfidation of $Ni(OH)_2 \cdot 0.75H_2O$	S_{doped}-Ni_5P_4	♥	56	104	43.6	(Chang et al. 2018b)
$NiPS_3$ Bulk	Electrochemical exfoliation of $NiPS_3$	Intercalated $NiPS_3$	♣	158		95	(X. Li et al. 2019)
$NiPS_3$ particles	H_2/Ar atmosphere + thermal treatment	$NiPS_3/Ni_2P$ epitaxy	♣	85		82	(Liang et al. 2019)
$NiPS_3$ Bulk	Ball-milling exfoliation of $NiPS_3$	Vacancy-$NiPS_3$	♣	126	200	65.4	(Tong et al. 2021)
$NiPS_3$ Bulk	Electrochemical exfoliation of $NiPS_3$	Thin $NiPS_3$ exfoliated layers	♣	205		74	(Luxa et al. 2020)
NF	Hydrothermal + Sulfo-Phosphidation	S_{doped}-Ni_2P	♣	179	280	62	(Huang et al. 2020)
NF	Phospho-Sulfidation	$Ni_2P/Ni_{0.96}S$	♦	72	239	149	(He et al. 2020)
Ni mesh	***Phospho-Sulfidation***	***Ni_5P_4-Ni_2P/NiS***	♥	***70***	***115***	***50***	★

NF: Nickel Foam, the current work is shown with ★, *: $mA.cm^{-2}$, **: $mV.dec^{-1}$, ♣: 1 M KOH, ♠: 1 M NaOH, ♥: 0.5 M H_2SO_4, ♦: 1 M KOH and 0.5 M urea.

Phospho-Sulfidation and Sulfo-Phosphidation are the two-step processes differing in order.

Table 2. 3. In-Situ Grown Epitaxial Heterojunction systems.

Source	Preparation process	Catalyst composition	solution	HER activity		
				η_{10}*	η_{100}*	Tafel Slope**
$NiPS_3$ particles	H_2/Ar atmosphere + thermal treatment	$NiPS_3/Ni_2P$ epitaxy	♣	85		82
$NiMoO_4$ Crystal	Selective Sulforation	N-$NiMoO_4/NiS_2$ nanowires/nanosheets epitaxy	♣	99	300	74.2
$NiCo_2O_4$ precursor	thermal annealing	Co-Ni3N	♣	194	290	156

As mentioned, this study does not present a champion electrocatalyst beating the current Pt bench market. However, it presents a new structure that has not been reported in the literature as shown in Table 2.2 and Table 2.3. Noticeably, all studies on the Ni-P-S ternary systems can be categorized into 4 groups based on the catalysts' compositions, as follows:

i. Producing intermediate nickel phosphosulfide compositions, like NiP_xS_{1-x}.
ii. Producing sulfur-doped nickel phosphide or phosphor-doped nickel sulfide,
iii. Producing stoichiometric compounds, like $NiPS_3$, NiS, and Ni_8P_3, and using further procedures such as ball-milling or electrochemical processes to exfoliate thin layers.
iv. Generating the in-situ epitaxial Ni_2P nanodomains on 2D $NiPS_3$ nanosheets

Thus, the presented comparison reiterates the novelty of the current study, in which a seamless 3D electrocatalyst is synthesized using sequential phase alterations on an ultrathin nickel mesh. The importance of the synthesized nanostructure relies on the epitaxial growth of NiS nanosheets out of the Ni_2P phase and, consequently, the formation of heterointerfaces near its nucleation sites.

Furthermore, to gain broader insights into the kinetics of the catalytic activity during HER catalysis, we use electrochemical impedance spectroscopy (EIS) techniques over a range of applied overpotentials from -100 to -450 mV vs. Ag/AgCl. In fact, assessing the catalytic activity at constant overpotentials beyond the onset potentials is a convenient method for comparing the electronic characters and the importance of structural development.(Z. Xiao et al. 2020) Anantharaj and Noda realized that a rational correlation could be found for the charge transfer resistances at the constant potentials in the catalytic turnover regions, in which the entire interface could be subjected to electrocatalytic activities (Anantharaj and Noda 2020). Evaluating EIS responses as a function of applied overpotentials can also shed light on the role of heterointerfaces generated owing to the epitaxial growth. The Nyquist plot of EIS data for the NiPS3 electrocatalyst is demonstrated in Figure 2.9a. It exhibits a depressed semicircle for all studied potentials, indicating the HER activity can be characterized by one time constant and only controlled by the charge transfer kinetics throughout the studied frequencies (Patil et al. 2022). The experimental data are fitted using the equivalent circuit shown as a sub-figure in Figure 2.9a. R_s represents the ohmic resistance imposed by all connections and the electrolyte. R_p and CPE elements indicate the polarization resistance and the pseudo-capacitance arising from the charge transfer at the interface between active catalytic sites and adsorbed protons.(J. Li et al. 2019) The CPE is used instead of the capacitance element due to depressed semicircles in Nyquist graphs. As shown in Figure 2.9b, the R_p reduces with applied potentials, in which the NiPS3 electrocatalyst demonstrates the lowest charge resistance at each potential, indicating a facilitated H* adsorption on the active catalytic sites (J. Li et al. 2019). Thus, we realize the electron exchangeability is significantly enhanced for the electrocatalyst containing the largest population of the epitaxial NiS nanosheets, thanks to the largest ECSA and its higher intrinsic catalytic sites compared to other catalysts. On the other hand, the NiP catalyst consisting of the Ni_5P_4-Ni_2P composition demonstrates the lowest electron transfer rate, leading to the weakest HER performance. Indeed, we realize a direct relation exists between raising the ECSA and decreasing the R_p trend. The measured R_p for the NiPS3 electrode shows the minimum resistance at each applied potential, implying that the transferring electrons to the

adsorbed H* species proceed with accelerated reaction kinetics during the HER performance (Zhao et al. 2021). These results confirm that the generated epitaxial interfaces and heterointerfaces significantly influence the HER performance. Indeed, the generation of the epitaxial NiS nanosheets lowers the charge transport resistance at the interfaces between Ni_2P and NiS phases and reinforces the electron transfer rate to the adsorbed H*.(Q. Liang et al. 2019) Further, the heterostructures emerging near the NiS nanosheets add to the structural and electronic improvements. These results are consistent with the overpotentials and Tafel slopes obtained for the electrocatalysts shown in Figure 2.7 b, c.

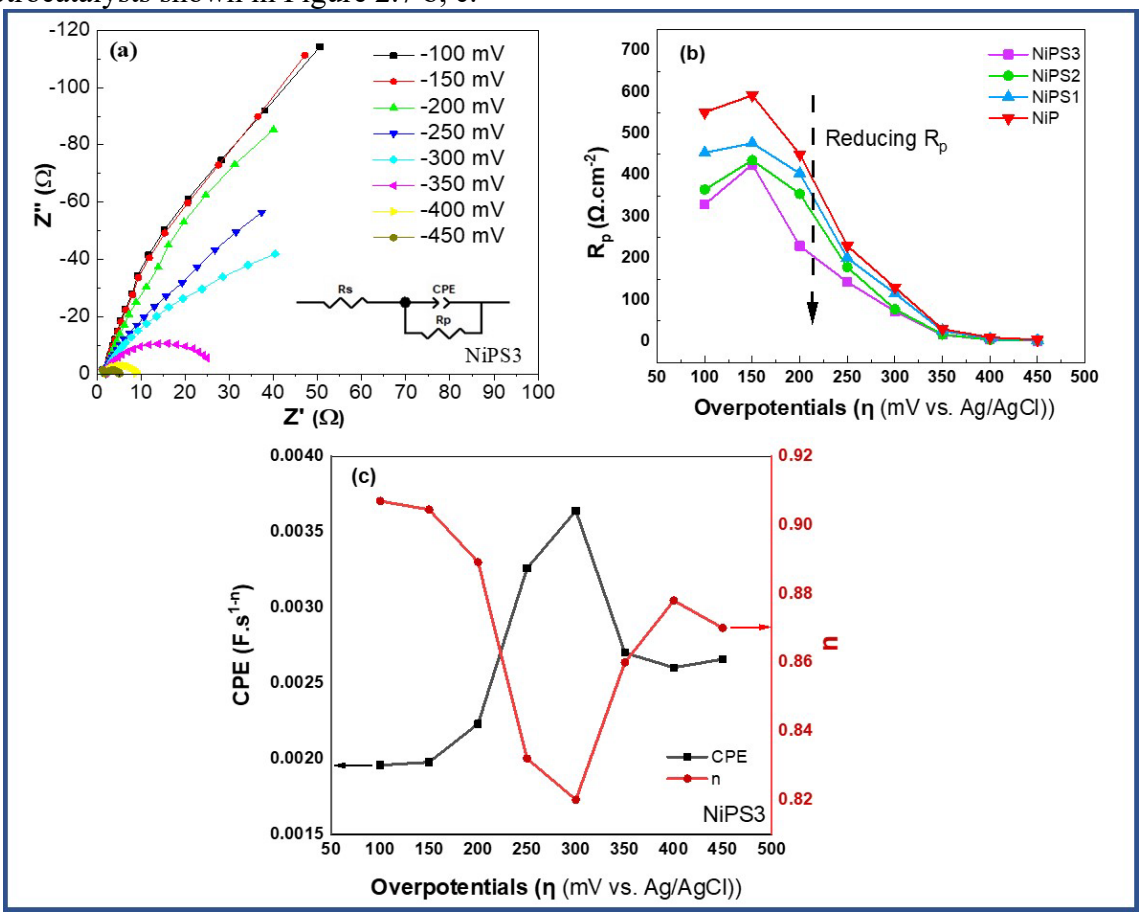

Figure 2-9: (a) Nyquist curves of electrochemical impedance spectroscopy (EIS) at overpotentials ranging from 100 to 450 mV, (b) charge transfer resistance (Rp) obtained from EIS data, (c) CPE and n profiles obtained from NiPS3 for different overpotentials.

The impedance of CPE can be expressed as:

$$Z_{CPE} = A(j\omega)^{-n} \qquad (1)$$

where $A=1/C_n$, n=1 (in the absence of frequency dispersion). It can be added that n is related to the surface condition of the electrocatalyst at different overpotentials. It is also utilized to alter the CPE to a pure capacity, where the closer to 1, the more the capacitance behavior can appear. Indeed, it is believed that n varies with the homogeneous distribution of active catalytic sites.(Morales et al. 2021) As shown in Figure 2.9c, we understand that the distribution of active sites varies with the applied overpotentials over the catalyst's surface, in which the homogeneity reduces with the applied potentials indicating that the number of active catalytic sites depletes and then mitigates at higher overpotentials (above 300 mV). In contrast, the CPE, representing the pseudo-capacitance of the formed double layer, increases with the applied potential until 300 mV, implying that the electron exchangeability rate over the active catalytic sites increases and then slightly reduces. Thus, it can be deduced that though the number of active sites is depleted, the activity of the remaining sites is intensified with the applied overpotential. The durability of NiP and NiPS3 electrodes are evaluated for 20 h and demonstrated by a chronopotentiometry plot for the cathodic potential of 10 mA. The data are shown in Figure 2.10. As apparent, the voltage change for NiPS3 catalysts is negligible, and the change of overpotential is also insignificant, which can be confirmed by the intersection LSV plot regarding NiPS3 electrode. However, the voltage increased during HER activity for the NiP electrocatalyst, indicating some surface deterioration. Noticeably, the SEM image from the surface of the NiP electrode after 20 h show the impact of catalytic activity in the forms of pits, while the surface of the NiPS3 electrode could sustain efficiently. The surface for NiPS3 catalysts does not show any pitting effect, and the structure could preserve some of the NiS nanosheets even after 20 h of HER activity.

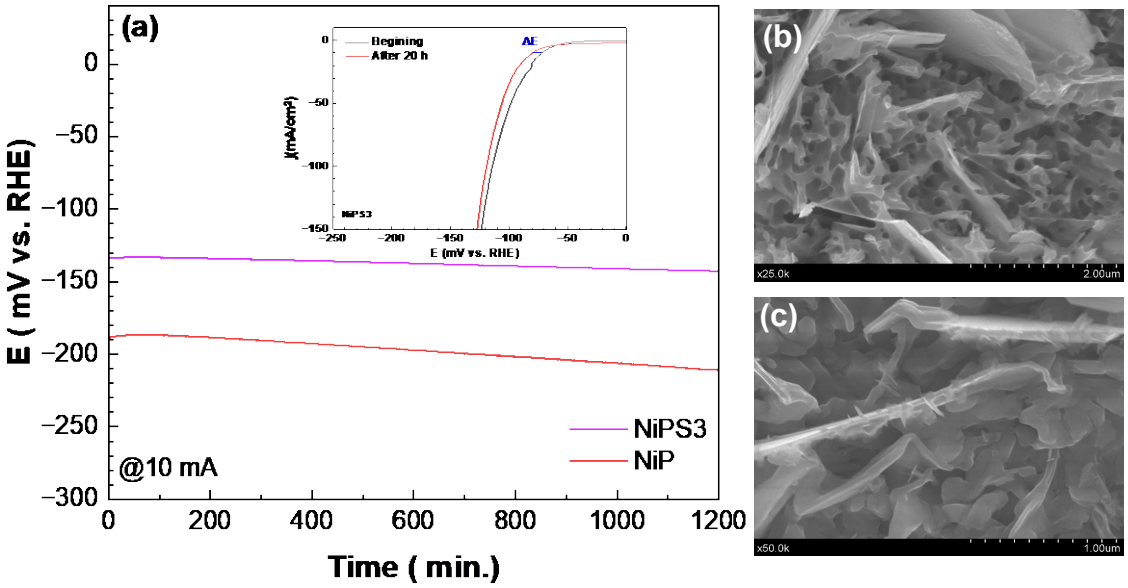

Figure 2-10: (a) chronopotentiometry plot of HER activity at 10 mA for 20 h with the intersection of LSV plot related to before and after 20 h stability test. (b and c) SEM images related to NiP and NiPS3 electrodes after 20 h catalytic activity.

The cartoon in Figure 2.11 illustrates the difference in the behavior of NiP and NiPS electrocatalysts in a range of reducing overpotentials. The cartoon explains that the ternary system provides a larger active catalytic surface area compared to the nickel phosphide catalyst while working at low overpotentials (< -300 mV vs. Ag/AgCl). After switching to high overpotentials, although some areas of the ternary NiPS system become inactive, those active catalytic areas accommodate a higher number of H_{ad} as an indication of compensating for inactive catalytic areas.

Taking into account the obtained results, we suggest the significant improvement observed for the catalytic activity of the Ni_5P_4-Ni_2P/NiS (plates/nanosheets) stems mainly from expanding ECSA because of growing the epitaxial NiS nanosheets and strengthening the intrinsic catalytic activity due to the generated heterointerfaces. We realize that the epitaxially grown nanosheets and heterointerface stabilize more significant H* adsorption over the active catalytic sites because of supporting the greater active surface area.(Q. Liang et al. 2019)

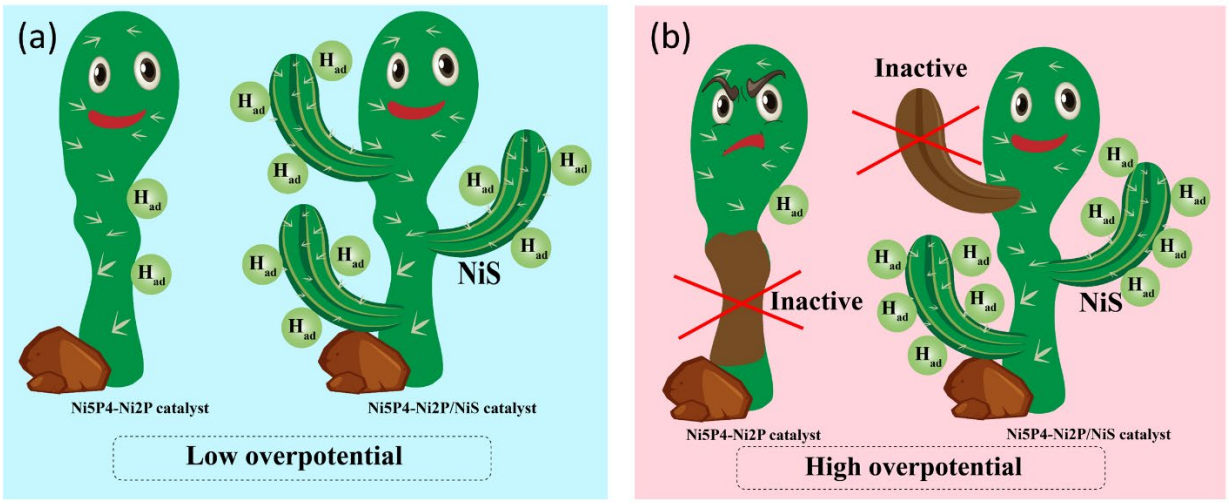

Figure 2-11: A cartoon representing the behavior of NiP and NiPS electrocatalysts during HER performance for low overpotentials (<-300 mV (vs. Ag/AgCl) and high overpotentials (>-300 mV)

The fundamental goal of the Ni-P-S ternary electrocatalytic system is to enhance electron transfer to adsorbed H* species. Generally, the HER activity can be optimized by enhancing the intrinsic catalytic activity or increasing the number of exposed active catalytic sites. The heterointerfaces chemically include a nanoscale mixture of various phases formed during the phosphidation and sulfidation procedures. Therefore, the catalytic activity of heterointerfaces may achieve the goal of hitting two birds with one stone, namely, enhancing the intrinsic catalytic activity by containing nanoscale defects and expanding the active surface areas simultaneously. In fact, introducing defects through creating heterointerfaces is an effective strategy to improve the catalytic activity, which may consequently modulate the electronic structure of the interface by reducing the adsorption-free energy of H* species during the HER performance.(Z. Hu et al. 2018) In addition, the heterointerfaces inherit a synergistic effect of different components, where the unique structure of the heterointerfaces can provide stronger affinity with H* species and thus improve HER catalytic activity.(Muthurasu, Maruthapandian, and Kim 2019)

The heterointerfaces are generated near the epitaxial NiS nanosheets, as evidenced in the structure and morphology characterizations. Thus, these heterostructures benefit from a long-range disordered structure and abundant defects in correspondence with the compositional and structural

variation. Another critical factor, although there are only limited studies/reports available at this time, is the chemistry of epitaxial interfaces that facilitates the enhanced catalytic activity for HER. Teng et al. reported significant improvement in the catalytic activity of hydrogen reduction due to the generation of abundant active sites via the formation of the heterogeneous structure.(Teng et al. 2018) Liu et al. also reported synthesizing a heterointerface between Ni_2P-NiP_2 as a successful strategy for establishing strong electronic coupling effects between various phases (Tong Liu et al. 2018). They showed electrons could transfer from P to Ni at the heterointerfaces, thereby reducing the adsorption energy of H* species. Thus, our understanding is that the nanoscale mixture of nickel phospho-sulfide in the heterointerfaces optimizes the intermediate hydrogen binding energy. To conclude that the chemically tailored heterointerfaces resulting from the mixture of different phases formed during the phosphidation and sulfidation procedures, where a controlled process dictates the chemistry of such interfaces formed, are the key to promoting the generation of abundant active sites, which in turn result in enhanced HER performance of the electrocatalysts designed in this work.

Chapter 3: Heterostructured Electrocatalyst of MoP-Mo2N@Mo for Stable Hydrogen Evolution Reactions

3.1. INTRODUCTION

Hydrogen as a clean alternative source is in stark contrast to fossil fuels, a leading cause of global warming and climate change, that promotes zero carbon emission during use, reduces harmful substances' release, and provides a potential for carbon-neutral production.(van Renssen 2020) However, there are challenges associated with hydrogen that must be overcome for it to become a sustainable and widespread energy source.(Ahmed et al. 2022; Mneimneh et al. 2023) The progress and expansion of "green" hydrogen production using the electrolysis method depend on developing durable electrocatalysts tolerating high current densities for a prolonged time. In addition, hydrogen evolution reaction (HER) is indeed limited by a significant overpotential. Platinum group metals (PGM) demonstrated relatively low overpotentials for HER across a wide pH range of electrolytes.(Zhang et al. 2017) However, the large-scale utilization of Pt electrocatalysts is hindered by their scarcity and the associated high cost limiting their widespread applications. Significant research efforts are focused on developing alternatives to reduce the reliance on PMG catalysts. These efforts aim to synthesize effective and affordable catalysts using abundant and low-cost elements and optimize their structures while maintaining high catalytic activity and stability for hydrogen production.(Zhao et al. 2018) The durability and longevity of electrocatalysts are essential because the degradation of catalysts over time decreases efficient operation and leads to higher energy costs. During the HER, the catalysts are subjected to harsh electrochemical conditions leading to various degradation mechanisms that can negatively impact the catalyst's stability and performance over time. The contribution of several factors determines the stability of electrocatalysts. The chemical, electrochemical, and morphological stability of

catalysts in the electrolyte environment is essential. The catalyst should resist dissolution, surface reconstruction, particle detachment, and reactions leading to the loss of active sites and withstand the high applied current densities in a broad pH range without significant alteration in its catalytic activity. In addition, poisoning or deactivation by adsorbed impurities and reaction intermediates reduces the catalytic activity. Therefore, researchers are actively exploring various synthesis strategies with different materials to enhance the stability of electrocatalysts for the HER.

Of the particular PGM-free catalysts, Mo-based compounds, such as MoS_2,(Z. Liu et al. 2022) S_{doped}-MoO_x,(Li et al. 2021) MoN_x,(Yao et al. 2021) and MoP(Pi et al. 2020) could demonstrate promising longevity with their efficient HER catalytic activities because of containing Pt-like d-band electronic configuration. Generally, P atoms with higher electronegativity draw electrons from transition metals and function as Lewis-base to attract positively charged protons in the HER process.(Kibsgaard et al. 2015) Further enhancement in HER catalytic activity could be achieved through S doping into MoP structure, where the synergistic effects between S and P created a more active electrode.(Kibsgaard et al. 2014) Introducing second anions generates heterostructured catalysts that the nanostructures and electronic features are tuned significantly.(Attarzadeh et al. 2023) From the perspective of the HER catalytic activity, most heterostructured catalysts, either with active/active or active/nonactive structures, highlight various advantages as follows. First, the number of active sites is increased significantly, and the electrical conductivity is enhanced because refining the nanostructure creates sufficient adsorption sites for the intermediates of HER.(Nikam et al. 2015) Second, using macroscopic and seamless substrates like mesh provides fast mass diffusion that can reduce overpotentials at high current densities.(Attarzadeh et al. 2023) Third, the electronegativity difference between different components of heterostructures accelerates the electron movements between components, which also results in electronic structure

refinement.(Wang et al. 2017; Zhou et al. 2016) Finally and most importantly, constructing heterostructures improves the catalysts' performance, durability, and longevity.(L. Yang et al. 2015) Therefore, the paramount strategy of introducing nonmetals such as N, P, and O into ternary or quaternary heterostructures is for tuning the chemical composition that can enhance the intrinsic catalytic activity, increase the number of active sites, and improve the longevity of efficient catalytic activity.

Recently, MoP-based heterojunction catalysts have been developed for efficient HER performance. Yang et al. successfully synthesized the heterostructure catalyst of MoS_2-MoP anchored on the N-doped porous carbon (NC) substrate. The heterojunction catalyst exhibited significant catalytic activity with remarkable stability for HER that could be derived from the presence of distinctive nanosheet morphology increasing active catalytic sites, the synergistic effect of MoP and MoS_2 phases, and efficient electron movements.(Y. Yang et al. 2021) Loomba et al. designed synthesizing porous nitrogen-doped $NiMo_3P$ (N-$NiMo_3P$) micro-sheets. They found that inducing nitrogen increased the corrosion resistance, and the higher electronegativity of nitrogen in metal-nitrogen bonds yielded greater stability of active sites. In fact, the electron-withdrawing capability of nitrogen causes metal ions to achieve a higher valence state, which improves the electron transition and enhances mobilizing of the electronic density of the catalysts.(Loomba et al. 2023) Gu et al. also synthesized a 2D porous MoP/Mo_2N heterojunction by controllable pyrolysis of 2D PMo_{12}-MA precursor. The HER performance could surpass the commercial Pt/c catalysts in a neutral medium.(Gu et al. 2021) Although significant development in various electrocatalysts has been achieved for increasing efficiency and boosting performance, less attention has been devoted to an insightful understanding of inducing nonmetals on the durability of TMPs through electrochemical studies.(Calvillo et al. 2018; Zhu et al. 2020) The fact that cannot be overlooked is the capability of active sites to undergo structural self-reconstruction during catalytic activity due to electrically driven structural reduction or oxidation processes.(Y. Liu et al. 2017) In fact, the self-reconstruction could crease or decrease the catalytic activity.(Nam

et al. 2018) The current ex-situ characterizations lack strong rationales for judiciously comprehending the rationale underlying the longevity of the catalyst's performance. However, operando or in situ techniques have attracted tremendous interest because of analyzing real-time HER, capturing dynamic evolutions in the structure and electronic features, and tracking the self-reconstruction of catalysts. The latter feature is crucial in extending the durability of a catalyst because it particularly creates more active sites via the electrochemical activation process of the catalysts, which results in further boosting the catalytic activity.(Ji et al. 2020; Su et al. 2019; Jiang et al. 2018)

Fascinated by above studies, we have synthesized MoP-Mo_2N@Mo heterostructured electrocatalyst for enhanced hydrogen evolution reactions (HER) performance. We have characterized the structure and composition of prepared electrodes using X-ray diffraction (XRD) analyses, Then, we employed scanning electron microscopy (SEM) to examine the surface morphology and structure of developed electrocatalysts. X-ray photoelectron microscopy is used to characterize and investigate the electronic properties of electrocatalysts. The electrocatalytic activity is evaluated using linear sweep voltammetry (LSV) and cyclic voltammetry (CV) in a range of 20-200 mV s^{-1} scanning rates. Operando electrochemical impedance spectroscopy (EIS) is used to investigate the prolonged stability of the prepared electrocatalysts.

3.2. EXPERIMENTAL METHODS

3.2.1. Synthesize

Preparation of porous MoPN on Mo meshes: A piece of Mo mesh (1 cm × 2 cm, ~0.002 g, GOODFELLOW CAMBRIDGE Ltd.) was washed under ultrasonication in propanol and ethanol for 10 min to degrease and then rinsed with DI water and allowed to dry in an oven at 60℃. The Mo mesh features a thickness of 1 mm and an open area of 75% (40 wire.cm^{-2}). Then, a quartz boat containing 0.2 g of red phosphorous powder (Sigma Aldrich, %99.99 pure) was covered partially by Mo mesh with keeping at 1 cm distance above the powders. After that, the

boat and mesh together were placed gently inside the quartz tube of the MTI Corporation chemical vapor deposition (CVD) furnace. The tube furnace was kept under vacuum pumping, and Ar was also purged for 10 min at a flow rate of 200 SCCM to evacuate the air and replace it with Ar. The furnace was heated to 800 ℃ at 10 ℃ min^{-1}, kept at the final temperature for 2 h with purging NH_3/Ar at the flow rate of 25 sccm, and then cooled down to room temperature at the same rate.

3.2.2. Material Characterization

We utilized various analytical techniques to characterize the structure, phase, morphology and microstructure, and chemical composition of synthesized Mo-P-N materials. Scanning electron microscopy (SEM) images were collected using Hitachi S4800 by applying 10 kV and 15 μA. X-ray diffraction (XRD) patterns were obtained using a Malvern Panalytical Empyrean Nano edition multipurpose X-ray diffractometer. To resolve peaks from the diffraction pattern, the step size and the integration time were 0.01˚and 0.85 s/step, respectively. A Cu Kα X-ray source with a wavelength of 0.154 nm was used to acquire the measurements. X-ray photoelectron spectroscopic (XPS) scans of the best Mo-P-N electrocatalyst samples were obtained employing Kratos Axis Ultra DLD spectrometer using Al Kα monochromatic X-ray source (1486.6 eV) and a high-resolution hemispherical analyzer. The XPS survey and high-resolution scans were recorded, and the data obtained were analyzed with the help of CasaXPS software employing Gaussian/Lorentzian (GL(30)) line shape, line asymmetry, and Shirley background correction.

3.2.3. Electrochemical Characterization and Performance Evaluation

Hydrogen evolution reaction (HER) measurements were carried out on a Solartron analytical-ModuLab Xm workstation using a conventional three-electrode system with Ag/AgCl, a graphite rod (99.99%) as the reference electrode, and the counter electrode, respectively. The prepared electrocatalysts from MO mesh were working electrodes. The reference electrode was

calibrated with respect to a reversible hydrogen electrode (RHE) before experiments. The electrolyte was 1.0 M H_2SO_4 aqueous solution made from DI water. The linear sweep voltammetry (LSV) was recorded at a scan rate of 2 mV s^{-1}. Before LSV measurement, the working electrode was kept at open circuit potential (OCP) for 1 h to reach a pseudo-Plato voltage. The electrochemical impedance spectroscopy (EIS) was collected using the same workstation. The amplitude was 5 mV, while the scan started from 100 kHz to 1 Hz. IR correction was performed to account for the cell resistance based on the EIS test at the open circuit potential (OCP). Cyclic voltammetry (CV) was performed at different scan rates ranging from 20 to 200 mV s^{-1} and at the non-Faradaic potential region. We prepared a Pt/C (20%) electrode using the conventional method. For that, 5 mg Pt/C (20%) was sonicated for 30 min in 1 ml solution of ethanol and Nafion (with the 9:1 ratio). We did drop-cast the prepared ink on the surface of a glassy carbon electrode. Then, the HER activity of the prepared Pt/C electrode was evaluated in an identical condition that the synthesized ternary electrocatalysts were tested.

3.3. Results and Discussion

3.3.1. Crystal Structure, Phase, and Chemical Composition Characterization

Illustration 1 shows the synthesizing path for the self-standing MoP and MoPN electrocatalysts. The seamless structures reduce internal resistivity and increase stability by preventing local corrosion. The etching step activates the surface while removing most of the surface oxides, making the surface patterned and increasing the suitable surface for growing the protrusion of MoP and Mo_2N. The method for Mo wires formation is to use a hot extrusion process. Therefore, the impact of extrusion forming becomes more apparent after etching in the boiling acid. After rinsing with DI water, the mesh samples are placed in the chemical vapor deposition (CVD) chamber and phosphor-nitriding at 800 ºC using P powder and purging a mixture flow of

NH_3 and Ar. This process is designed and implemented in our Lab, like previous work.(Attarzadeh et al. 2023)

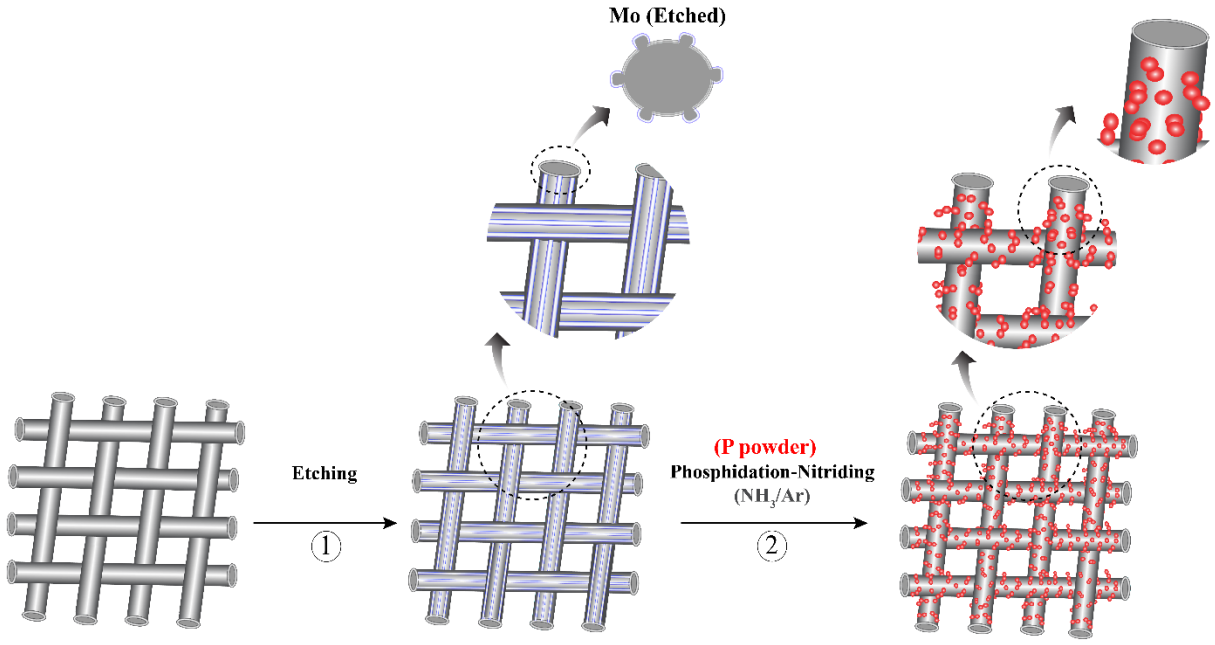

Illustration 3. 1. the synthesis path for Mott-Schottky MoP-Mo_2N@Mo heterostructured electrocatalyst

X-ray powder diffraction (XRD) analysis is employed to recognize the crystalline phases and structural variations of meshes after the first and second steps of synthesis. Figure 3.1a shows the XRD for MoP and MoPN electrodes demonstrating the electrodes' compositions after phosphidation and phosphor-nitriding processes. For the MoP electrode, it is apparent that MoP forms on the electrode because of obvious characteristic peaks at 27.8º, 31.9º, 42.8º, and 67.2º, being indexed to the (001), (010), (011), and (012) lattice planes of MoP based on ICSD#98-007-6367.

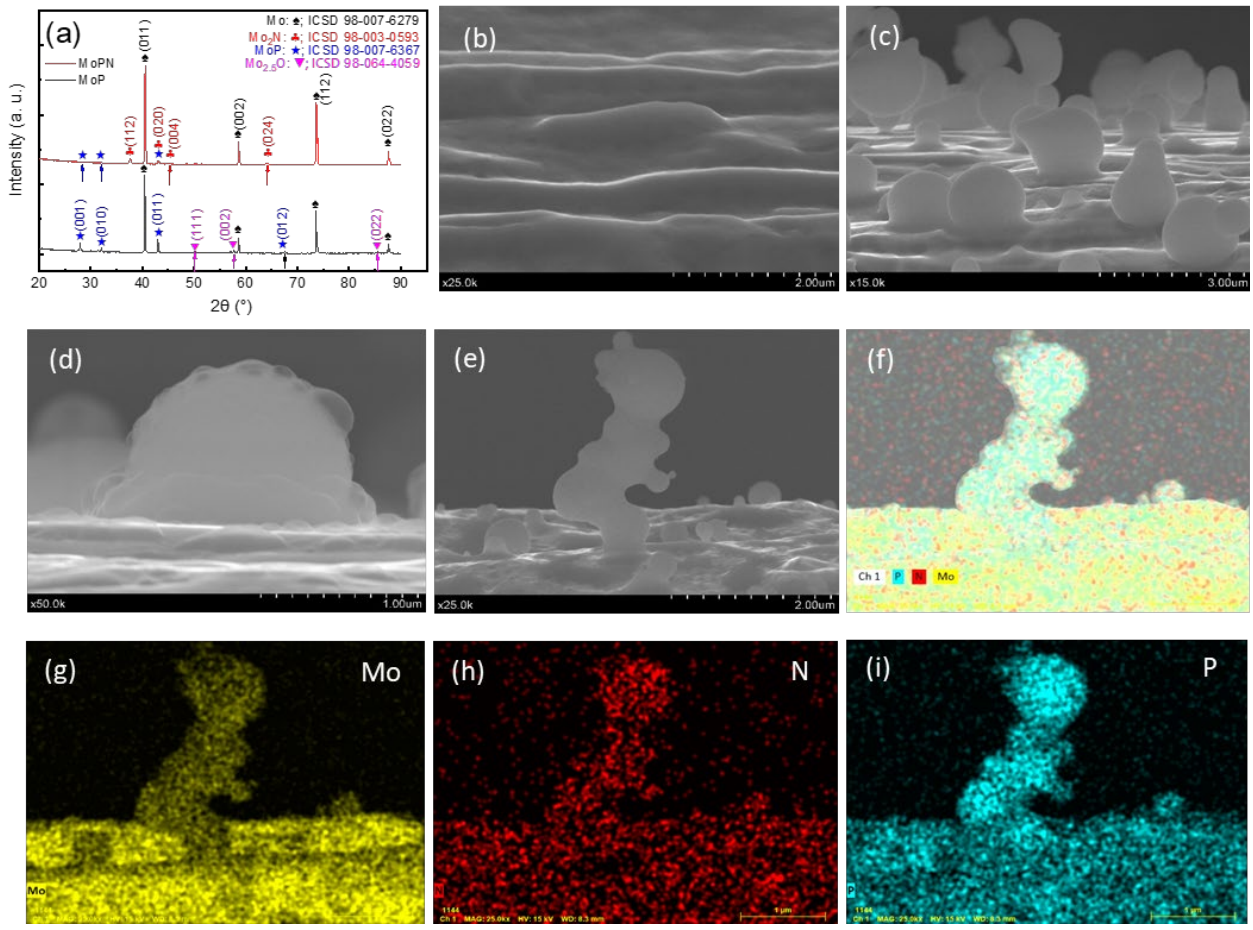

Figure 3-11: (a) XRD patterns of MoP and MoPN electrodes after phosphidation and phospho-nitriding process, SEM image from (b) etched Mo surface, (c-e) Phosopho-nitriding Mo surface for MoPN synthesized at the NH3/Ar flow of 25 sccm, (f-i) elemental mapping from MoPN electrodes for Mo, N, and P elements.

The characteristic diffraction peaks related to Mo are also evident because they are located at 40.5º, 58.6º, and 73.7º corresponding well to the (011), (002), and (112) planes of cubic Mo based on ICSD#98-007-6279 indicating that Mo remains on the surface and depth of the mesh wires. The lack of complete conversion of Mo to MoP creates the Mott-Schottky electrocatalyst causing enhanced catalytic performance. A slight amount of oxide remains even after etching in the form of $Mo_{2.5}O$ on the surface, with the characteristic peaks at 50.5º, 59º, and 88.3º representing the (111), (002), and (022) planes. For the MoPN electrode, we can recognize three phases of MoP,

Mo_2N, and the remaining Mo from XRD analyses. The characteristic peaks related to the tetragonal crystal of the Mo_2N phase are located at 37.7º, 43º, 45.3º, and 64.2º corresponding to (112), (020), (004), and (024) planes based on ICSD#98-003-0593. Therefore, we can deduce that the phospho-nitriding process on Mo mesh can create the Mott-Schottky MoP-Mo_2N@Mo heterostructured electrocatalyst.

To further characterize the structure and surface morphology of developed electrodes, we have used scanning electron microscopy (SEM) and elemental mapping using energy dispersive spectroscopy (EDS). Figure 3.1b shows the surface morphology of the Mo electrode after the etching process in the boiling solution of 3M chloride acid. The parallel lines on the surface are indications lines formed during the hot extrusion process of Mo wires, where the etching process makes them appear on the surface significantly. After phospho-nitriding process, SEM images in Figure 3.1c shows spheres form on the surface. The magnified SEM image in Figure 3.1d illustrates a semi sphere forming on the surface and gradually coming off from the surface, where the continuation of growth results either a bigger sphere or growing several spheres in the form of a hierarchy, like the hierarchy shown in Figure 3.1e. The EDS elemental analyses from the hierarchical sphere is show in Figure 3.1f-i. The presence of both P and N along with Mo indicates the formation and contribution of MoP, Mo_2N phases in the formed spheres and hierarchies.

X-ray photoelectron spectroscopy (XPS) has emerged as a powerful technique for characterizing and investigating the electronic properties of electrocatalysts. Mo-based electrocatalysts exhibit remarkable electrochemical performance attributed to their unique electronic structure and surface chemistry. The application of XPS in the analysis of Mo-based electrocatalysts offers valuable insights into the surface composition, chemical states, and binding energies of the molybdenum species, providing a fundamental understanding of their catalytic

mechanisms and contributing to the development of efficient electrochemical energy conversion devices. In this context, we employ XPS analyses on MoP and MoPN2 electrocatalysts with the use of casaXPS software to study these electrodes after their syntheses and changes that may occur after catalytic performance. Figure 3.2 demonstrates XPS results for both electrocatalysts with time. As shown in Figure 3.2a, the core level spectra for Mo $3d_{3/2}$ and Mo $3d_{5/2}$ of Mo^{4+} display peaks at 233.47 and 230.45 eV for the MoP I electrocatalyst, respectively.(Grünert et al. 1991) We realize that the binding energy shifts towards lower binding energy after catalytic activity for 6 h, where the core level spectra for Mo $3d_{3/2}$ and Mo $3d_{5/2}$ of Mo^{4+} stand at 232.6 and 229.2 eV for the MoP II electrocatalyst after 6 hours catalytic hydrogen evolution at 50 mA. We later explain the details of the catalytic activity in the electrochemical section. This phenomenon also appears in XPS spectrum shown in Figure 3.2b related to MoPN2 electrocatalyst. It is evident that Mo $3d_{3/2}$ and Mo $3d_{5/2}$ are located at 234.3 and 232.2 eV, respectively, for MoPN2 I electrocatalyst. After catalytic hydrogen evolution, we realize that there is a significant negative shift in the binding energy of the doublet for Mo^{4+}.

The shifting of binding energy for Mo 3d after catalytic activity can be attributed to several factors. Catalytic activity often involves the interaction of reactant molecules with the catalyst surface, leading to changes in the electronic structure of the catalyst. When reactant molecules adsorb onto the catalyst surface, they can interact with the Mo atoms, leading to electron transfer between the catalyst and reactant. This electron transfer can cause a shift in the binding energy of the Mo 3d electrons.(Q. Liu et al. 2020) Catalytic reactions can also induce changes in the oxidation state of the metal atoms in the catalyst. For example, Mo can undergo oxidation or reduction during a catalytic process. The change in oxidation state can influence the electronic environment around the Mo atoms, resulting in a shift in the binding energy of the Mo 3d

electrons.(Pandey et al. 2021) Catalytic reactions can induce surface reconstruction of the catalyst, where the arrangement of atoms on the surface undergoes changes. This reconstruction can lead to alterations in the local environment around the Mo atoms, affecting their binding energy.(Ji et al. 2020b; Saleh et al. 2022) During catalytic activity, new chemical species can form on the catalyst surface, such as adsorbed intermediates or reaction products. These surface species can interact with the Mo atoms and modify their electronic properties, leading to a shift in the binding energy of the Mo 3d electrons.(F. M. Li, Xia, and Xia 2022) Overall, the shifting of binding energy for Mo 3d after catalytic activity is a reflection of the changes in the electronic structure and chemical environment of the catalyst induced by the catalytic process.

For this study, the observed negative shift of binding energy for Mo 3d in XPS results can be attributed to the surface reconstruction during catalytic activity and changes in the oxidation state and the electronic structure of the Mo species during the catalytic process. During HER, Mo-based catalysts are commonly used, and they undergo changes in their oxidation state as they participate in the reaction. Mo catalysts can exist in different oxidation states, such as Mo^{6+} and Mo^{4+} and $Mo^{4+<x<6+}$. The reduction of Mo^{6+} to Mo^{4+} during HER involves the transfer of electrons to the catalyst from the reactants.

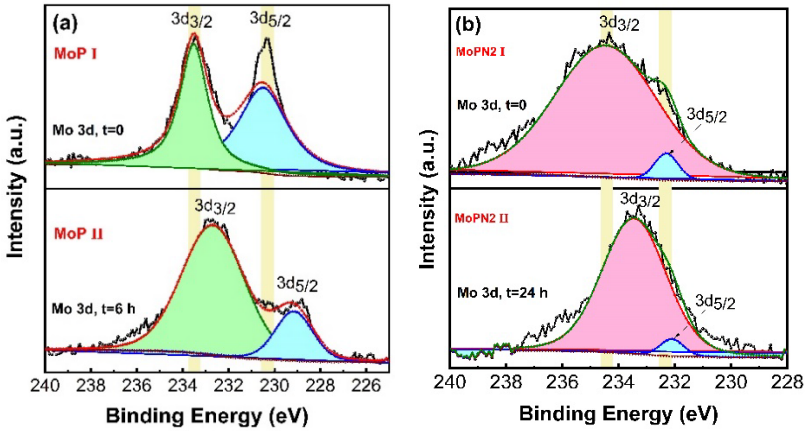

Figure 3-12: XPS results for the Mo doublets of Mo $3d_{3/2}$ and Mo $3d_{5/2}$ for (a) MoP and (b) MoPN2 electrocatalysts.

3.3.2. Evaluation of Catalytic Activity and Stability of Electrocatalysts

The electrocatalytic HER performance of the MoP-Mo_2N@Mo (MoPN1&2), MoP-$Mo_{2.5}O$@Mo (MoP), and commercial 20 Wt% Pt/C are investigated to determine the role of inducing nitrogen into the MoP crystal structure on the performance and durability of the developed catalysts. The HER activities are examined in Ar saturated 0.5 M solution using three electrode compartments, where Pt mesh (1 cm^2) and Ag/AgCl are the auxiliary and reference electrodes, respectively. The working electrode is the synthesized catalyst with an area of 1 cm^2. The electrocatalytic current density is normalized by considering the catalysts' geometry and active surface area. Figure 3.3a shows the IR-corrected linear sweep voltammetry (LSV) at the scan rate of 2 mV s^{-1}. It demonstrates that the Mott-Schottky MoP-Mo_2N@Mo (MoPN2) heterostructured electrocatalyst is the champion catalyst with the lowest overpotential. As shown by the LSV plots, developing the Mott-Schottky system and generating a heterostructure can be the reason behind boosting the electrocatalytic activity, where the overpotentials for the MoPN2 catalyst are 60 and 180 mV to attain the current densities of 10 and 100 mA cm^{-2}, respectively. The 3D bar chart in Figure 3.3b displays the overpotential values, and the values for the champion

catalyst are decent compared to the commercial Pt/C catalyst.(S. Liu et al. 2019) Even though obtained overpotentials do not beat values for the commercial Pt/C catalysts, this study is meant to show the importance of inducing the second nonmetal elements in modifying the durability and stability of an electrocatalyst. Based on Murthy et al. work, we used a linear fitting method on the polarization curves to obtain the Tafel slopes.(Murthy, Theerthagiri, and Madhavan 2018) The HER kinetics of the electrocatalysts are reflected by the Tafel slopes in Figure 3.3c. The plots show that the intrinsic catalytic activity is enhanced for the MoP-Mo_2N@Mo catalysts, where MoPN2 shows the value of 125 mV dec^{-1}.

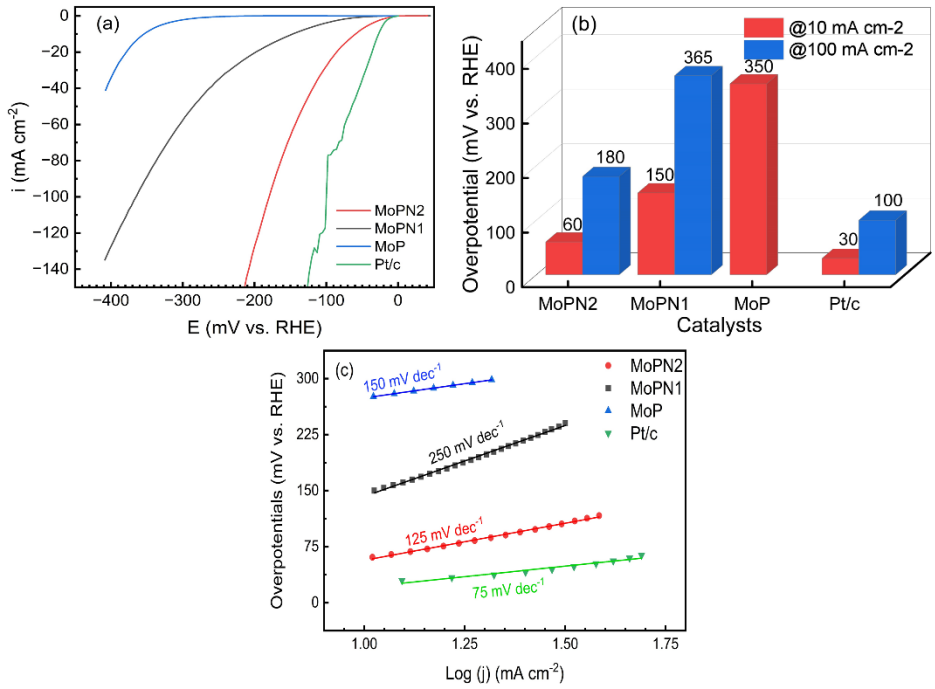

Figure 3-13: (a) IR-corrected linear sweep voltammetry (LSV) for HER performance, (b) the 3D bar chart for overpotential profiles of the developed catalysts, (c) Tafel slope plots for the developed overpotentials.

Stability and durability of the electrocatalysts are the key concern. To assess the HER stability of the synthesized materials, we apply a current of 50 mA to the electrodes and present their chronopotentiometry plots in Figure 3.4a. This type of durability test is designed to represent

the continuous electrolysis reaction of water in low currents. The MoP catalyst shows an abrupt change in its overpotential after 7 hours. Cyclic voltammetry in a range of (20-200 mV s^{-1}) scanning rates (noted by CV1 in cyan color, shown Figure 3.4a) is performed while the MoP electrocatalyst has been kept for 1 h in the open circuit potential and before initiating catalytic activity, which we call it "time zero", t=0. Double layer capacitance (C_{dl}) for the MoP electrocatalyst is measured and displayed in Figure 3.4b, 0.17 mF. Likewise, the stability test is carried out for MoPN1 and MoPN2 electrocatalysts. For MoPN2, the longest stability for the catalytic HER performance is recorded. Cyclic voltammetry in the same range of (20-200 mV s^{-1}) scanning rates is performed at three times with 24 h intervals. Figure 3.4c-e shows these three CVs which are noted by purple, green, and orange colors in figure 5a during the stability test for MoPN2 to realize the change of double layer capacitance. The plots and measured double layer capacitances (C_{dl}) for these three intervals are displayed with the same color in Figure 3.4b. As it is evident, C_{dl} increases significantly for t=24 and 48 h. The expansion in CVs with time and obtained C_{dl} indicates that the electrochemical surface area (ECSA) increases during catalytic HER performance. Figure 3.4b shows that the C_{dl} for MoPN2 varies from 10.4 to 32.5 mF. It seems there can be a connection between surface reconstruction and variation in double layer capacitance in certain electrochemical systems. In fact, C_{dl} is related to the charge accumulation at the interface between an electrode and an electrolyte. It is influenced by the surface properties of the electrode, including its structure, composition, and active sites. Surface reconstruction refers to the rearrangement of atoms or molecules on the surface of a material, leading to changes in its surface structure and morphology. This phenomenon can occur due to various factors, such as chemical reactions, adsorption/desorption processes, or exposure to reactive species.

The variation in double layer capacitance can be attributed to surface reconstruction for several reasons, such as surface area changes, active sites exposure, surface coverage, and electrolyte accessibility. Surface reconstruction can lead to changes in the surface area and roughness of the electrode. An increase in surface area can result in a higher double layer capacitance due to more available sites for charge accumulation. Surface reconstruction might also expose new active sites or alter the distribution of existing active sites on the electrode surface. This can affect the kinetics of charge transfer processes at the electrode-electrolyte interface and influence the double layer capacitance. In addition, some surface reconstruction processes may result in the formation of new adsorbates or species on the electrode surface. These adsorbates can affect the electric double layer formation and alter the double layer capacitance. It worth noting that changes in surface reconstruction can modify the accessibility of the electrolyte to the electrode surface. This can impact ion diffusion and charge accumulation in the electric double layer, leading to variations in double layer capacitance. The relationship between surface reconstruction and variation in double layer capacitance is a complex and active area of research, particularly in the field of electrocatalysis and energy storage materials. Experimental techniques like electrochemical impedance spectroscopy (EIS) are valuable tools to study and quantify these effects.

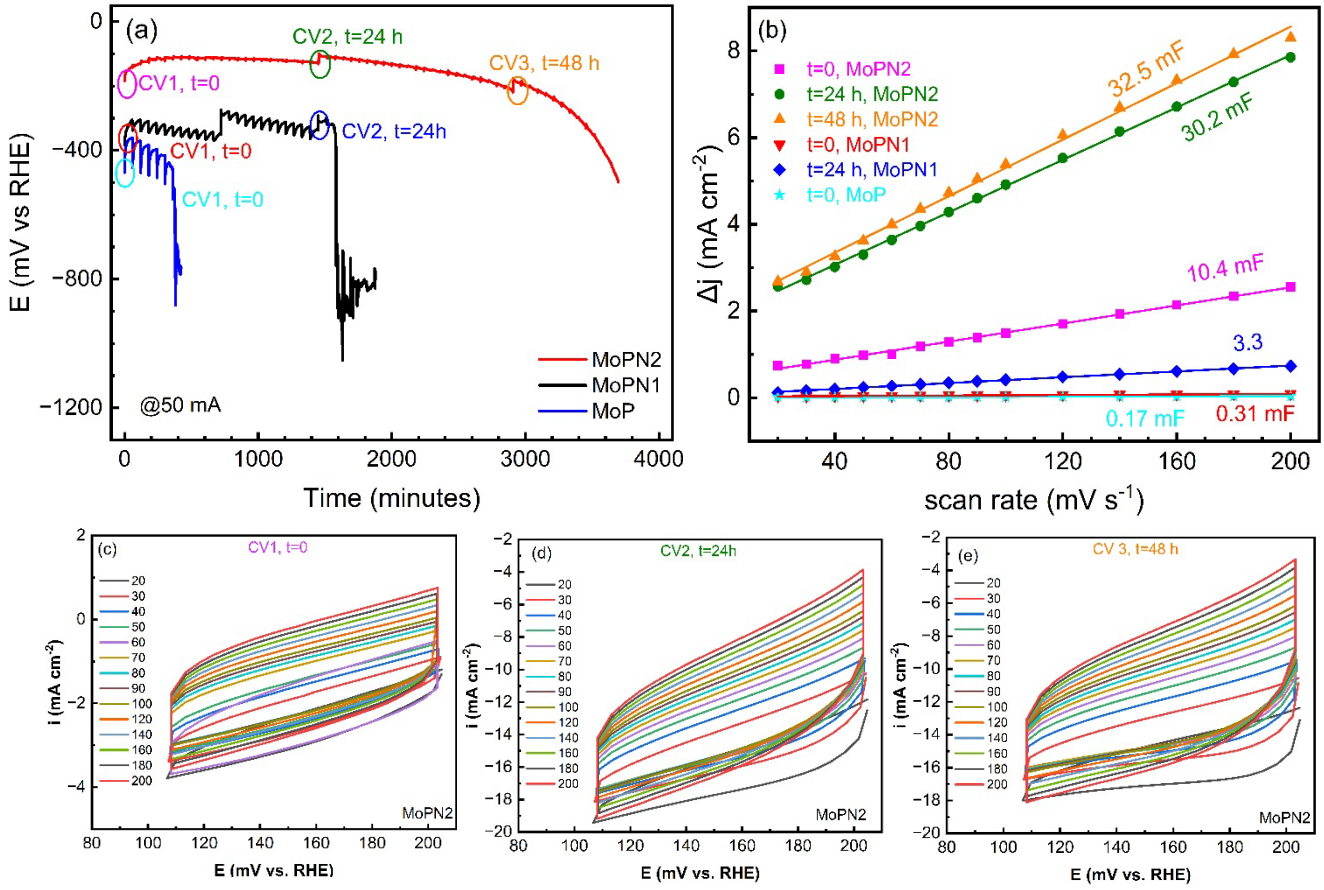

Figure 3-14: (a) Chronopotentiometry of the developed catalysts MoPN2, MoPN1, MoP at 50 mA, (b) double-layer capacitance (C_{dl}) plot of the catalysts corresponding to the stability time, (c-e) cyclic voltammetry of the MoPN2 catalyst at t=0, 24, and 48 h corresponding to the stability time.

Operando electrochemical impedance spectroscopy (EIS) offers several significant advantages in the assessment of the stability of HER electrocatalysts. Operando EIS allows for the real-time monitoring of the electrochemical performance of the HER electrocatalyst during the catalytic reaction. This provides valuable insights into the dynamic changes in the catalyst's behavior, which are not captured in static ex situ measurements. It enables us to observe the catalyst's stability under realistic operating conditions, which is crucial for evaluating its long-term performance. By continuously monitoring the impedance response during HER, operando EIS can

identify changes in the electrochemical behavior that may indicate degradation mechanisms or poisoning effects. This information is essential for understanding catalyst deactivation and designing more stable materials. Operando EIS provides mechanistic insights into the electrochemical processes occurring at the catalyst-electrolyte interface during HER. This deeper understanding can lead to the design of improved catalysts with enhanced stability and activity.

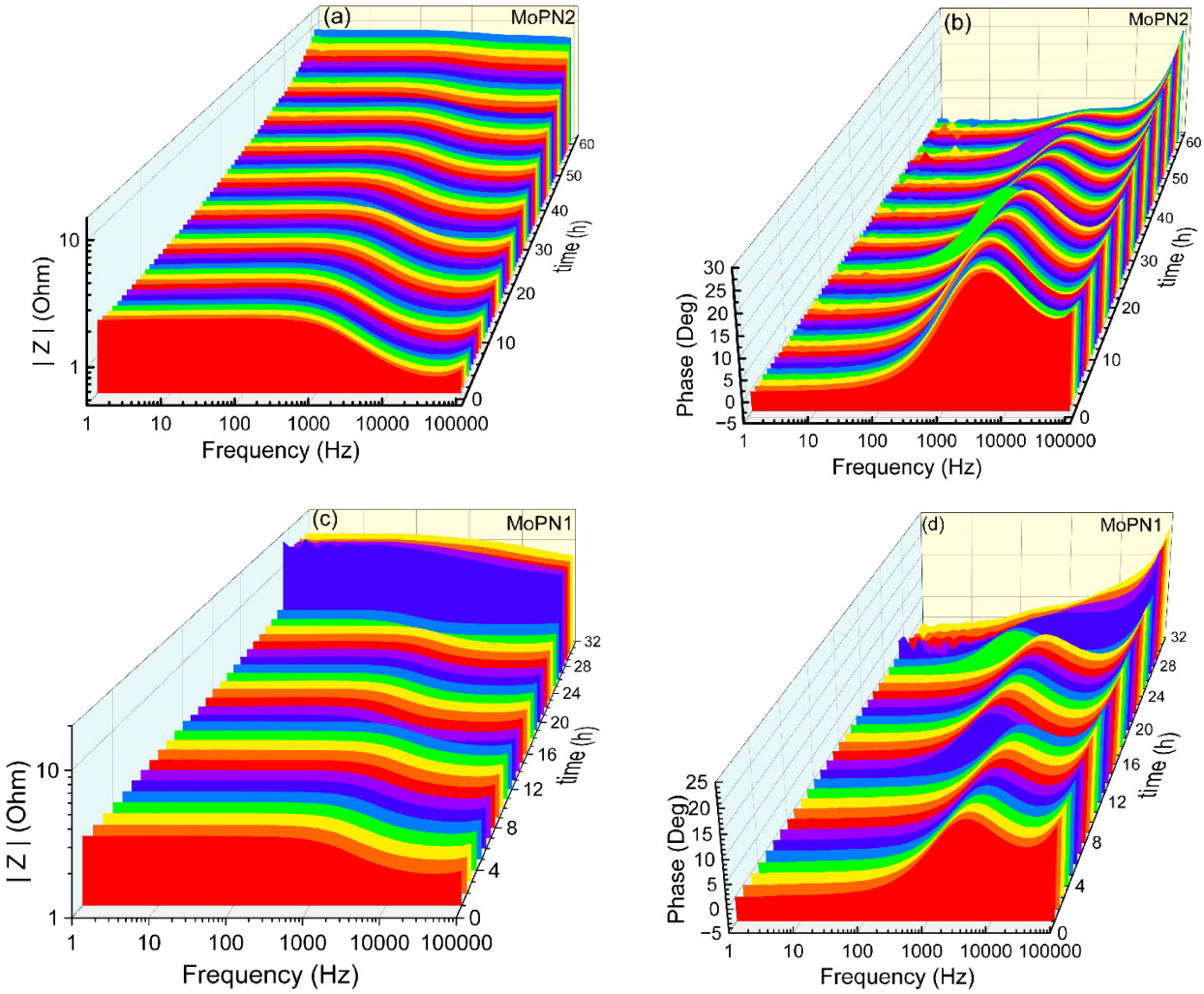

Figure 3-15: Operando EIS illustrating by Bode Z and Bode phase graphs.

Operando EIS results are shown in Figure 3-5. The 3D profile of Bode |Z| changes with time in Figure 3.5a, c provides valuable information from changing the resistance of MoPN2

electrocatalysts with time. The gradual increase during catalytic activity indicates the degradation occurs with increasing resistance at higher frequencies where the charge transfer resistance controls the EIS behavior.

Chapter 4: Conclusion and Summary of Research

Comprehensive studies performed on using transition metal phosphides for electrocatalyst applications to find a sustainable path for the future energy. Herein, the relationship between the structure and high electrocatalytic performance for TMPs is discussed. Although rapid progress has been made for TMPs to develop versatile catalysts, detailed information of reaction mechanisms and clear classification of strategies to facilitate catalytic activity is generally inadequate. Despite the increasing number of research efforts, there are numerous opportunities and challenges in the fabrication of TMPs with enhanced performance. While a deeper understanding of the influence of processing parameters on the growth and phase warrants continued efforts, there can be more interesting ways to improve the catalytic performance of TMPs by doping. Therefore, the effect of nonmetal doping on the structure and electrocatalytic performance will be interesting to design efficient catalysts. Although there are some efforts already in the literature, a more detailed account of such doping-induced effects is necessary, and further investigation is warranted. Studies in this dissertation can lead to a safe, simple, sustainable, and large-scale fabrication of TMPs. The use of innovative approaches in fabrication strategies opens new avenues for TMPs.

First, we demonstrate a controllable phospho-sulfidation process to synthesize the Ni_5P_4-Ni_2P/NiS (plates/nanosheets) electrocatalyst with abundant epitaxial heterointerfaces for hydrogen production. A regional prickly pear cactus with plentiful surface area motivates this study to design a synthesis strategy that led constructing a 3D heterostructure electrocatalyst with an abundant active catalytic area and enhanced intrinsic catalytic activity. We rationally employ an ultrathin nickel mesh to facilitate a uniform phase transformation and support spatial freedom for departing produced hydrogen. After the phosphidation process, the Ni_5P_4 and Ni_2P structures, known for their outstanding HER performance, form simultaneously on the mesh surface with two surface

features, protrusions and vertically aligned plates. We realize that Ni_5P_4 and Ni_2P phases coexist in the vertical plates, making nanoscale heterointerfaces and reinforcing electrical connectivity. After the sulfidation process, the epitaxial NiS nanosheets nucleate and grow primarily at the edges, kinks, or steps observed on the facets of the Ni_5P_4-Ni_2P plates. The *in-situ* epitaxial interfaces nucleate at the root of the NiS nanosheets interfacing with the Ni_2P phase and induce the heterointerfaces formation. We deduce that the electrochemical surface area (ECSA) expansion and intrinsic catalytic activity enhancement are the two influential factors optimizing the Ni_5P_4-Ni_2P/NiS electrocatalytic performance. The electrochemical studies, including EIS and CV analyses, verify the importance of emerging heterostructures in reinforcing electron mobility and stability at higher overpotentials. Our findings emphasize the importance of the successful growth of epitaxial nanosheets in improving electrocatalytic activities of the Ni_5P_4-Ni_2P/NiS heterostructures.

Second, the heterostructured electrocatalyst of MoP-Mo_2N@Mo are synthesized in a one-step phospho-nitriding process. The 3D structure and heterostructure of the catalysts participate in durability and stability of the electrocatalyst in longer time. The catalytic performance shows a low overpotential of 65 and 180 mV to attain the current density of 10 and 100 mA cm^{2-}, where the Tafel slope also indicates enhancing the intrinsic catalytic activity of MoP-Mo_2N@Mo electrocatalyst. The stability test indicates longer durability of electrocatalyst and gradual degradation of the catalyst with increasing resistance at higher frequencies.

Chapter 5: Future Directions

Hydrogen has emerged as a promising energy carrier for a sustainable and carbon-neutral future. As the world seeks to transition away from fossil fuels and reduce greenhouse gas emissions, hydrogen production through electrolysis has gained significant attention as a clean and efficient pathway. Transition metal-based electrocatalysts play a crucial role in enabling the hydrogen evolution reaction (HER) during electrolysis, providing efficient and cost-effective solutions. In this review, we delve into the future of hydrogen production for energy conversion and explore the current and potential role of transition metal-based electrocatalysts in driving this transformative energy landscape. The need for sustainable energy solutions has become more urgent than ever before, and hydrogen production is poised to play a pivotal role in the transition to a low-carbon economy. Electrolytic hydrogen generation via the hydrogen evolution reaction (HER) presents an attractive avenue for clean and renewable hydrogen production. Transition metal-based electrocatalysts, such as molybdenum, nickel, cobalt, and iron-based materials, have shown remarkable activity and stability in catalyzing the HER.

Hydrogen is envisioned as a versatile energy carrier that can facilitate the integration of renewable energy sources into various sectors, such as transportation, industry, and power generation. As the world strives to reduce carbon emissions and combat climate change, the demand for clean and sustainable energy solutions has surged. Hydrogen production through electrolysis offers a pathway to produce hydrogen using renewable electricity from sources like solar, wind, and hydropower. This "green" hydrogen can be harnessed for various applications, including fuel cells for transportation and stationary power, industrial processes, and energy storage. The hydrogen evolution reaction (HER) is a critical process in water electrolysis, where water molecules are split into hydrogen and oxygen gases. Transition metal-based electrocatalysts

have emerged as promising candidates for catalyzing the HER due to their high activity and stability. Materials like molybdenum phosphides, nickel phosphides, cobalt-based alloys, and others have shown remarkable performance in promoting the HER. These electrocatalysts exhibit unique electronic structures and surface properties that enhance the adsorption and activation of reaction intermediates, thus reducing the energy barrier for hydrogen production. Despite the progress in HER electrocatalysis, several challenges need to be addressed to enable large-scale hydrogen production with transition metal-based electrocatalysts:

a. Cost: Some transition metal-based materials, such as noble metals, can be expensive, hindering their commercial viability for widespread adoption. Efforts are being made to develop catalysts using earth-abundant elements to reduce costs.

b. Scalability: Transition metal-based electrocatalysts need to be synthesized and integrated into large-scale electrolyzer systems efficiently. Scalability is crucial to ensure cost-effective and continuous hydrogen production.

c. Long-term Stability: The durability of electrocatalysts is critical for long-term operation. Catalyst degradation and poisoning over time can lead to reduced efficiency and increased operational costs.

d. Catalyst Performance: While some transition metal-based electrocatalysts show promising activity under controlled laboratory conditions, their performance may vary in real-world environments, necessitating further optimization and understanding of catalyst behavior under different operating conditions.

To fully unlock the potential of hydrogen as a clean energy carrier, extensive research and development efforts are ongoing to address the aforementioned challenges. Researchers are focusing on:

a. Novel Catalyst Designs: Scientists are exploring innovative approaches to designing transition metal-based electrocatalysts with enhanced activity, selectivity, and stability. This includes advanced synthesis methods, defect engineering, and nanostructuring techniques.

b. Single-Atom Catalysis: Single-atom catalysts have emerged as a fascinating area of research, offering superior catalytic activity and atom efficiency. Researchers are investigating the potential of single-atom transition metal-based electrocatalysts for efficient HER.

c. Heteroatom Doping: Introducing heteroatoms into the catalyst structure can alter its electronic properties and enhance the catalytic activity for the HER. This avenue holds promise for developing high-performance electrocatalysts.

d. Advanced Characterization Techniques: In-depth characterization techniques, such as operando spectroscopy and in situ microscopy, are employed to gain insights into the catalyst's behavior during the HER under realistic operating conditions.

Transition metal-based electrocatalysts not only play a significant role in HER but also find application in other electrochemical processes, such as oxygen evolution reaction (OER) for water splitting and CO2 reduction for renewable fuels and chemical synthesis. Their versatility and tunability make them valuable tools for advancing sustainable energy conversion technologies.

The future of hydrogen production for energy conversion looks promising, and transition metal-based electrocatalysts are poised to be integral to this transformation. As research continues to advance the field of HER electrocatalysis, it is essential to address challenges related to cost, scalability, and long-term stability. The ongoing efforts in catalyst design, coupled with advancements in characterization techniques, will pave the way for efficient and sustainable hydrogen production, contributing to a cleaner and greener energy future.

References

Ahmed, Shams Forruque, M. Mofijur, Samiha Nuzhat, Nazifa Rafa, Afla Musharrat, Su Shiung Lam, and Alberto Boretti. 2022. "Sustainable Hydrogen Production: Technological Advancements and Economic Analysis." *International Journal of Hydrogen Energy* 47 (88): 37227–55. https://doi.org/10.1016/J.IJHYDENE.2021.12.029.

Amanda E. Henkes, and Yolanda Vasquez, and Raymond E. Schaak. 2007. "Converting Metals into Phosphides: A General Strategy for the Synthesis of Metal Phosphide Nanocrystals." *Journal of the American Chemical Society* 129 (7): 1896–97. https://doi.org/10.1021/JA068502L.

An, Li, Jianrui Feng, Yu Zhang, Rui Wang, Hanwen Liu, Gui-Chang Wang, Fangyi Cheng, et al. 2019. "Epitaxial Heterogeneous Interfaces on N-NiMoO4/NiS2 Nanowires/Nanosheets to Boost Hydrogen and Oxygen Production for Overall Water Splitting." *Advanced Functional Materials* 29 (1): 1805298. https://doi.org/10.1002/ADFM.201805298.

Anantharaj Sengeni, and Suguru Noda. 2020. "Appropriate Use of Electrochemical Impedance Spectroscopy in Water Splitting Electrocatalysis." *ChemElectroChem* 7 (10): 2297–2308. https://doi.org/10.1002/CELC.202000515.

Anantharaj Sengeni, Suguru Noda, Vasanth Rajendiran Jothi, Sung Chul Yi, Matthias Driess, and Prashanth W. Menezes. 2021. "Strategies and Perspectives to Catch the Missing Pieces in Energy-Efficient Hydrogen Evolution Reaction in Alkaline Media." *Angewandte Chemie International Edition* 60 (35): 18981–6. https://doi.org/10.1002/ANIE.202015738.

Ping, Liu, and José A. Rodriguez. 2005. "Catalysts for Hydrogen Evolution from the [NiFe] Hydrogenase to the Ni2P(001) Surface: The Importance of Ensemble Effect." *Journal of the American Chemical Society* 127 (42): 14871–78. https://doi.org/10.1021/JA0540019.

Anjum, Mohsin Ali Raza, Mahesh Datt Bhatt, Min Hee Lee, and Jae Sung Lee. 2018. "Sulfur-Doped Dicobalt Phosphide Outperforming Precious Metals as a Bifunctional Electrocatalyst for Alkaline Water Electrolysis." *Chemistry of Materials* 30 (24): 8861–70. https://doi.org/10.1021/ACS.CHEMMATER.8B03908.

Attarzadeh, Navid, Ravindra Nuggehalli, and C. V. Ramana. 2022. "Application of Transition Metal Phosphides to Electrocatalysis: An Overview." *JOM* 74 (2): 381–95. https://doi.org/10.1007/S11837-021-05058-2/FIGURES/10.

Attarzadeh, Navid, Debabrata Das, Srija N. Chintalapalle, Susheng Tan, V. Shutthanandan, and C. V. Ramana. 2023. "Nature-Inspired Design of Nano-Architecture-Aligned Ni5P4-Ni2P/NiS Arrays for Enhanced Electrocatalytic Activity of Hydrogen Evolution Reaction (HER)." *ACS Applied Materials and Interfaces* 15. https://doi.org/10.1021/ACSAMI.3C00781.

Bae, Seok Hu, Ji Eun Kim, Hyacinthe Randriamahazaka, Song Yi Moon, Jeong Young Park, and Il Kwon Oh. 2017. "Seamlessly Conductive 3D Nanoarchitecture of Core–Shell Ni-Co Nanowire Network for Highly Efficient Oxygen Evolution." *Advanced Energy Materials* 7 (1): 1601492. https://doi.org/10.1002/AENM.201601492.

Bai, Ningning, Qing Li, Daoyong Mao, Daikun Li, and Hongzhou Dong. 2016. "One-Step Electrodeposition of Co/CoP Film on Ni Foam for Efficient Hydrogen Evolution in Alkaline Solution." *ACS Applied Materials and Interfaces* 8 (43): 29400–407. https://doi.org/10.1021/ACSAMI.6B07785.

Browne, Michelle P, Zdeněk Sofer, and Martin Pumera. 2019. "Layered and Two-Dimensional Metal Oxides for Electrochemical Energy Conversion." *Energy & Environmental Science* 12 (1): 41–58. https://doi.org/10.1039/C8EE02495B.

C.V., Ramana, S. Utsunomiya, R. C. Ewing, and C. M. Julien, and U. Becker. 2006. “Structural Stability and Phase Transitions in WO3 Thin Films.” *Journal of Physical Chemistry B* 110 (21): 10430–35. https://doi.org/10.1021/JP056664I.

C. V., Ramana, A. Ait-Salah, S. Utsunomiya, U. Backer, A. Mauger, F. Gendron, and C. M. Julien. 2006. “Structural Characteristics of Lithium Nickel Phosphate Studied Using Analytical Electron Microscopy and Raman Spectroscopy.” *Chemistry of Materials* 18 (16): 3788–94. https://doi.org/10.1021/CM061137C.

C. V., Ramana, Mallesham Bandi, Aruna N Nair, Felicia S. Manciu, Sreeprasad Sreenivasan, and Vaithiyalingam Shutthanandan. 2021. “Electronic Structure, Chemical Bonding, and Electrocatalytic Activity of Ba(Fe0.7Ta0.3)O3-ΔCompounds.” *ACS Applied Energy Materials* 4 (2): 1313–22. https://doi.org/10.1021/ACSAEM.0C02548.

C. V., Ramana, A. Mauger, and C. M. Julien. 2021. “Growth, Characterization and Performance of Bulk and Nanoengineered Molybdenum Oxides for Electrochemical Energy Storage and Conversion.” *Progress in Crystal Growth and Characterization of Materials* 67 (3): 100533. https://doi.org/10.1016/J.PCRYSGROW.2021.100533.

C. V., Ramana, Swadipta Roy, Vishal Zade, Anil K. Battu, Nanthakishore Makeswaran, and V. Shutthanandan. 2021. “Electronic Structure and Chemical Bonding in Transition-Metal-Mixed Gallium Oxide (Ga2O3) Compounds.” *Journal of Physics and Chemistry of Solids* 157 (October): 110174. https://doi.org/10.1016/J.JPCS.2021.110174.

Cabán-Acevedo, Miguel, Michael L. Stone, J. R. Schmidt, Joseph G. Thomas, Qi Ding, Hung Chih Chang, Meng Lin Tsai, Hau He, and Song Jin. 2015. “Efficient Hydrogen Evolution Catalysis Using Ternary Pyrite-Type Cobalt Phosphosulphide.” *Nature Materials 2015 14:12* 14 (12): 1245–51. https://doi.org/10.1038/nmat4410.

Callejas, Juan F., Carlos G. Read, Christopher W. Roske, Nathan S. Lewis, and Raymond E. Schaak. 2016a. “Synthesis, Characterization, and Properties of Metal Phosphide Catalysts for the Hydrogen-Evolution Reaction.” *Chemistry of Materials* 28 (17): 6017–44. https://doi.org/10.1021/ACS.CHEMMATER.6B02148.

Callejas, Juan F., Carlos G. Read, Christopher W. Roske, Nathan S. Lewis, and Raymond E. Schaak. 2016“Synthesis, Characterization, and Properties of Metal Phosphide Catalysts for the Hydrogen-Evolution Reaction.” *Chemistry of Materials* 28 (17): 6017–44. https://doi.org/10.1021/ACS.CHEMMATER.6B02148.

Calvillo, L., F. Carraro, O. Vozniuk, V. Celorrio, L. Nodari, A. E. Russell, D. Debellis, et al. 2018. “Insights into the Durability of Co–Fe Spinel Oxygen Evolution Electrocatalysts via Operando Studies of the Catalyst Structure.” *Journal of Materials Chemistry A* 6 (16): 7034–41. https://doi.org/10.1039/C7TA10892C.

Cao, Shuai, Ning You, Li Wei, Cheng Huang, Xiaoming Fan, Kun Shi, Zeheng Yang, and Weixin Zhang. 2020. “CoP Microscale Prism-like Superstructure Arrays on Ni Foam as an Efficient Bifunctional Electrocatalyst for Overall Water Splitting.” *Inorganic Chemistry* 59 (12): 8522–31. https://doi.org/10.1021/ACS.INORGCHEM.0C00959.

Chang, Jinfa, Kai Li, Zhijian Wu, Junjie Ge, Changpeng Liu, and Wei Xing. 2018. “Sulfur-Doped Nickel Phosphide Nanoplates Arrays: A Monolithic Electrocatalyst for Efficient Hydrogen Evolution Reactions.” *ACS Applied Materials and Interfaces* 10 (31): 26303–11. https://doi.org/10.1021/ACSAMI.8B08068.

Chang, Jinfa, Liang Liang, Chenyang Li, Minglei Wang, Junjie Ge, Changpeng Liu, and Wei Xing. 2016. “Ultrathin Cobalt Phosphide Nanosheets as Efficient Bifunctional Catalysts for a Water

Electrolysis Cell and the Origin for Cell Performance Degradation." *Green Chemistry* 18 (8): 2287–95. https://doi.org/10.1039/C5GC02899J.

Chen, Tianyun, Shan Qin, Min Qian, Haojiang Dai, Yingyan Fu, Yaqi Zhang, Bo Ye, Qinhan Lin, and Qinghua Yang. 2021a. "Defect-Rich Fe-Doped CoP Nanosheets as Efficient Oxygen Evolution Electrocatalysts." *Energy & Fuels* 35 (13): 10890–97. https://doi.org/10.1021/ACS.ENERGYFUELS.1C01301.

Chen, Tianyun, Shan Qin, Min Qian, Haojiang Dai, Yingyan Fu, Yaqi Zhang, Bo Ye, Qinhan Lin, and Qinghua Yang. 2021. "Defect-Rich Fe-Doped CoP Nanosheets as Efficient Oxygen Evolution Electrocatalysts." *Energy & Fuels* 35 (July): 14. https://doi.org/10.1021/ACS.ENERGYFUELS.1C01301.

Chen, Yuanzhi, Houde She, Xiaohua Luo, Guang Hui Yue, and Dong Liang Peng. 2009. "Solution-Phase Synthesis of Nickel Phosphide Single-Crystalline Nanowires." *Journal of Crystal Growth* 311 (4): 1229–33. https://doi.org/10.1016/J.JCRYSGRO.2008.11.094.

Cheng, Fangyi, Yi Su, Jing Liang, Zhanliang Tao, and Jun Chen. 2009. "MnO2-Based Nanostructures as Catalysts for Electrochemical Oxygen Reduction in Alkaline Media†." *Chemistry of Materials* 22 (3): 898–905. https://doi.org/10.1021/CM901698S.

Cova, Camilla M., Alessio Zuliani, Mario J. Muñoz-Batista, and Rafael Luque. 2018. "A Sustainable Approach for the Synthesis of Catalytically Active Peroxidase-Mimic ZnS Catalysts." *ACS Sustainable Chemistry & Engineering* 7 (1): 1300–1307. https://doi.org/10.1021/ACSSUSCHEMENG.8B04968.

Chen, Xinhong, Qing Li, Qijun Che, Yashi Chen, Ya Tan, and Xi Xu. 2019. "Self-Supported Ni/NiSPx Microdendrite Structure for Highly Efficient and Stable Overall Water Splitting in

Simulated Industrial Environment." *ACS Sustainable Chemistry and Engineering* 7 (13): 11778–86. https://doi.org/10.1021/ACSSUSCHEMENG.9B02061.

Dai, Zhengfei, Hongbo Geng, Jiong Wang, Yubo Luo, Bing Li, Yun Zong, Jun Yang, et al. 2017. "Hexagonal-Phase Cobalt Monophosphosulfide for Highly Efficient Overall Water Splitting." *ACS Nano* 11 (11): 11031–40. https://doi.org/10.1021/ACSNANO.7B05050.

Dang, Yanliu, Junkai He, Tianli Wu, Linping Yu, Peter Kerns, Liaoyong Wen, Jing Ouyang, and Steven L. Suib. 2019. "Constructing Bifunctional 3D Holey and Ultrathin CoP Nanosheets for Efficient Overall Water Splitting." *ACS Applied Materials & Interfaces* 11 (33): 29879–87. https://doi.org/10.1021/ACSAMI.9B08238.

Danielsen, Hilmar K., John Hald, Flemming B. Grumsen, and Marcel A.J. Somers. 2006. "On the Crystal Structure OfZ-Phase Cr(V,Nb)N." *Metallurgical and Materials Transactions A 2006 37:9* 37 (9): 2633–40. https://doi.org/10.1007/BF02586098.

Doan-Nguyen, Vicky V. T., Sen Zhang, Edward B. Trigg, Rahul Agarwal, Jing Li, Dong Su, Karen I. Winey, and Christopher B. Murray. 2015. "Synthesis and X-Ray Characterization of Cobalt Phosphide (Co2P) Nanorods for the Oxygen Reduction Reaction." *ACS Nano* 9 (8): 8108–15. https://doi.org/10.1021/ACSNANO.5B02191.

Dong, Youzhen, Yongmin Wu, Mengjia Liu, and Jinghong Li. 2013. "Electrocatalysis on Shape-Controlled Titanium Nitride Nanocrystals for the Oxygen Reduction Reaction." *ChemSusChem* 6 (10): 2016–21. https://doi.org/10.1002/CSSC.201300331.

Du, Cuicui, Mengxiang Shang, Jianxin Mao, and Wenbo Song. 2017. "Hierarchical MoP/Ni2P Heterostructures on Nickel Foam for Efficient Water Splitting." *Journal of Materials Chemistry A* 5 (30): 15940–49. https://doi.org/10.1039/C7TA03669H.

Duan, Jingjing, Sheng Chen, and Chuan Zhao. 2018. “Strained Nickel Phosphide Nanosheet Array.” *ACS Applied Materials and Interfaces* 10 (36): 30029–34. https://doi.org/10.1021/ACSAMI.8B09147.

Fang, Liang, Yanping Xie, Peiyin Guo, Jingpei Zhu, Shuhui Xiao, Shujie Sun, Wei Zi, and Hongbin Zhao. 2021. “In Situ Formation of Highly Exposed NiPS3 Nanosheets on Nickel Foam as an Efficient 3D Electrocatalyst for Overall Water Splitting.” *Sustainable Energy & Fuels* 5 (9): 2537–44. https://doi.org/10.1039/D1SE00110H.

Fang, Zhiwei, Lele Peng, Yumin Qian, Xiao Zhang, Yujun Xie, Judy J. Cha, and Guihua Yu. 2018. “Dual Tuning of Ni–Co–A (A = P, Se, O) Nanosheets by Anion Substitution and Holey Engineering for Efficient Hydrogen Evolution.” *Journal of the American Chemical Society* 140 (15): 5241–47. https://doi.org/10.1021/JACS.8B01548.

Fang, Liang, Yanping Xie, Peiyin Guo, Jingpei Zhu, Shuhui Xiao, Shujie Sun, Wei Zi, and Hongbin Zhao. 2021. “In Situ Formation of Highly Exposed NiPS3 Nanosheets on Nickel Foam as an Efficient 3D Electrocatalyst for Overall Water Splitting.” *Sustainable Energy & Fuels* 5 (9): 2537–44. https://doi.org/10.1039/D1SE00110H.

Feng, Ligang, Heron Vrubel, Michaël Bensimon, and Xile Hu. 2014. “Easily-Prepared Dinickel Phosphide (Ni2P) Nanoparticles as an Efficient and Robust Electrocatalyst for Hydrogen Evolution.” *Physical Chemistry Chemical Physics* 16 (13): 5917–21. https://doi.org/10.1039/C4CP00482E.

Gao, Shiyuan, Ali Zavabeti, Bin Wang, Rui Ren, Chunhui Yang, Zhongqing Liu, and Yichao Wang. 2021a. “Nickel Phosphides Electrodeposited on TiO2 Nanotube Arrays as Electrocatalysts for Hydrogen Evolution.” *ACS Applied Nano Materials* 4 (5): 4542–51. https://doi.org/10.1021/ACSANM.1C00134.

Grünert, Wolfgang, Aleksander Yu Stakheev, Reinhard Feldhaus, Klaus Anders, Efim S. Shpiro, and Khabib M. Minachev. 1991. "Analysis of Mo(3d) XPS Spectra of Supported Mo Catalysts: An Alternative Approach." *Journal of Physical Chemistry* 95 (3): 1323–28. https://doi.org/10.1021/J100156A054/ASSET/J100156A054.FP.PNG_V03.

Gu, Ying, Aiping Wu, Yanqing Jiao, Huiru Zheng, Xueqi Wang, Ying Xie, Lei Wang, Chungui Tian, and Honggang Fu. 2021. "Two-Dimensional Porous Molybdenum Phosphide/Nitride Heterojunction Nanosheets for PH-Universal Hydrogen Evolution Reaction." *Angewandte Chemie* 133 (12): 6747–55. https://doi.org/10.1002/ANGE.202016102.

Guo, Yanru, Chunmei Zhang, Yong Wu, Hongen Yu, Shaojun Zhang, Aijun Du, Kostya (Ken) Ostrikov, Jie Zheng, and Xingguo Li. 2020. "Direct Conversion of Metal Organic Frameworks into Ultrafine Phosphide Nanocomposites in Multicomponent Plasma for Wide PH Hydrogen Evolution." *Journal of Materials Chemistry A* 8 (20): 10402–8. https://doi.org/10.1039/D0TA02768E.

Habelitz, S., T. Höche, R. Hergt, G. Carl, and C. Rüssel. 1999. "Microstructural Design through Epitaxial Growth in Extruded Mica Glass-Ceramics." *Acta Materialia* 47 (9): 2831–40. https://doi.org/10.1016/S1359-6454(99)00135-4.

Halim, Joseph, Sankalp Kota, Maria R Lukatskaya, Michael Naguib, Meng-Qiang Zhao, Eun Ju Moon, Jeremy Pitock, et al. 2016. "Synthesis and Characterization of 2D Molybdenum Carbide (MXene)." *Advanced Functional Materials* 26 (18): 3118–27. https://doi.org/10.1002/ADFM.201505328.

Han, Yechuang, Pengfei Li, Zhenfei Tian, Chao Zhang, Yixing Ye, Xiaoguang Zhu, and Changhao Liang. 2019. "Molybdenum-Doped Porous Cobalt Phosphide Nanosheets for Efficient Alkaline

Hydrogen Evolution." *ACS Applied Energy Materials* 2 (9): 6302–10. https://doi.org/10.1021/ACSAEM.9B00924.

He, Maoxiao, Chuanqi Feng, Ting Liao, Shengnan Hu, Huimin Wu, and Ziqi Sun. 2020. "Low-Cost Ni2P/Ni0.96S Heterostructured Bifunctional Electrocatalyst toward Highly Efficient Overall Urea-Water Electrolysis." *ACS Applied Materials and Interfaces* 12 (2): 2225–33. https://doi.org/10.1021/ACSAMI.9B14350.

Hu, Cun, Jinguang Cai, Shuai Liu, Chao Lv, Junhong Luo, Ming Duan, Changan Chen, et al. 2020. "General Strategy for Preparation of Porous Nickel Phosphide Nanosheets on Arbitrary Substrates toward Efficient Hydrogen Generation." *ACS Applied Energy Materials* 3 (1): 1036–45. https://doi.org/10.1021.

Hu, Zehua, Zhangting Wu, Cheng Han, Jun He, Zhenhua Ni, and Wei Chen. 2018. "Two-Dimensional Transition Metal Dichalcogenides: Interface and Defect Engineering." *Chemical Society Reviews* 47 (9): 3100–3128. https://doi.org/10.1039/C8CS00024G.

Huang, Kuo-Yen, Yi-Hsiang Luo, Hsin-Ming Cheng, al -, Hanlin Guo, Rui Zhou, Xu Li, et al. 2020. "Flower-like S-Doped-Ni2P Mesoporous Nanosheet-Derived Self-Standing Electrocatalytic Electrode for Boosting Hydrogen Evolution." *Nanotechnology* 31 (46): 465401. https://doi.org/10.1088/1361-6528/ABAD5D.

Hu, Cun, Jinguang Cai, Shuai Liu, Chao Lv, Junhong Luo, Ming Duan, Changan Chen, et al. 2020. "General Strategy for Preparation of Porous Nickel Phosphide Nanosheets on Arbitrary Substrates toward Efficient Hydrogen Generation." *ACS Applied Energy Materials* 3 (1): 1036–45. https://doi.org/10.1021/ACSAEM.9B02067.

Hu, Zehua, Zhangting Wu, Cheng Han, Jun He, Zhenhua Ni, and Wei Chen. 2018. “Two-Dimensional Transition Metal Dichalcogenides: Interface and Defect Engineering.” *Chemical Society Reviews* 47 (9): 3100–3128. https://doi.org/10.1039/C8CS00024G.

Hülsey, Max J., Chia Wei Lim, and Ning Yan. 2020. “Promoting Heterogeneous Catalysis beyond Catalyst Design.” *Chemical Science* 11 (6): 1456–68. https://doi.org/10.1039/C9SC05947D.

Ji, Pengxia, Xu Luo, Ding Chen, Huihui Jin, Zonghua Pu, Weihao Zeng, Jianwei He, Huawei Bai, Yucong Liao, and Shichun Mu 2020b. “Significantly Improved Water Oxidation of CoP Catalysts by Electrochemical Activation.” *ACS Sustainable Chemistry and Engineering* 8 (48): 17851–59. https://doi.org/10.1021/ACSSUSCHEMENG.0C07169

Jiang, Hongliang, Qun He, Youkui Zhang, and Li Song. 2018. “Structural Self-Reconstruction of Catalysts in Electrocatalysis.” *Accounts of Chemical Research* 51 (11): 2968–77. https://doi.org/10.1021/ACS.ACCOUNTS.8B00449.

Jiang, Deli, Yan Xu, Rong Yang, Di Li, Suci Meng, and Min Chen. 2019. “CoP3/CoMoP Heterogeneous Nanosheet Arrays as Robust Electrocatalyst for PH-Universal Hydrogen Evolution Reaction.” *ACS Sustainable Chemistry & Engineering*. https://doi.org/10.1021/ACSSUSCHEMENG.9B00357.

Jiang, Kun, Samira Siahrostami, Tingting Zheng, Yongfeng Hu, Sooyeon Hwang, Eli Stavitski, Yande Peng, et al. 2018. “Isolated Ni Single Atoms in Graphene Nanosheets for High-Performance CO2 Reduction.” *Energy & Environmental Science* 11 (4): 893–903. https://doi.org/10.1039/C7EE03245E.

Jiang, Ping, Qian Liu, Yanhui Liang, Jingqi Tian, Abdullah M. Asiri, and Xuping Sun. 2014. “A Cost-Effective 3D Hydrogen Evolution Cathode with High Catalytic Activity: FeP Nanowire

Array as the Active Phase." *Angewandte Chemie International Edition* 53 (47): 12855–59. https://doi.org/10.1002/ANIE.201406848.

Jiang, Ping, Qian Liu, and Xuping Sun. 2014. "NiP2 Nanosheet Arrays Supported on Carbon Cloth: An Efficient 3D Hydrogen Evolution Cathode in Both Acidic and Alkaline Solutions." *Nanoscale* 6 (22): 13440–45. https://doi.org/10.1039/C4NR04866K.

Kibsgaard, Jakob, Thomas F Jaramillo, J Kibsgaard, and T F Jaramillo. 2014. "Molybdenum Phosphosulfide: An Active, Acid-Stable, Earth-Abundant Catalyst for the Hydrogen Evolution Reaction." *Angewandte Chemie* 126 (52): 14661–65. https://doi.org/10.1002/ANGE.201408222.

Kibsgaard, Jakob, Charlie Tsai, Karen Chan, Jesse D. Benck, Jens K. Nørskov, Frank Abild-Pedersen, and Thomas F. Jaramillo. 2015. "Designing an Improved Transition Metal Phosphide Catalyst for Hydrogen Evolution Using Experimental and Theoretical Trends." *Energy & Environmental Science* 8 (10): 3022–29. https://doi.org/10.1039/C5EE02179K.

Kibler, Ludwig A. 2006. "Hydrogen Electrocatalysis." *ChemPhysChem* 7 (5): 985–91. https://doi.org/10.1002/CPHC.200500646.

Kim, Jooyoung, Junhyeong Kim, Hyunki Kim, and Sang Hyun Ahn. 2019. "Nanoporous Nickel Phosphide Cathode for a High-Performance Proton Exchange Membrane Water Electrolyzer." *ACS Applied Materials & Interfaces* 11 (34): 30774–85. https://doi.org/10.1021/ACSAMI.9B08074.

Kong, Desheng, Haotian Wang, Judy J. Cha, Mauro Pasta, Kristie J. Koski, Jie Yao, and Yi Cui. 2013. "Synthesis of MoS2 and MoSe2 Films with Vertically Aligned Layers." *Nano Letters* 13 (3): 1341–47. https://doi.org/10.1021/NL400258T.

Laursen, A. B., K. R. Patraju, M. J. Whitaker, M. Retuerto, T. Sarkar, N. Yao, K. v. Ramanujachary, M. Greenblatt, and G. C. Dismukes. 2015. "Nanocrystalline Ni5P4: A Hydrogen Evolution

Electrocatalyst of Exceptional Efficiency in Both Alkaline and Acidic Media." *Energy & Environmental Science* 8 (3): 1027–34. https://doi.org/10.1039/C4EE02940B.

Laursen, Anders B., Robert B. Wexler, Marianna J. Whitaker, Edward J. Izett, Karin U. D. Calvinho, Shinjae Hwang, Ross Rucker, et al. 2018. "Climbing the Volcano of Electrocatalytic Activity While Avoiding Catalyst Corrosion: Ni3P, a Hydrogen Evolution Electrocatalyst Stable in Both Acid and Alkali." *ACS Catalysis* 8 (5): 4408–19. https://doi.org/10.1021/ACSCATAL.7B04466.

Ledendecker, Marc, Sandra Krick Calderón, Christian Papp, Hans-Peter Steinrück, Markus Antonietti, and Menny Shalom. 2015. "The Synthesis of Nanostructured Ni5P4 Films and Their Use as a Non-Noble Bifunctional Electrocatalyst for Full Water Splitting." *Angewandte Chemie International Edition* 54 (42): 12361–65. https://doi.org/10.1002/ANIE.201502438.

Li, Fu Min, Chenfeng Xia, and Bao Yu Xia. 2022. "Exploration and Insight of Dynamic Structure Evolution for Electrocatalysts." *Accounts of Materials Research*, May. https://doi.org/10.1021/ACCOUNTSMR.2C00261.

Li, Jiayuan, Han Xuan Liu, Wangyan Gou, Mingkai Zhang, Zhaoming Xia, Sai Zhang, Chun Ran Chang, Yuanyuan Ma, and Yongquan Qu. 2019. "Ethylene-Glycol Ligand Environment Facilitates Highly Efficient Hydrogen Evolution of Pt/CoP through Proton Concentration and Hydrogen Spillover." *Energy & Environmental Science* 12 (7): 2298–2304. https://doi.org/10.1039/C9EE00752K.

Liang, Hanfeng, and Husam N. Alshareef. 2017. "A Plasma-Assisted Route to the Rapid Preparation of Transition-Metal Phosphides for Energy Conversion and Storage." *Small Methods* 1 (7): 1700111. https://doi.org/10.1002/SMTD.201700111.

Li, Qinliang, Cailei Yuan, Ting Yu, Lingchang Wang, Gaocan Qi, and Xijun Liu. 2021. "Sulfur Dopant-Enhanced Neutral Hydrogen Evolution Performance in MoO3 Nanosheets." *Nanotechnology* 33 (6): 065701. https://doi.org/10.1088/1361-6528/AC33D2.

Li, Qun, Zhicai Xing, Abdullah M. Asiri, Ping Jiang, Xuping Sun. 2014. "Cobalt Phosphide Nanoparticles Film Growth on Carbon Cloth: A High-Performance Cathode for Electrochemical Hydrogen Evolution." *International Journal of Hydrogen Energy* 39 (30): 16806–11. https://doi.org/10.1016/J.IJHYDENE.2014.08.099.

Li, Yang, Zihao Dong, Lifang Jiao. 2020. "Multifunctional Transition Metal-Based Phosphides in Energy-Related Electrocatalysis." *Advanced Energy Materials* 10 (11): 1902104. https://doi.org/10.1002/AENM.201902104.

Li, Yanguang, Hailiang Wang, Liming Xie, Yongye Liang, Guosong Hong, and Hongjie Dai. 2011. "MoS2 Nanoparticles Grown on Graphene: An Advanced Catalyst for the Hydrogen Evolution Reaction." *Journal of the American Chemical Society* 133 (19): 7296–99. https://doi.org/10.1021/JA201269B.

Li, Xinzhe, Yiyun Fang, Jun Wang, Bin Wei, Kun Qi, Hui Ying Hoh, Qiaoyan Hao, et al. 2019. "High-Yield Electrochemical Production of Large-Sized and Thinly Layered NiPS3 Flakes for Overall Water Splitting." *Small* 15 (30): 1902427. https://doi.org/10.1002/SMLL.201902427.

Liang, Qinghua, Lixiang Zhong, Chengfeng Du, Yubo Luo, Jin Zhao, Yun Zheng, Jianwei Xu, et al. 2019. "Interfacing Epitaxial Dinickel Phosphide to 2D Nickel Thiophosphate Nanosheets for Boosting Electrocatalytic Water Splitting." *ACS Nano* 13 (7): 7975–84. https://doi.org/10.1021/ACSNANO.9B02510.

Liang, Yanhui, Qian Liu, Abdullah M. Asiri, Xuping Sun, and Yonglan Luo. 2014. “Self-Supported FeP Nanorod Arrays: A Cost-Effective 3D Hydrogen Evolution Cathode with High Catalytic Activity.” *ACS Catalysis* 4 (11): 4065–69. https://doi.org/10.1021/CS501106G.

Liu, Mengjia, Youzhen Dong, Yongmin Wu, Hongbin Feng, and Jinghong Li. 2013. “Titanium Nitride Nanocrystals on Nitrogen-Doped Graphene as an Efficient Electrocatalyst for Oxygen Reduction Reaction.” *Chemistry – A European Journal* 19 (44): 14781–86. https://doi.org/10.1002/CHEM.201302425.

Liu, Qian, Jingqi Tian, Wei Cui, Ping Jiang, Ningyan Cheng, Abdullah M. Asiri, and Xuping Sun. 2014. “Carbon Nanotubes Decorated with CoP Nanocrystals: A Highly Active Non-Noble-Metal Nanohybrid Electrocatalyst for Hydrogen Evolution.” *Angewandte Chemie International Edition* 53 (26): 6710–14. https://doi.org/10.1002/ANIE.201404161.

Liu, Qian, Ziqian Xue, Baoming Jia, Qinglin Liu, Kang Liu, Yiyang Lin, Min Liu, Yinle Li, and Guangqin Li. 2020. “Hierarchical Nanorods of MoS2/MoP Heterojunction for Efficient Electrocatalytic Hydrogen Evolution Reaction.” *Small* 16 (32): 2002482. https://doi.org/10.1002/SMLL.202002482.

Liu, Shuai, Cun Hu, Chao Lv, Jinguang Cai, Ming Duan, Junhong Luo, Jiangfeng Song, et al. 2019. “Facile Preparation of Large-Area Self-Supported Porous Nickel Phosphide Nanosheets for Efficient Electrocatalytic Hydrogen Evolution.” *International Journal of Hydrogen Energy* 44 (33): 17974–84. https://doi.org/10.1016/J.IJHYDENE.2019.05.100.

Liu, Tingting, Lisi Xie, Jianhui Yang, Rongmei Kong, Gu Du, Abdullah M Asiri, Xuping Sun, et al. 2017. “Self-Standing CoP Nanosheets Array: A Three-Dimensional Bifunctional Catalyst Electrode for Overall Water Splitting in Both Neutral and Alkaline Media.” *ChemElectroChem* 4 (8): 1840–45. https://doi.org/10.1002/CELC.201700392.

Liu, Tong, Anran Li, Chengbo Wang, Wei Zhou, Shijie Liu, and Lin Guo. 2018. "Interfacial Electron Transfer of Ni2P–NiP2 Polymorphs Inducing Enhanced Electrochemical Properties." *Advanced Materials* 30 (46): 1803590. https://doi.org/10.1002/ADMA.201803590.

Liu, Wen, Enyuan Hu, Hong Jiang, Yingjie Xiang, Zhe Weng, Min Li, Qi Fan, Xiqian Yu, Eric I. Altman, and Hailiang Wang. 2016. "A Highly Active and Stable Hydrogen Evolution Catalyst Based on Pyrite-Structured Cobalt Phosphosulfide." *Nature Communications 2016 7:1* 7 (1): 1–9. https://doi.org/10.1038/ncomms10771.

Liu, Yaoda, Paranthaman Vijayakumar, Qianyi Liu, Thangavel Sakthivel, Fuyi Chen, and Zhengfei Dai. 2022. "Shining Light on Anion-Mixed Nanocatalysts for Efficient Water Electrolysis: Fundamentals, Progress, and Perspectives." *Nano-Micro Letters 2021 14:1* 14 (1): 1–41. https://doi.org/10.1007/S40820-021-00785-2.

Liu, Yuanyue, Jingjie Wu, Ken P. Hackenberg, Jing Zhang, Y. Morris Wang, Yingchao Yang, Kunttal Keyshar, et al. 2017. "Self-Optimizing, Highly Surface-Active Layered Metal Dichalcogenide Catalysts for Hydrogen Evolution." *Nature Energy 2017 2:9* 2 (9): 1–7. https://doi.org/10.1038/nenergy.2017.127.

Liu, Zhengqing, Kunkun Nie, Xiaoyan Qu, Xinghua Li, Binjie Li, Yanling Yuan, Shaokun Chong, et al. 2022. "General Bottom-Up Colloidal Synthesis of Nano-Monolayer Transition-Metal Dichalcogenides with High 1T′-Phase Purity." *Journal of the American Chemical Society* 144 (11): 4863–73. https://doi.org/10.1021/JACS.1C12379

Loomba, Suraj, Muhammad Waqas Khan, Muhammad Haris, Seyed Mahdi Mousavi, Ali Zavabeti, Kai Xu, Anton Tadich, et al. 2023. "Nitrogen-Doped Porous Nickel Molybdenum Phosphide Sheets for Efficient Seawater Splitting." *Small* 19 (18): 2207310. https://doi.org/10.1002/SMLL.202207310.

Lu, Y., C. D. Gu, X. Ge, H. Zhang, S. Huang, X. Y. Zhao, X. L. Wang, J. P. Tu, and S. X. Mao. 2013. "Growth of Nickel Phosphide Films as Anodes for Lithium-Ion Batteries: Based on a Novel Method for Synthesis of Nickel Films Using Ionic Liquids." *Electrochimica Acta* 112 (December): 212–20. https://doi.org/10.1016/J.ELECTACTA.2013.09.035.

Lukowski, Mark A., Andrew S. Daniel, Fei Meng, Audrey Forticaux, Linsen Li, and Song Jin. 2013. "Enhanced Hydrogen Evolution Catalysis from Chemically Exfoliated Metallic MoS2 Nanosheets." *Journal of the American Chemical Society* 135 (28): 10274–77. https://doi.org/10.1021/JA404523S.

Luna, Phil de, Christopher Hahn, Drew Higgins, Shaffiq A. Jaffer, Thomas F. Jaramillo, and Edward H. Sargent. 2019. "What Would It Take for Renewably Powered Electrosynthesis to Displace Petrochemical Processes?" *Science* 364 (6438). https://doi.org/10.1126/SCIENCE.AAV3506

Luo, Jie, Haiyan Wang, Geng Su, Yulian Tang, Huangqing Liu, Fenyang Tian, and Deliang Li. 2017. "Self-Supported Nickel Phosphosulphide Nanosheets for Highly Efficient and Stable Overall Water Splitting." *Journal of Materials Chemistry A* 5 (28): 14865–72. https://doi.org/10.1039/C7TA02651J.

Lv, Yang and Xianbao Wang. 2017. "Nonprecious Metal Phosphides as Catalysts for Hydrogen Evolution, Oxygen Reduction and Evolution Reactions." *Catalysis Science & Technology* 7 (17): 3676–91. https://doi.org/10.1039/C7CY00715A.

Lv, Yuan, Yuhui Lin, Liu Yang, Zhuang Cai, Baojian Jing, Jia Yu, Xiankai Jiang, Zipeng Xing, and Jinlong Zou. 2018. "Iron (III) Metaphosphate/Iron Phosphide Heterojunctions Embedded in Partly-Graphitized Carbon for Enhancing Charge Transfer and Power Generation in Microbial Fuel Cells." *Chemical Engineering Journal* 342 (June): 228–37. https://doi.org/10.1016/J.CEJ.2018.02.083.

Luna, Phil de, Christopher Hahn, Drew Higgins, Shaffiq A. Jaffer, Thomas F. Jaramillo, and Edward H. Sargent. 2019. “What Would It Take for Renewably Powered Electrosynthesis to Displace Petrochemical Processes?” *Science* 364 (6438). https://doi.org/10.1126/SCIENCE.AAV3506.

Luo, Jie, Haiyan Wang, Geng Su, Yulian Tang, Huangqing Liu, Fenyang Tian, and Deliang Li. 2017. “Self-Supported Nickel Phosphosulphide Nanosheets for Highly Efficient and Stable Overall Water Splitting.” *Journal of Materials Chemistry A* 5 (28): 14865–72. https://doi.org/10.1039/C7TA02651J.

Luxa, Jan, Štěpán Cintl, Lucie Spejchalová, Jeng Yu Lin, and Zdeněk Sofer. 2020. “Potential Dependent Electrochemical Exfoliation of NiPS3 and Implications for Hydrogen Evolution Reaction.” *ACS Applied Energy Materials* 3 (12): 11992–99. https://doi.org/10.1021/ACSAEM.0C02168.

Mahmood, Nasir, Chenzhen Zhang, Jie Jiang, Fei Liu, Prof. Yanglong Hou. 2013. “Multifunctional Co3S4/Graphene Composites for Lithium Ion Batteries and Oxygen Reduction Reaction.” *A European Journal* 19 (16): 5183–90. https://doi.org/10.1002/CHEM.201204549.

Makeswaran, Nanthakishore, Debabrata Das, Vishal Zade, Paul Gaurav, V. Shutthanandan, Susheng Tan, and C. v. Ramana. 2021. “Size- And Phase-Controlled Nanometer-Thick β-Ga2O3Films with Green Photoluminescence for Optoelectronic Applications.” *ACS Applied Nano Materials* 4 (4): 3331–38. https://doi.org/10.1021/ACSANM.1C00378.

Marghussian, Vahak. 2015. “Glass Crystallization.” In *Nano-Glass Ceramics Processing, Properties and Applications*, edited by Vahak Marghussian, 1–62. William Andrew Publishing. https://doi.org/10.1016/B978-0-323-35386-1.00001-3.

Men, Yana, Peng Li, Juanhua Zhou, Gongzhen Cheng, Shengli Chen, and Wei Luo. 2019. “Tailoring the Electronic Structure of Co2P by N Doping for Boosting Hydrogen Evolution Reaction at All PH Values.” *ACS Catalysis* 9 (4): 3744–52. https://doi.org/10.1021/ACSCATAL.9B00407.

Mneimneh, Farah, Hasan Ghazzawi, Mohammad Abu Hejjeh, Matteo Manganelli, and Seeram Ramakrishna. 2023. “Roadmap to Achieving Sustainable Development via Green Hydrogen.” *Energies 2023, Vol. 16, Page 1368* 16 (3): 1368. https://doi.org/10.3390/EN16031368.

Morales, Daniela v., Catalina N. Astudillo, Veronica Anastasoaie, Baptiste Dautreppe, Bruno F. Urbano, Bernabé L. Rivas, Chantal Gondran, et al. 2021. “A Cobalt Oxide–Polypyrrole Nanocomposite as an Efficient and Stable Electrode Material for Electrocatalytic Water Oxidation.” *Sustainable Energy & Fuels* 5 (18): 4710–23. https://doi.org/10.1039/D1SE00363A.

Murthy, Arun Prasad, Jayaraman Theerthagiri, and Jagannathan Madhavan. 2018. “Insights on Tafel Constant in the Analysis of Hydrogen Evolution Reaction.” *Journal of Physical Chemistry C* 122 (42): 23943–49. https://doi.org/10.1021/ACS.JPCC.8B07763.

Muthurasu, Alagan, Viruthasalam Maruthapandian, and Hak Yong Kim. 2019. “Metal-Organic Framework Derived Co3O4/MoS2 Heterostructure for Efficient Bifunctional Electrocatalysts for Oxygen Evolution Reaction and Hydrogen Evolution Reaction.” *Applied Catalysis B: Environmental* 248 (July): 202–10. https://doi.org/10.1016/J.APCATB.2019.02.014.

Nam, Dae Hyun, Oleksandr S. Bushuyev, Jun Li, Phil De Luna, Ali Seifitokaldani, Cao Thang Dinh, F. Pelayo García De Arquer, et al. 2018. “Metal-Organic Frameworks Mediate Cu Coordination for Selective CO2 Electroreduction.” *Journal of the American Chemical Society* 140 (36): 11378–86. https://doi.org/10.1021/JACS.8B06407

Nikam, Revannath Dnyandeo, Ang Yu Lu, Poonam Ashok Sonawane, U. Rajesh Kumar, Kanchan Yadav, Lain Jong Li, and Yit Tsong Chen. 2015. “Three-Dimensional Heterostructures of MoS2

Nanosheets on Conducting MoO2 as an Efficient Electrocatalyst to Enhance Hydrogen Evolution Reaction." *ACS Applied Materials and Interfaces* 7 (41): 23328–35. https://doi.org/10.1021/ACSAMI.5B07960

Pan, Yuan, Yanru Liu, Jinchong Zhao, Kang Yang, Jilei Liang, Dandan Liu, Wenhui Hu, Dapeng Liu, Yunqi Liu, and Chenguang Liu. 2014. "Monodispersed Nickel Phosphide Nanocrystals with Different Phases: Synthesis, Characterization and Electrocatalytic Properties for Hydrogen Evolution." *Journal of Materials Chemistry A* 3 (4): 1656–65. https://doi.org/10.1039/C4TA04867A.

Pandey, Shobhit A., Chi Zhang, Daniah H. Ibrahim, Elise A. Goldfine, Jill K. Wenderott, Roberto Dos Reis, Rick L. Paul, et al. 2021. "Hidden Complexity in the Chemistry of Ammonolysis-Derived 'γ-Mo2N': An Overlooked Oxynitride Hydride." *Chemistry of Materials* 33 (17): 6671–84. https://doi.org/10.1021/ACS.CHEMMATER.1C00617

Patil, Swati J, Nilesh R Chodankar, Seung-Kyu Hwang, Ganji Seeta, Rama Raju, Yun-Suk Huh, Young-Kyu Han, et al. 2022. "Fluorine Engineered Self-Supported Ultrathin 2D Nickel Hydroxide Nanosheets as Highly Robust and Stable Bifunctional Electrocatalysts for Oxygen Evolution and Urea Oxidation Reactions." *Small* 18 (7): 2103326. https://doi.org/10.1002/SMLL.202103326.

Ping Liu, José A. Rodriguez, Takeshi Asakura, João Gomes, and Kenichi Nakamura. 2005. "Desulfurization Reactions on Ni2P(001) and α-Mo2C(001) Surfaces: Complex Role of P and C Sites." *Journal of Physical Chemistry B* 109 (10): 4575–83. https://doi.org/10.1021/JP044301X.

Popczun, Eric J., James R. McKone, Carlos G. Read, Adam J. Biacchi, Alex M. Wiltrout, Nathan S. Lewis, and Raymond E. Schaak. 2013. "Nanostructured Nickel Phosphide as an Electrocatalyst

for the Hydrogen Evolution Reaction." *Journal of the American Chemical Society* 135 (25): 9267–70. https://doi.org/10.1021/JA403440E.

Popczun, Eric J., Carlos G. Read, Christopher W. Roske, Nathan S. Lewis, and Raymond E. Schaak. 2014. "Highly Active Electrocatalysis of the Hydrogen Evolution Reaction by Cobalt Phosphide Nanoparticles." *Angewandte Chemie International Edition* 53 (21): 5427–30. https://doi.org/10.1002/ANIE.201402646.

Popczun, Eric J., Christopher W. Roske, Carlos G. Read, J. Chance Crompton, Joshua M. McEnaney, Juan F. Callejas, Nathan S. Lewis, and Raymond E. Schaak. 2015. "Highly Branched Cobalt Phosphide Nanostructures for Hydrogen-Evolution Electrocatalysis." *Journal of Materials Chemistry A* 3 (10): 5420–25. https://doi.org/10.1039/C4TA06642A.

Pu, Zonghua, Ibrahim Saana Amiinu, Chengtian Zhang, Min Wang, Zongkui Kou, and Shichun Mu. 2017. "Phytic Acid-Derivative Transition Metal Phosphides Encapsulated in N,P-Codoped Carbon: An Efficient and Durable Hydrogen Evolution Electrocatalyst in a Wide PH Range." *Nanoscale* 9 (10): 3555–60. https://doi.org/10.1039/C6NR09883E.

Pu, Zonghua, Qian Liu, Ping Jiang, Abdullah M. Asiri, Abdullah Y. Obaid, and Xuping Sun. 2014. "CoP Nanosheet Arrays Supported on a Ti Plate: An Efficient Cathode for Electrochemical Hydrogen Evolution." *Chemistry of Materials* 26 (15): 4326–29. https://doi.org/10.1021/CM501273S.

Puli, Venkata S., Shiva Adireddy, and C. V. Ramana. 2015. "Chemical Bonding and Magnetic Properties of Gadolinium (Gd) Substituted Cobalt Ferrite." *Journal of Alloys and Compounds* 644 (September): 470–75. https://doi.org/10.1016/J.JALLCOM.2015.05.031.

Pi, Chaoran, Chao Huang, Yixuan Yang, Hao Song, Xuming Zhang, Yang Zheng, Biao Gao, Jijiang Fu, Paul K. Chu, and Kaifu Huo. 2020. "In Situ Formation of N-Doped Carbon-Coated Porous

MoP Nanowires: A Highly Efficient Electrocatalyst for Hydrogen Evolution Reaction in a Wide PH Range." *Applied Catalysis B: Environmental* 263 (April): 118358. https://doi.org/10.1016/J.APCATB.2019.118358.

Qin, Qing, Haeseong Jang, Ping Li, Bing Yuan, Xien Liu, and Jaephil Cho. 2019. "A Tannic Acid–Derived N-, P-Codoped Carbon-Supported Iron-Based Nanocomposite as an Advanced Trifunctional Electrocatalyst for the Overall Water Splitting Cells and Zinc–Air Batteries." *Advanced Energy Materials* 9 (5): 1803312. https://doi.org/10.1002/AENM.201803312.

Qin, Zhixiao, Yubin Chen, Zhenxiong Huang, Jinzhan Su, Zhidan Diao, and Liejin Guo. 2016. "Composition-Dependent Catalytic Activities of Noble-Metal-Free NiS/Ni3S4 for Hydrogen Evolution Reaction." *Journal of Physical Chemistry C* 120 (27): 14581–89. https://doi.org/10.1021/ACS.JPCC.6B05230.

Renssen, Sonja van. 2020. "The Hydrogen Solution?" *Nature Climate Change 2020 10:9* 10 (9): 799–801. https://doi.org/10.1038/s41558-020-0891-0.

Riyajuddin, Sk, Kashif Azmi, Mansi Pahuja, Sushil Kumar, Takahiro Maruyama, Chandan Bera, and Kaushik Ghosh. 2021. "Super-Hydrophilic Hierarchical Ni-Foam-Graphene-Carbon Nanotubes-Ni2P–CuP2 Nano-Architecture as Efficient Electrocatalyst for Overall Water Splitting." *ACS Nano* 15 (3): 5586–99. https://doi.org/10.1021/ACSNANO.1C00647.

Ryu, Jaeyune, Namgee Jung, Jong Hyun Jang, Hyoung-Juhn Kim, and Sung Jong Yoo. 2015. "In Situ Transformation of Hydrogen-Evolving CoP Nanoparticles: Toward Efficient Oxygen Evolution Catalysts Bearing Dispersed Morphologies with Co-Oxo/Hydroxo Molecular Units." *ACS Catalysis* 5 (7): 4066–74. https://doi.org/10.1021/ACSCATAL.5B00349.

Saadi, Fadl H., Azhar I. Carim, Walter S. Drisdell, Sheraz Gul, Jack H. Baricuatro, Junko Yano, Manuel P. Soriaga, and Nathan S. Lewis. 2017. "Operando Spectroscopic Analysis of CoP Films

Electrocatalyzing the Hydrogen-Evolution Reaction." *Journal of the American Chemical Society* 139 (37): 12927–30. https://doi.org/10.1021/JACS.7B07606.

Saadi, Fadl H., Azhar I. Carim, Erik Verlage, John C. Hemminger, Nathan S. Lewis, and Manuel P. Soriaga. 2014. "CoP as an Acid-Stable Active Electrocatalyst for the Hydrogen-Evolution Reaction: Electrochemical Synthesis, Interfacial Characterization and Performance Evaluation." *Journal of Physical Chemistry C* 118 (50): 29294–300. https://doi.org/10.1021/JP5054452.

Saleh, Amina A., Doha M. Sayed, Liam A.V. Nagle-Cocco, Giorgio Divitini, Loujain G. Ghanem, Caterina Ducati, and Nageh K. Allam. 2022. "Deciphering the in Situ Surface Reconstruction of Supercapacitive Bimetallic Ni-Co Oxyphosphide during Electrochemical Activation Using Multivariate Statistical Analyses." *ACS Applied Energy Materials* 5 (6): 7661–73. https://doi.org/10.1021/ACSAEM.2C01122.

She, Zhi Wei, Jakob Kibsgaard, Colin F. Dickens, Ib Chorkendorff, Jens K. Nørskov, and Thomas F. Jaramillo. 2017. "Combining Theory and Experiment in Electrocatalysis: Insights into Materials Design." *Science*. American Association for the Advancement of Science. https://doi.org/10.1126/science.aad4998.

Shi, Yanmei, and Bin Zhang. 2016. "Recent Advances in Transition Metal Phosphide Nanomaterials: Synthesis and Applications in Hydrogen Evolution Reaction." *Chemical Society Reviews* 45 (6): 1529–41. https://doi.org/10.1039/C5CS00434A.

Song, Bo, Kai Li, Ying Yin, Tao Wu, Lianna Dang, Miguel Cabán-Acevedo, Jiecai Han, et al. 2017. "Tuning Mixed Nickel Iron Phosphosulfide Nanosheet Electrocatalysts for Enhanced Hydrogen and Oxygen Evolution." *ACS Catalysis* 7 (12): 8549–57. https://doi.org/10.1021/ACSCATAL.7B02575.

Stern, Lucas-Alexandre, Ligang Feng, Fang Song, and Xile Hu. 2015. “Ni2P as a Janus Catalyst for Water Splitting: The Oxygen Evolution Activity of Ni2P Nanoparticles.” *Energy & Environmental Science* 8 (8): 2347–51. https://doi.org/10.1039/C5EE01155H.

Su, Liang, Xiangzhi Cui, Ting He, Liming Zeng, Han Tian, Yiling Song, Kai Qi, and Bao Yu Xia. 2019. “Surface Reconstruction of Cobalt Phosphide Nanosheets by Electrochemical Activation for Enhanced Hydrogen Evolution in Alkaline Solution.” *Chemical Science* 10 (7): 2019–24. https://doi.org/10.1039/C8SC04589E.

Sun, Hongming, Xiaobin Xu, Zhenhua Yan, Xiang Chen, Fangyi Cheng, Paul S. Weiss, and Jun Chen. 2017. “Porous Multishelled Ni2P Hollow Microspheres as an Active Electrocatalyst for Hydrogen and Oxygen Evolution.” *Chemistry of Materials* 29 (19): 8539–47. https://doi.org/10.1021/ACS.CHEMMATER.7B03627/ASSET/IMAGES/LARGE/CM-2017-03627T_0005.JPEG.

Sun, Meng, Huijuan Liu, Jiuhui Qu, and Jinghong Li. 2016a. “Earth-Rich Transition Metal Phosphide for Energy Conversion and Storage.” *Advanced Energy Materials* 6 (13): 1600087. https://doi.org/10.1002/AENM.201600087.

Sun, Yugang, Farbod Alimohammadi, Dongtang Zhang, and Guangsheng Guo. 2017. “Enabling Colloidal Synthesis of Edge-Oriented MoS2 with Expanded Interlayer Spacing for Enhanced HER Catalysis.” *Nano Letters* 17 (3): 1963–69. https://doi.org/10.1021/ACS.NANOLETT.6B05346.

Sun, Hongming, Xiaobin Xu, Zhenhua Yan, Xiang Chen, Fangyi Cheng, Paul S. Weiss, and Jun Chen. 2017. “Porous Multishelled Ni2P Hollow Microspheres as an Active Electrocatalyst for Hydrogen and Oxygen Evolution.” *Chemistry of Materials* 29 (19): 8539–47. https://doi.org/10.1021/ACS.CHEMMATER.7B03627.

Sun, Meng, Huijuan Liu, Jiuhui Qu, and Jinghong Li. 2016. “Earth-Rich Transition Metal Phosphide for Energy Conversion and Storage.” *Advanced Energy Materials* 6 (13): 1600087. https://doi.org/10.1002/AENM.201600087.

Tang, Chun, Rong Zhang, Wenbo Lu, Liangbo He, Xiue Jiang, Abdullah M Asiri, Xuping Sun, et al. 2017. “Fe-Doped CoP Nanoarray: A Monolithic Multifunctional Catalyst for Highly Efficient Hydrogen Generation.” *Advanced Materials* 29 (2): 1602441. https://doi.org/10.1002/ADMA.201602441.

Teng, Yuan, Xu-Dong Wang, Jin-Feng Liao, Wen-Guang Li, Hong-Yan Chen, Yu-Jie Dong, Dai-Bin Kuang, et al. 2018. “Atomically Thin Defect-Rich Fe–Mn–O Hybrid Nanosheets as High Efficient Electrocatalyst for Water Oxidation.” *Advanced Functional Materials* 28 (34): 1802463. https://doi.org/10.1002/ADFM.201802463.

Tian, Jingqi, Qian Liu, Abdullah M. Asiri, and Xuping Sun. 2014. “Self-Supported Nanoporous Cobalt Phosphide Nanowire Arrays: An Efficient 3D Hydrogen-Evolving Cathode over the Wide Range of PH 0–14.” *Journal of the American Chemical Society* 136 (21): 7587–90. https://doi.org/10.1021/JA503372R.

Tian, Jingqi, Qian Liu, Ningyan Cheng, Abdullah M. Asiri, and Xuping Sun. 2014. “Self-Supported Cu3P Nanowire Arrays as an Integrated High-Performance Three-Dimensional Cathode for Generating Hydrogen from Water.” *Angewandte Chemie International Edition* 53 (36): 9577–81. https://doi.org/10.1002/ANIE.201403842.

Tong, Yun, Pengzuo Chen, Lu Chen, and Xinjiang Cui. 2021. “Dual Vacancies Confined in Nickel Phosphosulfide Nanosheets Enabling Robust Overall Water Splitting.” *ChemSusChem* 14 (12): 2576–84. https://doi.org/10.1002/CSSC.202100720.

Vesborg, Peter C. K., Brian Seger, and Ib Chorkendorff. 2015. "Recent Development in Hydrogen Evolution Reaction Catalysts and Their Practical Implementation." *Journal of Physical Chemistry Letters* 6 (6): 951–57. https://doi.org/10.1021/ACS.JPCLETT.5B00306.

Wang, Fengmei, Peng He, Yuanchang Li, Tofik Ahmed Shifa, Ya Deng, Kaili Liu, Qisheng Wang, et al. 2017. "Interface Engineered WxC@WS2 Nanostructure for Enhanced Hydrogen Evolution Catalysis." *Advanced Functional Materials* 27 (7): 1605802. https://doi.org/10.1002/ADFM.201605802.

Wang, Jun, Xinzhe Li, Bin Wei, Rong Sun, Wei Yu, Hui Ying Hoh, Haomin Xu, et al. 2020. "Activating Basal Planes of NiPS3 for Hydrogen Evolution by Nonmetal Heteroatom Doping." *Advanced Functional Materials* 30 (12): 1908708. https://doi.org/10.1002/ADFM.201908708.

Wang, Ling, Haijun Wu, Shibo Xi, Sing Teng Chua, Fenghe Wang, Stephen J. Pennycook, Zhi Gen Yu, Yonghua Du, and Junmin Xue. 2019. "Nitrogen-Doped Cobalt Phosphide for Enhanced Hydrogen Evolution Activity." *ACS Applied Materials & Interfaces* 11 (19): 17359–67. https://doi.org/10.1021/ACSAMI.9B01235.

Wang, Xiaoguang, Yury v. Kolen'Ko, Xiao Qing Bao, Kirill Kovnir, and Lifeng Liu. 2015. "One-Step Synthesis of Self-Supported Nickel Phosphide Nanosheet Array Cathodes for Efficient Electrocatalytic Hydrogen Generation." *Angewandte Chemie International Edition* 54 (28): 8188–92. https://doi.org/10.1002/ANIE.201502577.

Wang, Yang, Biao Kong, Dongyuan Zhao, Huanting Wang, and Cordelia Selomulya. 2017. "Strategies for Developing Transition Metal Phosphides as Heterogeneous Electrocatalysts for Water Splitting." *Nano Today* 15 (August): 26–55. https://doi.org/10.1016/J.NANTOD.2017.06.006.

Wu, Hao bin, Bao Yu Xia, Le Yu, Xin-Yao Yu, and Xiong Wen (David) Lou. 2015. "Porous Molybdenum Carbide Nano-Octahedrons Synthesized via Confined Carburization in Metal-Organic Frameworks for Efficient Hydrogen Production." *Nature Communications 2015 6:1* 6 (1): 1–8. https://doi.org/10.1038/ncomms7512.

Wu, Zishan, Xiaolin Li, Wen Liu, Yiren Zhong, Quan Gan, Xueming Li, and Hailiang Wang. 2017. "Materials Chemistry of Iron Phosphosulfide Nanoparticles: Synthesis, Solid State Chemistry, Surface Structure, and Electrocatalysis for the Hydrogen Evolution Reaction." *ACS Catalysis* 7 (6): 4026–32. https://doi.org/10.1021/ACSCATAL.7B00466.

Xiao, Peng, Wei Chen, and Xin Wang. 2015. "A Review of Phosphide-Based Materials for Electrocatalytic Hydrogen Evolution." *Advanced Energy Materials* 5 (24): 1500985. https://doi.org/10.1002/AENM.201500985.

Xiao, Zhaohui, Yu Cheng Huang, Chung Li Dong, Chao Xie, Zhijuan Liu, Shiqian Du, Wei Chen, et al. 2020. "Operando Identification of the Dynamic Behavior of Oxygen Vacancy-Rich Co3O4for Oxygen Evolution Reaction." *Journal of the American Chemical Society* 142 (28): 12087–95. https://doi.org/10.1021.

Xiao, Zhaohui, Yu Cheng Huang, Chung Li Dong, Chao Xie, Zhijuan Liu, Shiqian Du, Wei Chen, et al. 2020. "Operando Identification of the Dynamic Behavior of Oxygen Vacancy-Rich Co3O4for Oxygen Evolution Reaction." *Journal of the American Chemical Society* 142 (28): 12087–95. https://doi.org/10.1021/JACS.0C00257.

Xu, Jianbo, Ping Gao, and T. S. Zhao. 2012. "Non-Precious Co3O4 Nano-Rod Electrocatalyst for Oxygen Reduction Reaction in Anion-Exchange Membrane Fuel Cells." *Energy & Environmental Science* 5 (1): 5333–39. https://doi.org/10.1039/C1EE01431E.

Xu, Lei, Qianqian Jiang, Zhaohui Xiao, Xingyue Li, Jia Huo, Shuangyin Wang, and Liming Dai. 2016. “Plasma-Engraved Co3O4 Nanosheets with Oxygen Vacancies and High Surface Area for the Oxygen Evolution Reaction.” *Angewandte Chemie International Edition* 55 (17): 5277–81. https://doi.org/10.1002/ANIE.201600687.

Xu, You, Rui Wu, Jingfang Zhang, Yanmei Shi, and Bin Zhang. 2013. “Anion-Exchange Synthesis of Nanoporous FeP Nanosheets as Electrocatalysts for Hydrogen Evolution Reaction.” *Chemical Communications* 49 (59): 6656–58. https://doi.org/10.1039/C3CC43107J.

Yan, Kaiqiang, Yunhua Li, Xing Zhang, Xin Yang, Nuowei Zhang, Jinbao Zheng, Binghui Chen, and Kevin J. Smith. 2015. “Effect of Preparation Method on Ni2P/SiO2 Catalytic Activity for NaBH4 Methanolysis and Phenol Hydrodeoxygenation.” *International Journal of Hydrogen Energy* 40 (46): 16137–46. https://doi.org/10.1016/J.IJHYDENE.2015.09.145.

Yan, Liting, Lei Cao, Pengcheng Dai, Xin Gu, Dandan Liu, Liangjun Li, Ying Wang, and Xuebo Zhao. 2017. “Metal-Organic Frameworks Derived Nanotube of Nickel–Cobalt Bimetal Phosphides as Highly Efficient Electrocatalysts for Overall Water Splitting.” *Advanced Functional Materials* 27 (40): 1703455. https://doi.org/10.1002/ADFM.201703455.

Yang, Linjing, Weijia Zhou, Dongman Hou, Kai Zhou, Guoqiang Li, Zhenghua Tang, Ligui Li, and Shaowei Chen. 2015. “Porous Metallic MoO2-Supported MoS2 Nanosheets for Enhanced Electrocatalytic Activity in the Hydrogen Evolution Reaction.” *Nanoscale* 7 (12): 5203–8. https://doi.org/10.1039/C4NR06754A.

Yang, Yaoxia, Xuqin An, Mi Kang, Fengyao Guo, Lan Zhang, Qingtao Wang, Dongfei Sun, Yuan Liao, Zhiwang Yang, and Ziqiang Lei. 2021. “Distinctive MoS2-MoP Nanosheet Structures Anchored on N-Doped Porous Carbon Support as a Catalyst to Enhance the Electrochemical

Hydrogen Production." *New Journal of Chemistry* 45 (31): 14042–49. https://doi.org/10.1039/D1NJ02835A.

Yang, Yaqian, Han Mao, Rui Ning, Xu Zhao, Xiaohang Zheng, Jiehe Sui, and Wei Cai. 2021. "Ar Plasma-Assisted P-Doped Ni3S2 with S Vacancies for Efficient Electrocatalytic Water Splitting." *Dalton Transactions* 50 (6): 2007–13. https://doi.org/10.1039/D0DT03711G.

Yao, Na, Ran Meng, Jun Su, Zhengyin Fan, Pingping Zhao, and Wei Luo. 2021. "Dual-Phase Engineering of MoN/Co4N with Tailored Electronic Structure for Enhanced Hydrogen Evolution." *Chemical Engineering Journal* 421 (October): 127757. https://doi.org/10.1016/J.CEJ.2020.127757.

Ye, Ruquan, Paz del Angel-Vicente, Yuanyue Liu, M. Josefina Arellano-Jimenez, Zhiwei Peng, Tuo Wang, Yilun Li, et al. 2016. "High-Performance Hydrogen Evolution from MoS2(1–x)P Solid Solution." *Advanced Materials* 28 (7): 1427–32. https://doi.org/10.1002/ADMA.201504866.

Yin, Huajie, Shenlong Zhao, Kun Zhao, Abdul Muqsit, Hongjie Tang, Lin Chang, Huijun Zhao, Yan Gao, and Zhiyong Tang. 2015. "Ultrathin Platinum Nanowires Grown on Single-Layered Nickel Hydroxide with High Hydrogen Evolution Activity." *Nature Communications 2015 6:1* 6 (1): 1–8. https://doi.org/10.1038/ncomms7430.

Yin, Ying, Yumin Zhang, Tangling Gao, Tai Yao, Xinghong Zhang, Jiecai Han, Xianjie Wang, et al. 2017. "Synergistic Phase and Disorder Engineering in 1T-MoSe2 Nanosheets for Enhanced Hydrogen-Evolution Reaction." *Advanced Materials* 29 (28): 1700311. https://doi.org/10.1002/ADMA.201700311.

Yu, Linping, Jian Zhang, Yanliu Dang, Junkai He, Zachary Tobin, Peter Kerns, Yuhai Dou, Yao Jiang, Yuehui He, and Steven L. Suib. 2019. "In Situ Growth of Ni2P–Cu3P Bimetallic Phosphide with Bicontinuous Structure on Self-Supported NiCuC Substrate as an Efficient

Hydrogen Evolution Reaction Electrocatalyst." *ACS Catalysis* 9 (8): 6919–28. https://doi.org/10.1021/ACSCATAL.9B00494.

Zhang, Haojie, A. Wouter Maijenburg, Xiaopeng Li, Stefan L. Schweizer, and Ralf B. Wehrspohn. 2020. "Bifunctional Heterostructured Transition Metal Phosphides for Efficient Electrochemical Water Splitting." *Advanced Functional Materials* 30 (34): 2003261. https://doi.org/10.1002/ADFM.202003261.

Zhang, Lihan, Lili Han, Haoxuan Liu, Xijun Liu, and Jun Luo. 2017. "Potential-Cycling Synthesis of Single Platinum Atoms for Efficient Hydrogen Evolution in Neutral Media." *Angewandte Chemie International Edition* 56 (44): 13694–98. https://doi.org/10.1002/ANIE.201706921.

Zhang, Xiaoyan, Shan Zhang, Jing Li, and Erkang Wang. 2017. "One-Step Synthesis of Well-Structured NiS–$Ni_2P_2S_6$ Nanosheets on Nickel Foam for Efficient Overall Water Splitting." *Journal of Materials Chemistry A* 5 (42): 22131–36. https://doi.org/10.1039/C7TA05285E.

Zhao, Guoqiang, Kun Rui, Shi Xue Dou, Wenping Sun, G Q Zhao, K Rui, S X Dou, and W P Sun. 2018. "Heterostructures for Electrochemical Hydrogen Evolution Reaction: A Review." *Advanced Functional Materials* 28 (43): 1803291. https://doi.org/10.1002/ADFM.201803291.

Zhao, Tingwen, Xiangjian Shen, Yuan Wang, Rosalie K Hocking, Yibing Li, Chengli Rong, Kamran Dastafkan, et al. 2021. "In Situ Reconstruction of V-Doped Ni2P Pre-Catalysts with Tunable Electronic Structures for Water Oxidation." *Advanced Functional Materials* 31 (25): 2100614. https://doi.org/10.1002/ADFM.202100614.

Zhou, Xiaoli, Yun Liu, Huanxin Ju, Bicai Pan, Junfa Zhu, Tao Ding, Chunde Wang, and Qing Yang. 2016. "Design and Epitaxial Growth of MoSe2-NiSe Vertical Heteronanostructures with Electronic Modulation for Enhanced Hydrogen Evolution Reaction." *Chemistry of Materials* 28 (6): 1838–46. https://doi.org/10.1021/ACS.CHEMMATER.5B05006.

Zhu, Changrong, An-Liang Wang, Wen Xiao, Dongliang Chao, Xiao Zhang, Nguyen Huy Tiep, Shi Chen, et al. 2018. “In Situ Grown Epitaxial Heterojunction Exhibits High-Performance Electrocatalytic Water Splitting.” *Advanced Materials* 30 (13): 1705516. https://doi.org/10.1002/ADMA.201705516.

Zhu, Yanping, Jiali Wang, Hang Chu, You Chiuan Chu, and Hao Ming Chen. 2020. “In Situ/ Operando Studies for Designing Next-Generation Electrocatalysts.” *ACS Energy Letters* 5 (4): 1281–91. https://doi.org/10.1021/ACSENERGYLETT.0C00305

Zuliani, Alessio, Manuel Cano, Federica Calsolaro, Alain R. Puente Santiago, Juan J. Giner-Casares, Enrique Rodríguez-Castellón, Gloria Berlier, Giancarlo Cravotto, Katia Martina, and Rafael Luque. 2021. “Improving the Electrocatalytic Performance of Sustainable Co/Carbon Materials for the Oxygen Evolution Reaction by Ultrasound and Microwave Assisted Synthesis.” *Sustainable Energy & Fuels* 5 (3): 720–31. https://doi.org/10.1039/D0SE01505A.

Zuliani, Alessio, Mario J. Muñoz-Batista, and Rafael Luque. 2018. “Microwave-Assisted Valorization of Pig Bristles: Towards Visible Light Photocatalytic Chalcocite Composites.” *Green Chemistry* 20 (13): 3001–7. https://doi.org/10.1039/C8GC00669E.

Vita

Navid earned his BSc and MSc degrees in materials engineering from Iran. He joined the research institute of petroleum industry and worked for two years on several team-work projects related to failure analyses and corrosion management. Then, he earned his second master's degree in chemical engineering, where he worked at the Institute of Energy and Environment (IEE) for three years and obtained significant experience in current and emerging new strategies for managing internal and external product development and research projects. He also received a PhD degree in environmental engineering, where he studied synthesizing and developing catalysts for hydrogen and oxygen production. He joined the center for advanced materials research (CMR) at the university of Texas at El Paso in January 2021. He synthesized and designed nickel and molybdenum phosphosulfide electrodes for energy storage applications. He has substantial experience in advanced electrochemical techniques like cyclic voltammetry and impedance spectroscopy (EIS) to optimize electrochemical systems and worked in developing anodes for Li-ion batteries and cathode electrodes for Zn-ion air batteries over three years. He has strong hands-on experience in advanced materials characterization like SEM, TEM, XPS, XRD, and Raman spectroscopy. I am confident that his background and qualifications align with the requirements of the electrochemistry engineer position, and he will become an asset to the FuelCell Energy community.

Navid Attarzadeh

nattarzadeh@utep.edu